Multilevel analysis of the human immune response to *Aspergillus fumigatus* infection: Characteristic molecular signatures and individual risk factors

Analysen der humanen Immunantwort auf eine Infektion mit *Aspergillus fumigatus*: Charakteristische molekulare Signaturen und individuelle Risikofaktoren

Doctoral thesis for a doctoral degree at the Graduate School of Life Sciences,
Julius-Maximilians-Universität Würzburg,
Section Infection and Immunity

submitted by

Tamara Zoran

from

Maribor

Würzburg, 2022

Submitted on: ……..……..

Members of the Thesis Committee

Chairperson: Prof. Dr. Markus Sauer

Primary Supervisor: Prof. Dr. Jürgen Löffler

Supervisor (Second): Prof. Dr. med. Oliver Kurzai

Supervisor (Third): Dr. Jörg Linde

Supervisor (Fourth): Prof. Dr. Andreas Beilhack

Date of Public Defence: ……..……

Date of Receipt of Certificates: …….

Table of contents

Abbreviations

alloSCT	Allogeneic stem cell transplantation
ATCC	American Type Culture Collection
BAL	Bronchoalveolar lavage
BALF	Bronchoalveolar lavage fluid
cDNA	Complementary DNA
CO_2	Carbon dioxide
CRP	C-reactive protein
CV	Coefficient of variation
CXCL	Chemokine (C-X-C motif) ligand
CYP51A	Cytochrome P450 14-alpha sterol demethylase
DEG	Differentially expressed gene
DEM	Differentially expressed miRNA
DNA	Deoxyribonucleic acid
ELISA	Enzyme-linked immunosorbent assay
ELISPOT	Enzyme-linked immune absorbent spot
EORTC	European Organisation for Research and Treatment of Cancer
EtOH	Ethanol
FCS	Fetal calf serum
GM-CSF	Granulocyte-macrophage colony-stimulating factor
GvHD	Graft versus host disease
HR-CT	High-resolution computed tomography
hrs	Hours
HSCT	Hematopoietic stem-cell transplantation
ICU	Intensive care unit
IFN-γ	Interferon gamma
IL	Interleukin
LPS	Lipopolysaccharide
MALDI-TOF MS	Matrix-assisted laser desorption - ionisation-time of flight mass spectrometry
miRNA	Micro RNA
MSGERC	Mycoses Study Group Education and Research Consortium
NF-κB	Nuclear factor-kappa B

PBMCs	Peripheral blood mononuclear cells
PCR	Polymerase chain reaction
pH	Potential of hydrogen
qPCR	Quantitative real-time PCR
RIN	RNA integrity number
RNA	Ribonucleic acid
RPKM	Reads per kilobase million
RPMI	Roswell Park Memorial Institute
Ta	Annealing temperature
TNF	Tumour necrosis factor
TRL	Toll-like receptor
UTR	Untranslated region

Summary

Although the field of fungal infections advanced tremendously, diagnosis of invasive pulmonary aspergillosis (IPA) in immunocompromised patients continues to be a challenge. Since IPA is a multifactorial disease, investigation from different aspects may provide new insights, helpful for improving IPA diagnosis. This work aimed to characterize the human immune response to *Aspergillus fumigatus* in a multilevel manner to identify characteristic molecular candidates and risk factors indicating IPA, which may in the future support already established diagnostic assays. We combined *in vitro* studies using myeloid cells infected with *A. fumigatus* and longitudinal case-control studies investigating patients post allogeneic stem cell transplantation (alloSCT) suffering from IPA and their match controls.

Characteristic miRNA and mRNA signatures indicating *A. fumigatus*-infected monocyte-derived dendritic cells (moDCs) demonstrated the potential to differentiate between *A. fumigatus* and *Escherichia coli* infection. Transcriptome and protein profiling of alloSCT patients suffering from IPA and their matched controls revealed a distinctive IPA signature consisting of *MMP1* induction and *LGAL2* repression in combination with elevated IL-8 and caspase-3 levels. Both, *in vitro* and case-control studies, suggested cytokines, matrix-metallopeptidases and galectins are important in the immune response to *A. fumigatus*. Identified IPA characteristic molecular candidates are involved in numerous processes, thus a combination of these in a distinctive signature may increase the specificity. Finally, low monocyte counts, severe GvHD of the gut (grade ≥ 2) and etanercept administration were significantly associated with IPA diagnosis post alloSCT. Etanercept in monocyte-derived macrophages (MDM) infected with *A. fumigatus* downregulates genes involved in the NF-κB and TNF-α pathway and affects the secretion of CXCL10.

Taken together, identified characteristic molecular signatures and risk factors indicating IPA may in the future in combination with established fungal biomarkers overcome current diagnostic challenges and help to establish tailored antifungal therapy. Therefore, further multicentre studies are encouraged to evaluate reported findings.

Zusammenfassung

Obwohl im Bereich der Erforschung invasiver Pilzinfektionen aktuell enorme Fortschritte erzielt wurden, stellt die Diagnose der Invasiven Pulmonalen Aspergillose (IPA) bei immunsupprimierten Patienten weiterhin eine grosse Herausforderung dar. Da es sich bei der IPA um eine multifaktorielle Erkrankung handelt, können Untersuchungen unter verschiedenen Fragestellungen neue Erkenntnisse liefern, die zur Verbesserung der IPA Diagnose beitragen. In dieser Arbeit wurde die humane Immunantwort auf *Aspergillus fumigatus* auf mehreren Ebenen untersucht, um charakteristische molekulare Kandidaten und Risikofaktoren zu identifizieren, die auf eine IPA hinweisen um so in Zukunft bereits etablierte diagnostische Tests unterstützen zu können. Wir kombinierten *in vitro* Studien mit *A. fumigatus* infizierten, myeloischen Zellen mit longitudinalen Case-Control-Studien, in denen an IPA erkrankte Patienten und ihre passenden Kontrollpatienten nach allogener Stammzelltransplantation (alloSZT) untersucht wurden.

Charakteristische miRNA und mRNA Signaturen von *A. fumigatus*-infizierten Monozyten-abgeleiteten dendritischen Zellen (moDCs) zeigten das Potenzial, zwischen *A. fumigatus* und *Escherichia coli* Infektionen zu unterscheiden. Transkriptom- und Protein- Analysen von alloSZT Patienten, die an einer IPA erkrankten, und den passenden Kontrollpatienten ergaben charakteristische IPA Signaturen, bestehend aus einer *MMP1* Induktion und einer *LGALS2* Repression, in Kombination mit erhöhten IL-8 und Caspase-3 Konzentrationen. Sowohl die *in vitro* Daten als auch die Fall-Kontroll- Studien zeigten, dass Zytokine, Matrix-Metallopeptidasen und Galectine eine wichtige Rolle bei der Immunantwort auf *A. fumigatus* spielen. Die in IPA identifizierten charakteristischen molekularen Kandidaten sind an mehreren Prozessen beteiligt, so dass eine Kombination dieser molekularen Kandidaten die Spezifität mittels charakteristischer Signatur erhöhen könnte. Schließlich waren niedrige Monozytenzahlen, eine schwere GvHD des Darms (Grad $\geq$ 2) und die Anwendung von Etanercept signifikant mit einer IPA Diagnose nach alloSZT assoziiert. Etanercept in Makrophagen, die mit *A. fumigatus* ko-kultiviert wurden, reguliert Gene herunter, die am NF-κB- und TNF-α-Signalweg beteiligt sind, und beeinflusst die Sekretion von CXCL10.

Zusammenfassend lässt sich festhalten, dass die identifizierten charakteristischen molekularen Signaturen und Risikofaktoren, die auf eine IPA hinweisen, in Zukunft in Kombination mit etablierten Pilz-Biomarkern die derzeitigen diagnostischen Limitationen überwinden könnten und dazu beitragen könnten, eine patientenindividuelle antimykotische Therapie zu etablieren.

Es werden jedoch weitere multizentrische Studien notwendig sein, um diese Ergebnisse umfassend zu bewerten.

1. Introduction

1.1 Aspergillosis in immunocompromised patients

1.1.1 Opportunistic pathogen *Aspergillus fumigatus*

The genus *Aspergillus* consists of ubiquitous, saprophytic moulds widely distributed in nature, found worldwide. Among *Aspergillus* spp., *A. fumigatus* belonging to section *Fumigati* is the most frequently associated with aspergillosis (Latge, 1999). Other clinically relevant species causing an infection are *A. terreus, A. flavus, A. niger* and *A. nidulans* (Latge and Chamilos, 2019). One of the major characteristics that make *A. fumigatus* ubiquitous in the environment and the prevalent species associated with aspergillosis are abundant sporulation, small and hydrophobic conidia which are easily dispersed in the air, ability to survive wide temperature and pH range and adaptation to the host environment (Kwon-Chung and Sugui, 2013).

A. fumigatus is commonly found in the air as well as decaying vegetation and is reported as the dominant fungi in the greenhouse soil and gardens (Jensen, 1931; Kwon-Chung and Sugui, 2013). While the optimal temperature for its growth is 37° C, this species can tolerate temperatures between 12 °C and 65 °C. On the standard fungal media such as Sabouraud dextrose agar (SDA) or potato dextrose agar (PDA), *A. fumigatus* form velvety green-grey culture, white to pale yellow on the reverse. Among typical microscopic *A. fumigatus* features are uniseriate conidial head with phialides (flask-shaped hyphae) covering up to three-quarters of the vesicle and pigmented, spherical conidia, 2.5-3 μm in size, produced on phialides (Latge, 1999).

1.1.2 Pathogenesis and innate immune response to *A. fumigatus*

The infection with *A. fumigatus* mainly occurs by inhalation of airborne conidia, which are due to their small size, able to reach the lower respiratory tract, thus the common site of infection is the lungs (Latge, 1999). In healthy individuals, inhaled conidia are removed by host defence mechanisms daily. These defence mechanisms include an intact epithelial layer with mucus, alveolar macrophages and neutrophils (Challa, 2018). In individuals with a weakened immune system such as alloSCT patients, the immune response is weak or delayed, leading to the germination of conidia and the development of the disease. Dissemination usually occurs when hyphae escape host defences and disseminate from the lung via the bloodstream to other organs. Innate immunity has therefore crucial role in the clearance of *A. fumigatus* conidia (Dagenais

and Keller, 2009). The respiratory epithelium presents a mechanical barrier, protecting from the invasion of conidia and is important in the recognition of *A. fumigatus* through the expression of pattern-recognition receptors (e.g., dectin-1, TLRs) (Sun *et al*., 2012). Essential cells responsible for phagocytosis of *A. fumigatus* conidia are alveolar macrophages, which via dectin-1 recognize β-glucan (Steele *et al*., 2005). These immune cells phagocyte conidia by releasing reactive oxygen species (ROS) in lysosomes, produce cytokines and chemokines and recruit neutrophils to the site of the infection (Bhatia *et al.*, 2011; Challa, 2018). Inhaled conidia, which escape macrophages and germinate to hyphae are targeted by neutrophils, which damage hyphae and starve *A. fumigatus* by binding iron to lactoferrin (Dagenais and Keller, 2009; Challa, 2018). Neutrophils are known as the most important effector cells against *A. fumigatus*, therefore, any condition leading to neutropenia presents a high risk for the development of IPA (Schaffner *et al*., 1982; Baddley, 2011).

Besides macrophages and neutrophils, also other immune cells play an important role in efficient defence against *A. fumigatus*. Murine studies demonstrated Natural killer (NK) cells are the major source of IFN-γ in the lungs of neutropenic mice with aspergillosis and their recruitment to the lungs is important for early host defence (Morrison *et al*., 2003; Park *et al*., 2009). Monocytes, bone marrow-derived cells are circulating in the blood and in the response to stimuli migrate into tissue and differentiate into macrophages and dendritic cells (Serbina *et al*., 2009). Monocytes and their derivatives are crucial in orchestrating immune responses to *A. fumigatus* infections by phagocytizing and killing conidia, transferring conidia to the lymph nodes, production of cytokines that enhance the fungicidal activity of neutrophils and facilitating adaptive immune responses by antigen presentation (Palucka and Banchereau, 1999; Heung, 2020).

1.1.3 Clinical manifestations of aspergillosis

Aspergillosis refers to a wide spectrum of diseases that are depending on the host immune status, categorized into allergic, chronic and invasive aspergillosis (Latge and Chamilos, 2019). In immunocompetent patients, *Aspergillus* spp. can cause noninvasive, chronic form, leading to the development of aspergilloma or chronic pulmonary aspergillosis (CPA). These forms of diseases occur in patients with structural lung diseases such as chronic obstructive pulmonary disease (COPD) or patients post tuberculosis or sarcoidosis (Cadena *et al*., 2021). Fungal balls or aspergillomas are usually formed due to colonization of *Aspergillus* spp. of preexisting pulmonary cavities. Chronic pulmonary aspergillosis is described as slow progressive

destruction of lung parenchyma evolving over months (> three months). Allergic bronchopulmonary aspergillosis (ABPA) is the most severe form of aspergillosis in atopic patients and is characterized as a hypersensitivity disease of the lung. This form of aspergillosis develops as sensitization to *A. fumigatus* allergens, mostly in patients with asthma, cystic fibrosis or individuals with a predisposition for ABPA (Latge and Chamilos, 2019). IPA develops in case of immune dysfunction and commonly presents in patients with symptoms such as chest pain, shortness of breath, cough, hemoptysis and fever. Due to the weak immune response, profoundly immunosuppressed or neutropenic patients might show only a few or no symptoms, which often leads to late diagnosis (Cadena *et al*., 2021). IPA has been reported as the most prevalent invasive fungal infection among hematopoietic stem cell transplant and solid-organ recipients (Cordonnier *et al*., 1986; Neofytos *et al*., 2009).

1.1.4 Epidemiology and risk factors

Neutropenia which may be inherited or acquired and corticosteroid treatment are both considered among the major risk factors for IPA (Patterson *et al.*, 2016). Pulmonary complications post HSCT are frequent, and patients undergoing HSCT are highly susceptible to opportunistic infections due to the weakened immune system. Major risk factors for IPA among HSCT patients are high-dose chemoradiotherapy, immunosuppressive therapy, neutropenia, defects in cell-mediated immunity and the type of HSCT (Cordonnier *et al*., 1986; Nucci and Anaissie, 2009). AlloSCT, an important treatment strategy for adults with AML, present a higher risk for IPA compared to autologous HSCT (Ganapule *et al*., 2017). A common complication following alloSCT is GvHD, characterized as inflammation in different organs due to donor T cells attacking the patient's healthy cells and has also been associated with IPA diagnosis (Jaglowski and Devine, 2014; Cadena *et al*., 2021). The highest risk for developing IPA is in the first four weeks post alloSCT, with a second peak three to four months post alloSCT, which is mostly associated with GvHD and subsequent immunosuppressive therapy (Cadena *et al*., 2021). Incidence of IPA among alloSCT patients was reported up to 23%, with a mortality rate of 20 to 75% (Neofytos *et al.*, 2008; Garcia-Vidal *et al*., 2015; Robin *et al*., 2019). Considering aspergillosis occurs by inhalation of conidia, the environment has a great impact on the epidemiology of the disease. Over the last few decades, IPA has been commonly associated with air-handling equipment effects as well as hospital constructions (Patterson *et al*., 2016).

Patients undergoing solid transplantation, in particular lung transplant recipients, are also at increased risk for developing IPA (Patterson *et al*., 2000). Increased risk for IPA has been reported for the patients in the ICU, associated with lung structural diseases (e.g., COPD) and subsequent corticosteroid therapy as well as acute respiratory distress syndrome (ARDS) (Koulenti *et al*., 2014). IPA has been associated also with critically ill patients, CMV viremia and respiratory viral infections. It has been suggested, that IPA occurs following respiratory infections due to injured epithelium and dysfunctional mucociliary clearance which allow growth and invasion of *Aspergillus* spp. (Kuo *et al*., 2021; Chala, 2018). Recently, aspergillosis has been reported as a secondary infection in patients with Coronavirus disease 2019 (COVID-19). COVID-19-associated pulmonary aspergillosis (CAPA) has been mostly associated with severe COVID-19, increasing mortality (Cadena *et al*., 2021; Feys *et al*., 2021). In a recent report, summarizing 48 studies investigating CAPA cases mostly in Europe, Feys *et al.* (2021) reported an incidence of CAPA between 0.7 and 34.4 %. It has been suggested that the treatment of COVID-19 with corticosteroids and tocilizumab is the major risk for CAPA (Feys *et al*., 2021).

With the latest advancements in the therapy for haematological malignancies and autoimmune diseases, new risk groups are emerging. IPA has been recently reported in patients receiving monoclonal antibodies, small-molecule protein kinases inhibitors (e.g., ibrutinib) and CAR T-cell therapy (Nedel *et al*., 2009; Alkharabsheh *et al*., 2021; Stewart and Henden, 2021; Wudhikarn *et al*., 2021). Therefore, to improve the overall management of IPA, continuous research on risk factors and epidemiologic surveillance of IPA is essential.

1.1.5 Antifungal treatment

Prompt treatment is essential for good outcomes, especially in immunocompromised patients suffering from IPA. Thus, in patients with a strong suspicion of IPA, antifungal treatment is recommended while the diagnostic tests are conducted (Patterson *et al*., 2016). Several antifungals are available for routine clinical use. Preferred antifungals of choice, triazoles (e.g., voriconazole, posaconazole) are inhibiting ergosterol synthesis by targeting 14-α-demethylase (encoded by *CYP51*), an enzyme that converts lanosterol to ergosterol (Lass-Flörl, 2011). While voriconazole is the primary choice of treatment for IPA, posaconazole is the antifungal of choice for prophylaxis in alloSCT and neutropenic patients. In case voriconazole administration is not possible, Amphotericin B, targeting ergosterol which leads to membrane leakage and

fungal cell death, is considered a good alternative for initial or salvage therapy (Patterson *et al*., 2016; Latge and Chamilos, 2019).

Besides side effects and high costs of antifungals, an additional challenge in IPA management presents antifungal resistance (Krueger and Nelson, 2009). The azole resistance mostly occurs by mutations in the *CYP51A* and develops either due to long-duration therapy or as a consequence of using azoles in agriculture (Chowdhary *et al*., 2013; Cadena *et al*., 2021). Thus, continuous research on developing new therapeutic strategies and antifungals, along with improving the use of antifungals through antifungal stewardship intervention is crucial.

1.1.6 EORTC/MSGERC classification

To improve IPA outcomes in high-risk patients, early diagnosis and prompt antifungal treatment are crucial (Jenks and Hoenigl, 2018). Despite diagnostic advancements in the last two decades, the management of IPA is still challenging. One of the major diagnostics improvements in the last years has been standardized EORTC/MSGERC criteria for IPA diagnosis (Donnelly *et al*., 2020). These criteria were established mainly for clinical research studies to help with the standardization of IPA definitions and not for clinical decision making (De Pauw *et al*., 2008). EORTC/MSGERC criteria categorize IPA patients according to the certainty of disease based on radiological, clinical and mycological evidence into possible, probable and proven IPA cases. The established classification applies to immunocompromised patients and not the other risk groups such as critically ill patients in the ICU (Donnelly *et al*., 2020). Proven IPA is considered in the case of positive histopathology or culture by detection of *Aspergillus* spp. from sterile specimens. Considering the risk of complications due to the invasive procedure, a biopsy is often not feasible. The category of proven IPA is applied regardless of whether the patient is immunocompromised, whereas probable and possible IPA categories are suggested for immunocompromised patients only. The category of probable IPA presents cases with host factor (e.g., neutropenia, HSCT, corticosteroids), clinical feature (positive HR-CT scan) and mycological evidence (culture, positive galactomannan ELISA or *Aspergillus* DNA PCR). Cases with host factors and clinical evidence yet without mycological evidence are considered as possible IPA (Donnelly *et al*., 2020) (Figure 1).

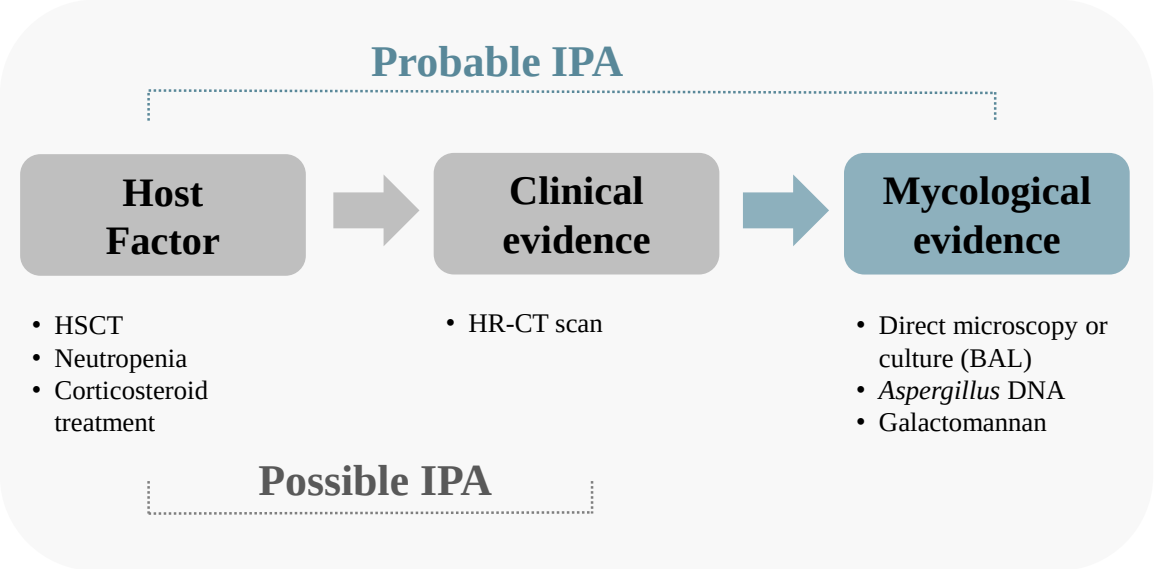

Figure 1: Revised EORTC/MSGERC guidelines. According to recently revised EORTC/MSGERC criteria, probable IPA cases are defined by a combination of host factors, clinical and mycological evidence. Cases having host factors and clinical evidence, without mycological evidence are classified as possible IPA (Donnelly *et al*., 2020).

1.1.7 Diagnosis of IPA in immunocompromised patients

Clinical symptoms and signs for IPA are often nonspecific and differentiation between colonization and invasive disease is difficult. Blood cultures for *Aspergillus* spp. are generally negative. Considering airway-invasive growth, BAL and lung biopsies are specimens of choice for IPA diagnosis (Simoneau *et al*., 2005; Lass-Flörl, 2017). Among the greatest challenges in IPA, diagnosis is finding an ideal diagnostic marker or test providing high specificity and sensitivity, which currently used diagnostic assays are often lacking. To achieve adequate sensitivity, the diagnosis of IPA is currently based on the combination of multiple diagnostic assays from radiology to the detection of fungal biomarkers (Ullmann *et al*., 2018).

HR-CT is recommended in immunocompromised patients to evaluate pulmonary abnormalities indicating IPA such as nodules commonly surrounded by a “halo sign”. However, detection of the “halo sign” is only possible in the early time of IPA and later radiological signs become non-specific or appear too late for guiding treatment decisions (Caillot *et al*., 2001; Cruciani *et al*., 2019). Conventional methods based on culture and microscopy are commonly used, yet due to the low sensitivity often in combination with newer diagnostics assays. (Ullmann *et al*., 2018). MALDI-TOF MS has been reported as a fast, cost-effective and accurate method for the identification of *Aspergillus* spp., including cryptic species. Yet, the performance of the method depends on the used library. While expanded in house libraries showed better performance

compared to commercially available libraries, the creation of new databases is an expensive, slow and labour intensive process (Vidal-Acuna *et al*., 2018). Challenges in obtaining invasive specimens (e.g., biopsies) in high-risk patients, as well as the need for early diagnosis, increased interest in the establishment of non-invasive and non-culture based diagnostic methods such as detection of polysaccharide-based antigens of *Aspergillus* spp. cell wall and *Aspergillus* DNA (Patterson and Donnelly, 2019; Feinstein *et al*., 2021).

Galactomannan is the cell wall component of *Aspergillus* spp., released during fungal growth, detectable in biofluids such as BAL and serum. Detection of galactomannan by ELISA is a well-established method, already widely used in the clinics and is included also in the current EORTC/MSGERC criteria (Bretagne *et al*., 1997; Donnelly *et al.*, 2020). Compared to conventional methods, in immunocompromised patients, galactomannan testing showed a higher sensitivity for IPA diagnosis. The overall sensitivity of this method (44 %-90 %) depends on the host immune status and it has been reported higher in high-risk patients with haematological malignancies compared to other non-risk patients (ICU patients) (Maertens *et al*., 2001; Cadena *et al*., 2021; Reinwald *et al*., 2021). Moreover, higher sensitivity was observed in BAL specimens compared to serum. In immunocompromised patients, according to the FDA, the optical density index (ODI) of ≥ 0.5 is considered positive. To avoid false-positive results in other non-risk patient groups, a higher cut-off is recommended (Arastehfar *et al*., 2021). The optimal ODI cut-off is still debatable and recently updated EORTC/MSGERC criteria have proposed an ODI of ≥ 1 for positive galactomannan in serum or BAL (Donnelly *et al*., 2020; Siopi *et al*., 2021).

β-D-glucan is another component detectable in biofluids, yet compared to galactomannan is not specific for *Aspergillus* spp. and it is part of the cell wall of other fungi such as *Candida*, *Fusarium*, *Trichosporon*. Some fungi such as Mucorales and *Cryptococcus* are not detectable by the β-D-glucan test (Odabasi *et al*., 2006; Patterson and Donelly, 2019). The detection of β-D glucan has been recently excluded from ERTC/MSGERC criteria (Donnelly *et al*., 2020).

Detection of *Aspergillus* DNA by PCR has been widely studied, nevertheless, diagnostic accuracy and specificity of PCR testing for IPA diagnosis have been debatable for many years. The major challenges faced by researchers have been the variation in diagnostic performances across studies and the lack of standardization due to the use of different techniques (Spreadbury *et al*., 1993; Arastehfar *et al*., 2021). Despite high BAL PCR sensitivity, there is a lack of specificity as it cannot distinguish between colonization from invasive growth (Latge and Chamilos, 2019). In a recent study, Cruciani *et al.* (2019) reported moderate diagnostic

accuracy for blood PCR in the case of IPA screening in high-risk patients, however a high negative predictive value. Among 29 evaluated studies, conducted between 1980 and 2015, reported PCR sensitivity and specificity in the case of two consecutive positive blood PCR tests were 59.6 % and 95.1 %, respectively. A combination of galactomannan and PCR tests has been proposed to increase diagnostic accuracy (Cruciani *et al*., 2019). Many efforts were undertaken for PCR protocol standardization and PCR has been recently included in the revised EORTC/MSGERC criteria to help to define probable IPA (Donnelly *et al*., 2020). Similar to the galactomannan test, PCR is most useful in high-risk (e.g., neutropenic) patients not receiving mould prophylaxis, whereas in other non-neutropenic patients PCR showed limited utility. Antifungal prophylaxis and treatment affect the performance of both diagnostics assays (Reinwald *et al*., 2012; Arastehfar *et al*., 2021). In immunocompromised patients, monitoring based on a combination of serum galactomannan and *Aspergillus* PCR has been associated with earlier IPA diagnoses (Aguado *et al*., 2015). Detection of both fungal markers has been reported to increase diagnostic accuracy and reduce the unnecessary use of antifungals (Reinwald *et al*., 2012; Cruciani *et al*., 2019).

1.1.7.1 Novel concepts in IPA diagnostics

In the last decade, several novel concepts and tests for IPA detection have been developed and are under evaluation (White and Price, 2021). Emerging antifungal resistance in *Aspergillus* spp. has led to the development of molecular approaches for the detection of clinically relevant *Aspergillus* spp. and the most frequent mutations associated with azole resistance (*cyp*51A). For example, the commercially available diagnostic PCR kit AsperGenius® (PathoNostic, Netherlands), enables the identification and detection of clinically relevant *Aspergillus* spp. together with azole-resistance markers TR34 and TR46 (Pelzer *et al*., 2020). Point of care diagnostic tools like lateral flow devices detecting *Aspergillus* antigens are in development and showed promising results for rapid IPA diagnosis in immunocompromised patients (Mercier *et al*., 2020). Similar was suggested also for assays targeting *Aspergillus* specific functional T-cells by ELISPOT, ELISA or flow cytometry (Bacher *et al*., 2015). However, due to the challenges linked to the pre-test conditions, lack of standardization and optimization, more research is necessary (White and Price, 2021). These tests have shown promising results in immunocompromised patients, especially when combined with galactomannan and *Aspergillus* DNA detection, however, more research is necessary to standardize and evaluate their performance (Patterson and Donnelly, 2019; White and Price, 2021).

1.2 Investigation of molecular signatures indicating infection

Characterization of human immune response to *A. fumigatus* infection may lead to the identification of potential human biomarker candidates indicating aspergillosis and to novel host-directed therapeutic strategies (Bruno *et al*., 2020).

According to the National Institutes of Health Biomarkers Definitions Working Group, the term biomarker is defined as a "*characteristic that is objectively measured and evaluated as an indicator of normal biological processes, pathogenic processes, or pharmacologic responses to a therapeutic intervention or other health care intervention*" (Biomarkers Definitions Working Group, 2001). For instance, CRP is a human biomarker widely used for inflammation and infection, however, does not allow the discrimination between different infection types (Hjortdahl *et al*., 1991). Combining several human biomarkers or using characteristic host-based signatures might increase the specificity and even allow to discriminate between different respiratory pathogens (Zaas *et al*., 2009; Bhattacharya *et al*., 2017; Ashkenazi-Hoffnung *et al*., 2018).

Host biomarkers may have in the future an important role in the development of personalized medicine (Pfaffl, 2013). Recent advancements in "omics" methodologies (e.g., transcriptomics, genomics) allowed high-throughput biomarker screening and identification of a large number of potential candidates or characteristic signatures. Although from many identified biomarkers only a few have made the transition to clinical use, results are promising and further research is encouraged (Hanash, 2011; Quezada *et al*., 2017).

1.2.1 Transcriptome profiling using RNA-seq

A transcriptome is a complete collection of RNA transcripts and presents knowledge of gene regulation and protein content information in a given time under-investigated conditions (Wang *et al*., 2009). Host transcriptomics using RNA-seq is therefore a powerful approach for deciphering the pathophysiology of different types of infections and a better understanding of already described genes and pathways linked to investigated infection. Moreover, in the context of biomarker research, RNA-seq enables the identification of novel yet unknown RNAs and may provide a large number of potential molecular candidates or signatures indicating infection (Kukurba and Montgomery, 2015).

Several platforms are available and the Illumina HiSeq platform has been reported as the most commonly applied NGS technology for RNA-seq (Kukurba and Montgomery, 2015). The

simple workflow of RNA-seq investigation is shown in Figure 2. RNA-seq experiment starts with the extraction of RNA and is followed by the library preparation, which consists of cDNA synthesis, fragmentation, adapter ligation to the ends of cDNA fragments and amplification by PCR to increase library input before sequencing (Kukurba and Montgomery, 2015). RNA-seq libraries are thus collections of prepared fragments, ready for sequencing. Next, the library is loaded into a flow cell (sequencing chip), where each fragment via adapters anneals to the primers on the flow cell and is amplified through a series of amplification reactions termed bridge amplification, resulting in millions of copies of single-stranded DNA. These DNA templates are ready for the sequencing on Illumina platform, which uses the "sequencing by synthesis" approach (Illumina Inc., 2017, *Brochure*). In the sequencing step, nucleotides containing the fluorescent tag and reversible terminator which blocks incorporation of the next base, bind to the DNA templates. After the addition of a specific nucleotide, which is detected by a fluorescent signal, the terminator is cleaved and the next base can bind. DNA can be sequenced from only one end, termed single-end sequencing which is the simplest way of Illumina sequencing, economic and rapid. Another method is paired-end sequencing, where after sequencing a forward DNA strand, the reads are washed away and sequencing repeats for the reverse strand (Illumina Inc., 2017, *Brochure*). The final step in the RNA-seq is data analysis, where bioinformatics plays a crucial role. Raw sequencing reads are processed and aligned to the reference genome and further data analysis such as differential expression analysis are performed (Koch *et al*., 2018).

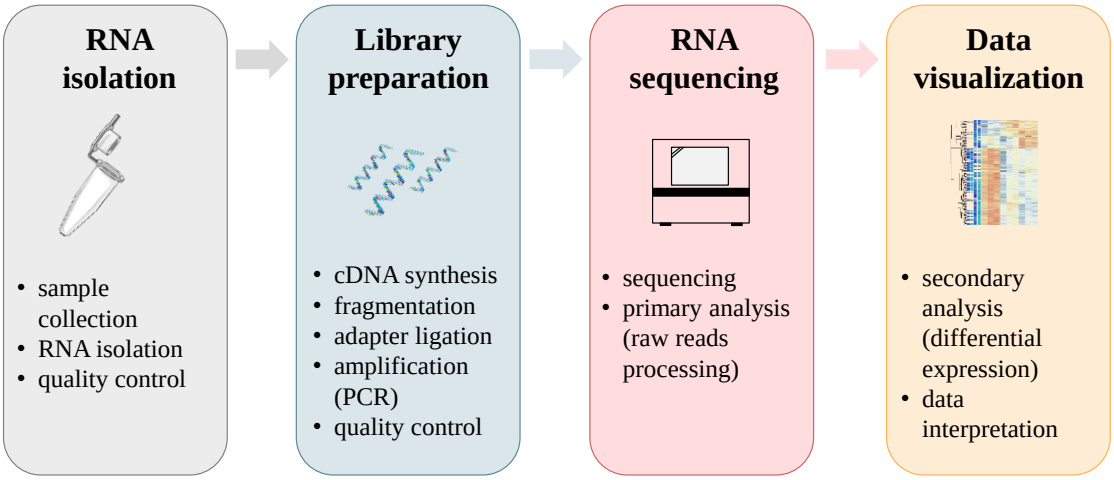

Figure 2: RNA-seq workflow. RNA-seq experiments start with sample collection and are followed by RNA isolation and library preparation. After RNA-seq, raw reads are processed and analysed. Illustrations were taken and modified from Servier Medical Art by Servier (available at https://smart.servier.com).

1.2.2 Transcriptome signatures and miRNAs

Changes in the transcriptome are one of the earliest responses to the infection (Di Lulio *et al.*, 2021). Gene transcription allows cells to rapidly adapt to external or physiological changes, therefore transcriptome signature may be a powerful tool for describing pathophysiological status and exposure to pathogens (Pfaffl., 2013). RNA molecules, especially protein-coding RNAs (mRNAs) have been extensively studied as non-invasive biomarkers in various medical fields (Matsushima *et al*., 2011; Xi *et al*., 2017; Ross *et al*., 2019; Katiyar *et al*., 2021). In the last years, non-coding RNAs have evoked interest as biomarkers due to their involvement in the gene regulation and immune response to infections and diseases (Ahmed *et al*., 2016; Ouyang *et al*., 2016; Xi *et al*., 2017). Among these, miRNAs have been suggested as promising non-invasive biomarkers (Chen *et al*., 2004). MiRNAs, first reported in 1993 in *Caenorhabditis elegans*, are single-stranded, small non-coding RNAs, involved in the regulation of the genes (Lee *et al*., 1993). They mostly regulate their target mRNA through binding to the complementary seed sequence at the 3' UTR. This binding affects the production of corresponding proteins due to the degradation of targeted mRNA or translation repression (Fabian *et al*., 2010; Xu *et al*., 2020).

Activation of immune cells is regulated by hsa-miR-9, hsa-miR-146a and hsa-miR-155. In the response to LPS, these miRNAs have a key role in the regulation of the proinflammatory transcription factor NF-κB and TLR-induced responses, which are crucial in pathogen

recognition (Taganov *et al*., 2006; O'Connell *et al*., 2007; Tsitsiou and Lindsay, 2009). Although miRNAs have recently become a topic of interest also in the fungal field, their role in the context of *Aspergillus* spp. is not well elucidated. Induction of hsa-miR-155 has been reported in myeloid cells infected with *A. fumigatus* (Das Gupta *et al*., 2014; Dix *et al*., 2017). Recently, it has been demonstrated that hsa-miR-146a negatively regulates TNF-α and IL-6 in *A. fumigatus*-infected macrophages (Tong *et al*., 2021). Dysregulation of hsa-miR-132 and hsa-miR-212 following *A. fumigatus* but not LPS exposure has been demonstrated in moDCs (Dix *et al*., 2017). Furthermore, characteristic signatures indicating *A. fumigatus* or aspergillosis have been recently demonstrated *in vitro* and *in vivo* (Chen *et al*., 2019; Dix *et al*., 2017). As studies on miRNAs expression in response to *A. fumigatus* infection are underrepresented, more research is necessary to better understand their role during aspergillosis.

1.2.3 Cytokine signatures

Cytokines including interleukins, chemokines, interferons, and tumour necrosis factors are small proteins, important in mediating immune responses to fungal pathogens. In response to *A. fumigatus*, cytokines are secreted by various immune cells such as epithelial cells, monocytes, alveolar macrophages, and dendritic cells and are crucial in cell-to-cell communication (Cenci *et al.*, 1997; Phadke and Mehrad, 2005).

Abnormal cytokines levels and their potential as biomarkers have been demonstrated in various diseases (Cenci *et al*., 1997; Burska *et al*., 2014; Li *et al*., 2018; Guo *et al*., 2021). Characteristic cytokine profiles have been previously demonstrated also in alloSCT patients suffering from IPA (Gonçalves *et al*., 2017). Up to date, elevated IL-6 and IL-8 have been reported as the most promising cytokines indicating IPA in alloSCT patients and have shown potential for treatment monitoring and outcome prediction (Chai *et al*., 2010; Gonçalves *et al*., 2017; Heldt *et al*., 2018; Thammasit *et al*., 2021). Due to easy detection in biofluids and promising findings, cytokine signatures may be a promising tool to support current diagnostic IPA approaches and monitoring the status of the disease (Heldt *et al*., 2017).

1.3 Aims of the PhD project

As currently used diagnostic assays are lacking sensitivity and specificity, a combination of various assays is used to overcome these difficulties (Lass-Flörl, 2017). The cutting-edge technologies have allowed high-throughput investigation of human immune response to *Aspergillus* spp. infections and highlighted the potential of diagnostic aids based on human immune response (White *et al*., 2018; Bruno *et al*., 2020). These personalized diagnostic and treatment approaches may provide valuable information regarding the onset and progression of IPA as well as response to the treatment (Bruno *et al*., 2020).

The main aim of the present PhD work was to investigate potential molecular candidates and novel risk factors indicating IPA post alloSCT, which might together with established diagnostic assays (e.g., detection of galactomannan) increase the diagnostic accuracy. Combing *in vitro* and *ex vivo* studies along with multilevel analysis, we aimed to identify potential molecular candidates and risk factors promising for further larger, multicentre studies. Briefly, this thesis was aiming to investigate the following three main topics:

I. *In vitro* investigation of human transcriptome profiles in response to *A. fumigatus* infection.

Considering the low incidence of IPA in alloSCT patients, clinical heterogeneity as well as the complexity of IPA and alloSCT, we aimed to investigate transcriptome signatures by RNA-seq using *in vitro* model based on moDCs infected with *A. fumigatus* germ tubes (Ribaud, 2006). Additionally, we aimed to explore the potential to differentiate between *E. coli* and *A. fumigatus*-infected moDCs based on obtained transcriptome profiles. *In vitro* model was therefore used as a pilot study to evaluate the feasibility of transcriptome profiling in particular miRNA and highlight the potential candidates for further follow up in collected patient samples.

II. Investigation of characteristic molecular signatures indicating IPA in patients post alloSCT.

Studies elucidating human immune response during IPA in alloSCT patients are underrepresented. Thus, in the second part of the project, we established a biobank comprising of blood samples collected from patients post alloSCT and conducted a pilot, longitudinal case-control study to characterize the immune response in patients suffering from IPA. Using RNA-seq and immunoassays, we aimed to identify potential molecular candidates indicating IPA in alloSCT patients.

III. Investigation of human risk factors contributing to the risk of invasive pulmonary aspergillosis in patients post alloSCT.

In the last part of the PhD project, we conducted a longitudinal, case-control study to investigate novel risk factors for developing IPA post alloSCT. We aimed to investigate significant associations between the diagnosis of IPA and collected clinical variables from IPA cases and their controls.

2. Methods and materials

2.1 *In vitro* investigation of human transcriptome profiles in response to *A. fumigatus* infection

2.1.1 Microorganisms

2.1.1.1 A. fumigatus

Cultivation and germ tubes generation

A. fumigatus ATCC 44645 strain was cultivated as previously described by Hefter *et al*. (2017). In short, *A. fumigatus* was cultured on malt extract agar plates which were kindly provided by the Institute for Hygiene and Microbiology, University of Würzburg (Würzburg, Germany), for two to three days at 37 °C. Conidia were harvested using endotoxin-free water (Fresenius Kabi, Germany) and filtered through a 40 µm cell strainer (BD Biosciences, USA). Conidia were counted using a hemocytometer (HBG Henneber-Sander, Germany) and stored at 4 °C until further experiments. Germ tubes were generated by inoculating a 25 ml RPMI 1640 medium (Thermo Fisher Scientific, USA) with conidial suspension (2 x10^8 conidia) in a loosely closed 50 ml falcon and incubated at 25 °C, 200 rpm for 10-12 hrs. The development of germ tubes was monitored by light microscopy.

Inactivation with EtOH

To avoid potential fungal overgrowth in the co-culture with immune cells, due to longer incubation time (12 hrs), germ tubes were inactivated with 100 % EtOH. All centrifugation steps during inactivation were performed at room temperature at 5000 x g for 10 min. Briefly, germ tubes were centrifuged, resuspended in 5 ml sterile 100 % EtOH and incubated for 45 min. After three washing steps with sterile endotoxin-free water, germ tubes were passed up to five times through a 20G needle (BD Biosciences, USA) to avoid aggregates in fungal suspension. Germ tubes were counted with Neubauer chamber (HBG Henneber-Sander, Germany), resuspended in serum-free CellGenix GMP dendritic cell medium (CellGenix, USA) supplemented with 120 µg/ml Refobacin (Merck, Germany) and stored at -20 °C. To investigate whether inactivation was successful, RPMI 1640 was inoculated with inactivated germ tubes and incubated overnight at 37 °C. The next day, the potential growth of inactivated germ tubes was investigated by light microscopy.

2.1.1.2 E. coli

Gram-negative bacteria *E. coli* was used as a model organism to investigate potential distinctive host molecular signatures response to fungal and bacterial exposure. With thimerosal inactivated clinical isolate of *E. coli* (BK 1546/3) was kindly provided by the Institute for Hygiene and Microbiology, University of Würzburg.

2.1.2 Cell culture of immune cells

All centrifugation steps were performed at room temperature unless mentioned differently. Cell number and viability were determined by a cell viability analyzer (Beckman Coulter, USA).

2.1.2.1 PBMC isolation

PBMCs were isolated from healthy anonymous blood donors (Institute of Transfusion Medicine and Haemotherapy, University Hospital Würzburg, Germany), by density gradient centrifugation. Blood from leukoreduction system (LRS) chambers was diluted with endotoxin-free HBSS, consisting of Hank's balanced solution (Sigma-Aldrich, USA) supplemented with 2 mM EDTA (Sigma-Aldrich, USA) to a final volume of 50 ml. Diluted blood samples were carefully transferred to a fresh 50 ml falcons with 20 mL of Biocoll separating solution (1.077 g/ml) (Biochrom, Germany) and centrifuged without break for 20 min at 800 x g. After centrifugation, PBMCs were collected into a new 50 ml falcon and washed two times with HBBS followed by centrifugation for 15 min at 120 x g without a break. After the final washing step, PBMCs were centrifuged for 10 min at 300 x g and resuspended in HBSS.

2.1.2.2 Monocyte isolation

Monocytes were purified from PBMCs by CD14 positive magnetic cell sorting following the manufacturer's instructions (Miltenyi Biotec, Germany). All centrifugation steps were performed at 4 °C. Briefly, freshly isolated PBMCs were resuspended in cold HBSS ($1x10^8$ PBMCs per 340 µl HBSS) and incubated with 60 µl of CD14 microbeads (Miltenyi Biotec, Germany) for 15 min at 4 °C in the dark. After incubation, cells were washed with 10 mL of HBSS buffer and centrifuged at 300 x g for 10 min. Meanwhile, LS columns (Miltenyi Biotec, Germany) were placed in the magnetic field of the MACS separator (Miltenyi Biotec, Germany) and washed with 3 mL of HBSS. After centrifugation, the cell pellet was resuspended in 2 mL HBSS and transferred to the LS columns (Miltenyi Biotec, Germany). Columns were washed three times with HBSS and afterwards placed on a 15 mL falcon. To the columns, 5 mL of HBSS was added and the positive fraction was eluted using a plunger supplied with the column,

washed with HBSS and centrifuged at 300 x g for 10 min. Afterwards, monocytes were counted and resuspended in the appropriate medium.

2.1.3 Generation of moDCs and infection with *A. fumigatus* and *E. coli*.

MoDCs were generated as described previously by Paijo *et al.* (2016). Briefly, monocytes at density 10^6 per mL were incubated in 6-well plates at 37 °C and 5 % CO_2 atmosphere in serum-free CellGenix GMP dendritic cell medium supplemented with 120 µg/ml Refobacin, 1000 U/ml GM-CSF (Miltenyi Biotec, Germany) and IL-4 (Miltenyi Biotec, Germany). Cells were used for experiments on day six at a concentration of 10^6 moDCs/mL.

Previously Dix and colleagues (2017) demonstrated a higher number of differentially expressed miRNAs in moDCs after 12 hrs compared to 6 hrs of infections with LPS and *A. fumigatus*. Therefore, we infected moDCs with inactivated *E. coli* (MOI 5) and *A. fumigatus* germ tubes (MOI 1) for 12 hrs at 37 °C and 5 % CO_2 atmosphere in serum-free CellGenix GMP dendritic cell medium supplemented with 120 µg/ml Refobacin.

2.1.4 Transcriptome profiling

2.1.4.1 Total RNA isolation

Cells were harvested by washing wells with 400 µl RNAprotect Cell Reagent (Qiagen, Germany), a stabilization reagent that preserves gene expression profiles by immediate stabilization of RNA molecules. Samples were stored at -80 until RNA extraction. Prior RNA isolation samples were thawed and centrifuged for 5 min at 4 °C and 5000 x g. Total RNA including miRNAs was extracted with a miRNeasy mini kit (Qiagen, Germany) following the manufacturer's protocol. RNA was eluted in 25-30 µl RNase-free water after 1 min centrifugation at 8000 x g. Finally, RNA purity as well concentration were determined by NanoDrop 1000 (Peqlab, Germany) and RNA integrity was investigated by Agilent 2100 Bioanalyzer (Agilent Technologies, Germany) the manufacturer’s instructions. Determined RIN values were between 8.1 and 9.4, indicating the high quality of RNA of all investigated samples.

2.1.4.2 DNase treatment

DNase treatment was performed with TURBO DNA-free™ Kit (Thermo Fisher Scientific, USA), following the manufacturer's protocol for routine DNase treatment. Briefly, RNA samples with a concentration above 200 ng/µl were diluted in a final volume of 40 µl. DNase digestion reagents were mixed and added to extracted RNA as follows: 0.1 volume of 10X

TURBO DNase™ Buffer and 1 µl TURBO DNase™ per RNA sample. Samples were gently mixed and incubated at 37 °C for 20-30 min. After incubation, 0.1 volume of DNase inactivation reagent was added. The samples were incubated at room temperature for 5 min and mixed occasionally (2-3 times). Afterwards, samples were centrifuged at 10.000 x g for 1.5 min and the supernatant was carefully transferred to a new-labelled 1.5 ml tube. DNase treated RNA samples were stored at -80 °C until further analysis.

2.1.4.3 RNA-seq and data processing

Removal of rRNA, library preparation and RNA–sequencing were performed at IMGM Laboratories (Germany) using Illumina next-generation sequencing system based on sequencing by the synthesis method. To obtain mRNA expression profiles, one RNA-seq library was prepared from all the RNA-seq libraries generated using the Illumina TruSeq® A small RNA-seq library was prepared using the NEBNext® small RNA Library Prep Kit for Illumina (New England BioLabs, USA). The quality of generated sequencing libraries for mRNA and miRNA sequencing was determined by 2100 Bioanalyzer using DNA 1000 LabChip kit (mRNA) and High Sensitivity DNA LabChip kits, respectively (Agilent Technologies, USA). All libraries were quantified by fluorescent dye-based Qubit® DNA HS Assay Kit (Invitrogen, USA) using the Qubit instrument (Invitrogen, USA). Next, the sequencing library pool was generated by pooling single libraries with an equal amount of DNA per sample and was quantified by the Qubit system. RNA-seq was performed on the Illumina Next® 500 next-generation sequencing system (Illumina, USA) (75 bp, single-end reads).

Raw reads processing including quality control was kindly performed by Bastian Seelbinder and Dr. Sascha Schäuble in collaboration with Systems Biology and Bioinformatics at Leibniz Institute for Natural Product Research and Infection Biology–Hans Knöll Institut (Jena, Germany). Differential expression was detected as described previously by GEO2RNAseq (mRNAs) and QuickMIRSeq (miRNAs) (Seelbinder *et al.*, 2019; Zhao *et al.*, 2017). Differential expression was considered significant if all used tools (DESeq1, DESeq2, Limma and EdgeR) were reported significant (mRNA: $q < 0.01$ and $\log2FC \geq 2$; miRNA $q < 0.05$ and $\log2FC \geq 1$). For each tool, p-values were adjusted for multiple testing by the false discovery rate (FDR) method. Heatmaps with hierarchical clustering were generated with the ward.D2 clustering method using MRN gene-abundance data with pheatmap (R package version 1.0.12). Raw sequencing files are accessible under the Gene Expression Omnibus accession number GSE174827.

FungiFun2 was used for enrichment analysis of identified DEGs and Venn Diagrams were generated using DeepVenn established by Hulsen *et al*. (2008).

2.1.4.4 Integration of miRNA-mRNAs profiles and investigation of interaction sites

In silico investigation of miRNAs and their targets was performed in collaboration with the Systems Biology and Bioinformatics at Leibniz Institute for Natural Product Research and Infection Biology–Hans Knöll Institut (Jena, Germany). Integration of differentially expressed miRNAs and mRNAs was kindly performed by Bastian Seelbinder, using miRWalk2.0, an archive of experimentally validated miRNA-mRNA interactions (Sticht *et al*., 2018). Investigation of miRNA-mRNA interactions sites was kindly supported by Dr. Patricia Sieber. Interaction sites of hsa-132-3p, hsa-miR-204-5p and hsa-9-5p and their target genes (*ITGB3*, *IL1B*, *TLN2*, *LGR4*, *MAP3K3*, *RAB34*) were investigated using MiRanda, TargetScan and RNA22 as described previously by Oliviera *et al.* (2017).

2.1.4.5 mRNA expression analysis by qPCR

Sequencing results were validated in additional donors by, qPCR. First, RNA was transcribed using First Strand cDNA Synthesis Kit (Thermo Fisher Scientific, USA) according to the manufacturer's protocol in a Thermal Cycler (Eppendorf, Germany). Reagents for the RT-PCR master mix were prepared as shown in Table 1.

Table 1: Master mix reagents used for RT-PCR.

master mix	volume (µl)
5x Reaction Buffer	4
Ramdom hexamer primer (10 µM)	1
RiboLock Rnase Inhibitor (20 U/µl)	1
10 mM dNTP Mix	2
M-MuLV Reverse Transkriptase (20 U/µl)	2

RT-PCR was performed in 0.2 ml PCR reaction tubes (Biozym, Germany) using 250-500 ng of RNA diluted with nuclease-free water. Reaction tubes containing 10 µL of diluted RNA and 10 µL of the master mix were incubated for 5 min at 25 °C, followed by 60 min at 37 °C and5 min at 70 °C. Samples were stored at 4 °C if used immediately or at -20 °C until later qPCR investigation.

QPCR was performed using iTaq™ Universal SYBR® Green Supermix (Bio-Rad Laboratories, USA) and StepOnePlus™ system (Applied Biosystems, USA). Per reaction,

10 µL of iTaq USGS 2x, 1 µL of each, forward and reverse primer and 4 µL of water were added to a 1.5 ml Eppendorf tube and gently mixed. To designated wells in a 96-well plate (MicroAmp™ Fast Optical 96-Well Reaction Plate; Applied Biosystems, USA), 16 µL of the master mix and 4 µL of diluted cDNA (2.5 ng/ µL) were added. Next, the reaction plate was sealed with an optical adhesive strip (Sarstedt, Germany), briefly centrifuged and cycling was performed as shown in Table 2. In short, the hot-start activation step at 95 °C of 30 sec, was followed by amplification for 40 cycles under the following conditions: 15 sec at 95 °C (denaturation) and 60 sec at 60 °C (annealing/extension). Melting curve analysis started at 95°C for 15 min and ranged from 60°C to 95°C with a 0.5°C increase.

Table 2: Cycling protocol for mRNA expression investigation using iTaq™ SYBR Green system.

activation step:	**30 sec at 95 °C**
cycling:	40 cycles
denaturation	15 sec at 95 °C
annealing/extension	60 sec at 60-62 °C
melting curve:	15 sec at 95 °C
	6 0sec at 60 °C + 0.5 °C
	15 sec at 95 °C

Investigated samples and negative controls were run in at least duplicates. Raw data were analysed with StepOnePlus™ Software (version 2.3) (Applied Biosystems, USA) and expression levels (Log2FC) were calculated by the ΔΔCT method as described previously by Schmittgen and Livak, (2008). NormFinder was used to identify the most appropriate references genes for our experimental conditions (Andersen *et al.*, 2004). The combination of *ALAS* and *EIF2B2* gave the best stability value among tested candidates.

2.1.4.6 miRNA expression analysis by qPCR

The expression of selected miRNAs, identified by sequencing, was validated using the miScript PCR system (Qiagen, Germany), which enables the detection of multiple miRNAs from a single cDNA preparation. Reagents were thawed at room temperature, mixed by flicking the tubes, briefly centrifuged and during the experiments stored on ice.

Total RNA including miRNAs was used as starting material. Polyadenylation and reverse transcription for miRNA expression analysis was performed using the miScript Reverse Transcription kit (Qiagen, Germany) following the manufacturer's protocol.

Table 3: MiScript master mix reagents used for reverse transcription.

component	volume (µl)
5x miScript HiFlex/HiSpec Buffer	4
10x miScript Nucleic Mix	2
miScript Reverse Transcription Mix	2

RNA (100-500 ng) was diluted in nuclease-free water in a final volume of 12 µl. The reverse transcription master mix was prepared according to Table 3, gently mixed and transferred (8 µl) to the diluted RNA. Reverse transcription was performed in 0.2 µl reaction tubes using a Thermal Cycler as follows: 60 min to 37 °C and 5 min at 95 °C to inactivate miScript reverse transcriptase. QPCR was performed in the StepOnePlus™ system using miScript SYBR® Green PCR Kit (Qiagen, Germany) following the manufacturer's protocol. Reagents used in the qPCR reaction are shown in Table 4.

Table 4: MiScript SYBR Green reagents used for quantification of miRNA expression.

component	volume (µL)
2xQuantiTect SYBR Green PCR mmx	12,5
10x miScript Universal Primer	2,5
10x miRNA primer (FW)	1,25
water	6,25

QPCR reaction consisted of 22.5 µl master mix and 2.5 µl diluted cDNA (5 ng/ µL). PCR reaction started with activation of HotStarTaq DNA Polymerase, which is included in 2x QuantiTect SYBR Green PCR Master Mix (15 min at 95 °C). Thermal cycling conditions are shown in Table 5.

Table 5: Cycling protocol for miRNA expression investigation using miScript.

activation step	**15min at 95 °C**
3-step cycling:	45 cycles
denaturation	1 min at 94 °C
annealing	30 sec at 58 °C
extension	1 min at 72 °C
final extension	10 min at 72 °C

Expression levels of selected miRNAs were calculated by the ΔΔCT method as described previously (Schmittgen and Livak, 2008). Reference for the raw data normalization and gene expression analysis was selected according to the miRNA-sequencing results, which

demonstrated hsa-let7g-5p as miRNA with the most stable expression levels across investigated samples.

2.1.4.7 Primers

If not stated differently, primers were designed using the NCBI online tool Primer-BLAST. Primers ordered as desalted and lyophilized oligonucleotides (Sigma-Aldrich, USA) were diluted in nuclease-free water to a stock concentration of 100 μM and stored at −20 °C until further experiments. Primers were optimized by investigating appropriate concentration and annealing temperature (Ta) as described previously by Veselenak *et al.* (2015). A negative template control (NTC) was included to investigate whether primer pairs formed primer dimers. The quality of designed primers and specificity was evaluated by melting curve investigation and with agarose gel electrophoresis. Primer pairs used in the study, their concentration and annealing temperature used in the qPCR reaction are shown in Table 6.

The efficiency of used primers was in the range of 90-105% and it was determined by performing 4-5 series of 10-fold cDNA dilutions. Data analysis and calculation of efficiency were performed using StepOnePlus™ Software (version 2.3).

Table 6: Primers used for validation of RNA-seq results by qPCR.

gene/miRNA	direction	primer sequence	concentration (nM)	design
IL1B	fw	GGACAAGCTGAGGAAGATGC	500	Primer- BLAST
	rv	TCGTTATCCCATGTGTCGAA	500	
EIF2B2	fw	TCCACCCCACTCATCGTCTG	400	Maeß *et al.*, 2010
	rv	TGGCAGGACTTCTTCAGGAGC	200	
ITGB3	fw	CTCCGGCCAGATGATTC	500	KiCqStart
	rev	TCCTTCATGGAGTAAGACAG	500	(Sigma-Aldrich)
MAP3K3	fw	AGAGTCTCGGAGGATGTTGGCT	400	Primer- BLAST
	rv	CCAGTTGAAGGCTTACGGTGCT	200	
RAB34	fw	ATGCGCTGATGGAGAAAGACGC	100	Primer- BLAST
	rv	CTCGGACATTCTCACCAGTGAG	400	
TLN2	fw	CGGATGAGTGTGTGCAGAGT	100	Primer- BLAST
	rv	AGCCTCGTGTTTTGTGGGAT	100	
LGR4	fw	ACTCAGTTGCCAGAAGATGC	100	Primer- BLAST
	rv	CTCGAATGGCTTCACTGGGT	200	
ALAS	fw	GGCAGCACAGATGAATCAGA	500	Czakai, 2015
	rv	CCTCCATCGGTTTTCACACT	500	
hsa-miR-9-5p	fw	TCTTTGGTTATCTAGCTGTATGAA	500	Yoon *et al*., 2017
hsa-miR-132-3p	fw	TAACAGTCCACAGCCATGGT	500	Yoon *et al*., 2017
hsa-let-7g-5p	fw	TGAGGTAGTAGTTTGTACAGTTGC	500	Yoon *et al*., 2017
hsa-miR-204-5p	fw	miScript Primer Assays	500	miScript (Qiagen)

Due to the universal reverse primer provided with the miScript kit, only forward primers were designed for miRNA expression analysis (Table 6). Forward primers for selected miRNAs were designed as described by Yoon *et al*., using the Primer3 tool (available at *https://primer3.ut.ee/*) or ordered as predesigned miScript Primer Assays (Qiagen, Germany). All miRNA primers were validated and optimized as described above. The expected product length after amplification mentioned in the miScript protocol is 85-87 bp and Tm around 75 °C.

2.1.4.8 Agarose gel electrophoresis

The specificity of primers and the appropriate length of PCR products were investigated by 2-3 % (w/v) agarose (Roth, Germany) gel electrophoresis. For the gel preparation, 1 x TAE buffer diluted from UltraPure ™ 10x TAE buffer (Invitrogen, USA) was used. Two microliters of SERVA DNA Stain G (SERVA Electrophoresis, Germany) per 50 mL 1XTAE buffer were used to visualize the products under UV light. Quick-Load® Purple 100 bp DNA Ladder (New England Biolabs, USA) was used as a molecular weight marker according to the manufacturer's protocol. Samples were mixed with Gel Loading Dye, Purple (6X) (New England Biolabs, USA) following the manufacturer's recommendations. The electrophoresis was performed at 5-10 V/cm (product size smaller than 1kb) for 40-50 min. Gels were imaged using an AlphaImager™ Light Cabinet. (Biozym, Germany).

2.1.5 Protein quantification

2.1.5.1 IL-1β quantification

Levels of IL-1β in cell supernatants were determined by ELISA MAX™ Deluxe Set Human IL-1β kit (BioLegend, USA) following the manufacturer's protocol. Prior to the experiments, all reagents were calibrated to room temperature and prepared according to the manufacturer's protocol. Following reagents were not included in the kit: 10 x PBS (Thermo Fisher Scientific, USA), wash buffer (1xPBS + 0.05 % Tween; Sigma-Aldrich, USA) and stop solution (0.5 M H_2SO_4). Cell supernatants were thawed and kept on ice. A pilot run was performed to define appropriate sample dilution (10x) for later experiments. The colourimetric reaction was monitored for each experiment and stopped within 15 min after the addition of substrate solution by adding 100 µl of stop solution. Absorbance was measured at 450 nm and 570 nm with a microplate reader (Tecan, Infinite® 200 PRO, Switzerland) according to the manufacturer's protocol. Generation of the standard curve and data analysis were performed using GraphPad PRISM version 6.0.

2.1.6 Statistics

If not stated differently, data represent the means + SD of at least 3 independent experiments with moDCs generated from different healthy volunteers, each performed in duplicates. Significant differences were investigated by Mann – Whitney and Kruskal-Wallis with Dunn's based test for multiple test correction. Statistical significances between investigated groups are indicated by asterisks: *, 0.05; **, 0.01; ***, 0.001; ****, 0.0001.

All statistical analyses were performed in the statistical environment R (version 3.3) and/or GraphPad PRISM version 6.0.

2.2 Investigation of characteristic molecular signatures indicating IPA in patients post alloSCT

2.2.1 Investigated patient cohorts

The main investigated patient cohort in the present longitudinal, case-control study comprised of patients post alloSCT, recruited at the University Hospital of Würzburg, between March 2017 and December 2019. From these patients, we retrospectively collected blood samples after alloSCT (see chapter 2.2.2). All investigated alloSCT patients were categorized as cases and controls according to the EORTC/MSGERC criteria (Donnelly *et al.*, 2020). Considering the

criteria mentioned above, age of patients (> 20), the number of collected time points and a sufficient amount of RNA, we identified three probable IPA cases appropriate for profiling (Table 7). All three patients were neutropenic and had positive radiology (CT scan) and mycology (positive galactomannan ELISA and or *Aspergillus* DNA PCR in serum or BAL). Control patients did not show any signs of *Aspergillus* spp. infection and were matched to cases according to the underlying disease (acute myeloid leukaemia, AML), sex and similar age and collected time points post alloSCT (Table 7).

Table 7: Clinical characteristics of main investigated probable IPA cases and their matched controls, obtained from University Hospital of Würzburg (Würzburg cohort). Taken from Zoran *et al*., 2022. Nr, number of samples; M, male; F, female; VRC, voriconazole; PSC, Posaconazole; FLC, fluconazole; NT, no treatment.

patient	status	age	sex	antifungal treatment	prophylaxis	GvHD (grade)	nr. of Samples
P15	case	63	M	VRC	PSC, FLC	pulmonary (III)	11
P53	control	59	M	NT	FLC	no GvHD	9
P43	case	60	F	VRC, PSC	FLC	skin (III), intestinal (IV)	18
P18	control	51	F	NT	PSC	no GvHD	12
P55	case	62	M	Ambisome	PSC	skin (NA)	9
P63	control	55	M	NT	FLC	skin (III) and intestinal (I)	7

As selected three IPA cases (Würzburg cohort) developed IPA at different time post alloSCT, we established relative time to avoid consequent bias. Day 0 presented detected galactomannan or *Aspergillus* DNA in the serum or BAL along with positive radiology (CT scan). Overall, we profiled 66 samples of selected probable IPA cases and their matched controls, by RNA-seq and immunoassays (for a detailed analysis, see chapters 2.2.3–2.2.4). Additionally, we investigated gene expression and protein levels of selected candidates in three alloSCT patients suffering from severe GvHD (grade ≥ 2) (Suppl. Table S1). From these patients, we selected four consecutive time points per patient at the time of GvHD diagnosis.

In addition to the original Würzburg cohort we investigated protein levels (see chapter 2.2.4.) of molecular candidates in additional patient cohorts obtained from Public Health Wales, Microbiology Cardiff (Wales, United Kingdom): Cardiff I and Cardiff II cohort. Cardiff I cohort consisted of additional alloSCT patients categorized as probable IPA (N=6), possible IPA cases (N=5) and controls (N=6). The most common underlying disease among these patients was AML (N=12). Controls were matched to cases according to the same sex and similar age. Overall, we investigated 5-6 consecutive serum samples per patient after IPA diagnosis (Donnelly *et al*., 2020). Cardiff II cohort consisted of 20 CAPA cases and 45 COVID-

19 control patients. For each patient, we analysed one time point, overall, 65 serum samples. Clinical information of additional investigated patients is shown in Suppl. Table S1 and S2.

2.2.2 Sample collection and processing

Blood samples from patients (Würzburg cohort) were collected post alloSCT twice-weekly (whenever feasible) until day 100 post alloSCT. If a patient was readmitted to the hospital, the collection started again. Approximately 3 ml of blood was collected into Tempus Blood RNA Tube (Thermo Fisher Scientific, USA), a preservation tube that allows immediate RNA stabilization, crucial for gene expression investigation. Immediately after blood drawing, Tempus tubes were thoroughly mixed for at least 10 sec. Serum samples were collected into 9 ml SARSTEDT Monovette ® tubes (Sarstedt, Germany) and centrifuged for 10 min at 3000 x g. Tempus tubes and aliquoted serum samples were stored at -20 °C until profiling.

2.2.3 Whole blood transcriptome investigation

2.2.3.1 RNA isolation from whole blood

RNA from whole blood, collected in Tempus Blood RNA tubes, was isolated with a Tempus Spin RNA isolation kit (Thermo Fisher Scientific, USA), according to the manufacturer's instructions.

Before purification, stabilized blood was processed according to manufacturer protocol. In short, after thawing at room temperature samples were diluted with 1 x PBS in a falcon to a final volume of 12 ml. Diluted samples were vigorously vortexed for at least 30 seconds and centrifuged at 4 °C for 30 min at 3000 x g. After centrifugation, the supernatant was carefully discarded and falcons were inverted on absorbent paper for 2 min. The remaining drops were removed with a sterile cotton swab and 400 µl of RNA Purification Resuspension Solution was added. Samples were briefly vortexed and afterwards kept on ice until purification on filtration membranes.

The purification run was performed according to the manufacturer's protocol. Briefly, purification filters were pre-wetted with 100 µl RNA Purification Wash Solution 1. Resuspended RNA was transferred to a purification filter and centrifuged at 16.000 x g for 30 seconds. Flow-through was discarded and washing steps were performed. First with 500 µl RNA Purification Wash Solution 1 and afterwards two times with 500 µl RNA Purification Wash Solution 2. After the washing steps, the membranes were dried by centrifugation at 16.000 x g. Purification filters were transferred to new labelled collection tubes and 100 µl

Nucleic Acid Purification Elution Solution was added. After 2 min of incubation at 70 °C, samples were centrifuged at 16.000 x g for 30 seconds. RNA eluates were transferred back to the purification filters and centrifuged for 2 min at 16.00 x g. Approximately 80-90 µl of RNA eluate was transferred to a new labelled tube and RNA was stored at -80 °C until further experiments. The concentration and purity of isolated RNA were determined with NanoDrop ND-1000 and RNA integrity was evaluated by Agilent 2100 Bioanalyzer. Determined RIN values of investigated samples were in the range of 7.6-9.9.

2.2.3.2 DNase treatment

DNase treatment was performed using TURBO DNA-free™ Kit as previously described in chapter 2.1.4.2 DNase treatment. After the DNase treatment RNA samples were stored at -80 °C until further analysis

2.2.3.3 RNA-seq and data processing

Whole blood RNA-seq was performed at IMGM Laboratories (Germany) on the Illumina NextSeq® 500 next-generation sequencing system with 1 x 75 bp single-read chemistry. Previous studies have reported that RNA isolated from whole blood contains high levels of haemoglobin RNA, therefore depletion for library preparation together with bioinformatic removal of globin gene counts is recommended for reproducible RNA measurement in the blood transcriptome (Harrington *et al.*, 2020). For this purpose, RNA-seq libraries were prepared with the Illumina TruSeq® Stranded mRNA kit including Ribo-Zero Globin technology, which allows depletion of globin mRNA as well as cytoplasmic and mitochondrial rRNA.

RNA-seq data processing and identification of DEGs was performed by Dr. Sascha Schäuble in collaboration with Systems Biology and Bioinformatics at Leibniz Institute for Natural Product Research and Infection Biology–Hans Knöll Institut (Jena, Germany) according to Seelbinder *et al.* (2019) using GEO2RNAseq pipeline (v0.100.1) in R version 3.5.1. Briefly, RNA-seq reads were mapped to the reference genome GRCH 38 v109 and normalized as described previously by Anders and Huber (2010), using median-by-ration normalization (MRN). Raw files are available under GSE174827. To identify DEGs we used all profiled samples obtained from selected three IPA cases and compared them to all collected samples of control patients, without IPA. Significant DEGs were identified by DESeq2 (v.1.18.1) and EdgeR (v.3.20.7), using the false discovery rate method (q=FDR(p)). DEGs were considered significant if they were reported by both used tools ($q < 0.05$ and Log2 MRN$\geq$0.8). Heatmap

and hierarchical clustering were generated using pheatmap (R package version 1.0.12) and MRN data. Enrichment analysis was performed by FungiFun2.

2.2.3.4 Validation of RNA-seq by qPCR

RNA was transcribed using First Strand cDNA Synthesis Kit according to the manufacturer's instructions (previously described in chapter 2.1.4.2). Gene expression of selected biomarker candidates was further evaluated using TaqMan Assays® (Thermo Fisher Scientific, USA) according to the manufacturer protocol. PCR reaction mix was prepared as shown in Table 8.

Table 8:TaqMan reagents used in master mix preparation.

component	volume (µl)
TaqMan (R) Fast Advanced Master Mix (2x)	10
TaqMan assay (20x)	1
nuclease-free water	7

TaqMan Assays used in experiments were designed to span exons and were fluorescently labelled with FAM (6-Carboxyfluorescein) (Table 9). The amplification efficiency of TaqMan assays was investigated by performing five series of 10-fold cDNA dilutions and determined using StepOnePlusTM Software (version 2.3). All TaqMan assays exhibited amplification efficiency of 1.960-2.059 (92 %-102) %.

Table 9: TaqMan assays used in the case-control study investigating gene expression of potential molecular candidates indicating IPA in investigated alloSCT patients.

probe	assay ID	amplicon length
LGALS2	Hs00197810_m1	73
MMP1	Hs00899658_m1	64
MMP9	Hs00957562_m1	67
ITGB3	Hs01001469_m1	59
SRSF4	Hs00900675_m1	73
TAOK3	Hs00937694_m1	61

PCR reaction mix was mixed by flicking the tube, shortly centrifuged and 18 µl was transferred to the appropriate well of a 96 well optical reaction plate. To assigned wells, 2 µl of cDNA template (10 ng) or nuclease-free water (negative control) was added. The reaction plate was sealed with an optical adhesive film and briefly centrifuged. PCR reaction conditions are shown in Table 10.

Table 10: PCR reaction conditions using TaqMan chemistry.

PCR program	T (°C)	time
hold		
UNG incubation	50	2 min
polymerase activation	95	2 min
cycling (40x)		
denaturation	95	1 sec
anneal/extend	60	20 sec

PCR reaction started with 2 min at 50 °C, to activate Uracil-DNA glycosylase (UNG), which prevents carryover contamination and 2 min at 95 °C to activate DNA-polymerase. The activation step was followed by amplification for 40 cycles under the following condition: denaturation at 95 °C for 1 sec and annealing/extension at 60 °C for 20 sec.

All samples were measured in at least duplicates and gene expression levels were determined using the ΔΔCq method as previously described by Schmitgen and Livak (2008).

2.2.3.5 Selection of reference genes

In this longitudinal study integrated approach described previously by Sundaram and colleagues (2019) was used to identify the best candidates for reference genes. This approach is based on a combination of the CV analysis, NormFinder as well as a visual representation of mRNA fold changes. Reference genes were first investigated in obtained RNA-seq datasets of three profiled IPA cases and three control patients and later tested by qPCR. Top reference candidates were considered as genes with the lowest CV value and were visualized (Log2FC to first investigated time-point) as well as evaluated further by qPCR and NormFinder. Due to the limited RNA amount isolated from the collected whole blood of three profiled IPA cases and three controls, four time points per patient were investigated by qPCR. A combination of *TAOK3* and *SRSF4* showed the best results among investigated candidates (low CV, expression stability across tested time points) and was used as a reference.

2.2.3.6 Analysis of publicly available gene expression datasets

To support our findings, we further investigated publicly available gene expression datasets obtained from six *in vitro* studies characterizing host transcriptome response in different immune cells following *A. fumigatus* exposure (Cortez *et al*., 2006; GSE60729, GSE69723, GSE174827, GSE134344, GSE177040). Gene expression datasets were selected according to the identified number of DEGs (at least 1000) and experimental design (myeloid cells infected

with *A. fumigatus*). Altogether we analysed seven gene expression datasets obtained by microarrays (Cortez *et al*., 2006; GSE60729, GSE69723) or RNA-seq (GSE174827, GSE134344, GSE177040). Datasets were obtained either from supplementary files (Cortez *et al*., 2006) or Gene Expression Omnibus. DEGs from RNA-seq datasets were computed as described previously using the GEO2RNA pipeline (Seelbinder *et al*., 2019) or in the case of microarrays, GEO2R (Barrett *et al*., 2013).

2.2.4 Protein quantification in serum

Protein levels of selected molecular candidates were quantified by singleplex and multiplex immunoassays according to the manufacturer protocol (Table 11). Multiplex immunoassays (ProcartaPlex custom panel, Thermo Fisher Scientific, USA) were kindly performed by Antje Häder in collaboration with Fungal Septomics at Leibniz Institute for Natural Product Research and Infection Biology–Hans Knöll Institut (Jena, Germany). All reagents were prepared fresh on the day of the experiment and calibrated to room temperature before use. Multiplex assays were performed using undiluted patient sera. Before each singleplex ELISA experiment, a pilot run was performed to determine the appropriate dilution for the tested analytes (Table 11). Serum samples were diluted in the case of MMP9 (200x) and galectin-2 ELISA (50x). COVID-19 patient sera (Cardiff II) were diluted for caspase-3 (10x) and IL-8 ELISA (10x). Levels of MMP1, IL-8 and caspase-3 were additionally investigated *in vitro* and the sera of the additional patient cohort (Cardiff I and Cardiff II). Cell supernatants harvested from *A. fumigatus* and *E. coli*-infected moDCs were diluted 10x for MMP1 and IL-8 ELISA. Uninfected moDCs were investigated undiluted. Absorbance was measured with a microplate reader (Tecan, Infinite® 200 PRO, Germany) according to the manufacturer's protocol.

Table 11: Investigated molecular candidates on the protein level. Protein levels were quantified in sera of alloSCT patients obtained from the Cardiff I cohort (Ca I), Würzburg (Wü) cohort and COVID-19 cohort, Cardiff II cohort (Ca II). Additionally, protein levels were quantified in cell supernatants of moDCs infected either by *A. fumigatus* or *E. coli (in vitro).*

analyte	assay	manufacturer	investigated group
caspase-3	multiplex	Thermo Fisher Scientific, USA	Ca I, Wü
CD40	multiplex	Thermo Fisher Scientific, USA	Ca I, Wü
IL-8	multiplex	Thermo Fisher Scientific, USA	Ca I, Wü
MMP-1	multiplex	Thermo Fisher Scientific, USA	Ca I, Wü
PAI-1 (serpin)	multiplex	Thermo Fisher Scientific, USA	Ca I, Wü
VEGF-A	multiplex	Thermo Fisher Scientific, USA	Ca I, Wü
galectin-2	singleplex	Abbexa, UK	Ca I, Wü
ITGB3	singleplex	Abbexa, UK	Ca I, Wü
MMP9	singleplex	BioLegend, USA	Ca I, Wü
MMP-1	singleplex	Thermo Fisher Scientific, USA	Ca II, *in vitro*
IL-8	singleplex	BioLegend, USA	Ca II, *in vitro*
caspase-3	singleplex	Thermo Fisher Scientific, USA	Ca II, *in vitro*

2.2.5 Statistics

Data were analysed using GraphPad PRISM version 6.0 and/or *R*, version 3.5.1. Significant differences between investigated groups were investigated by Mann–Whitney test if not stated otherwise. Statistical significances are indicated by asterisks: *, 0.05; **, 0.01; ***, 0.001; ****, 0.0001.

Generated datasets of profiled alloSCT patients obtained from the Würzburg cohort were balanced to avoid bias due to sampling and time points. We selected four time points per investigated patient in the early onset of IPA (first five weeks after IPA onset, n=24) (Suppl. Table S3). In addition, we analysed all samples, collected up to 56 days after IPA onset (n=66).

2.2.6 Ethics approval

Ethical approval for the present study was obtained from the Ethics Committee of the University Hospital of Würzburg, Germany (#173/11 and #225/12). Before the study, written informed consent was obtained from all patients. Investigated serum samples from Public Health Wales, Microbiology Cardiff, UK were surplus clinical samples, which were analysed retrospectively and anonymously, therefore according to the NHS Health Research Authority decision, the ethical review was not required.

2.3 Investigation of human risk factors contributing to the risk of invasive pulmonary aspergillosis in patients post alloSCT

2.3.1 Selection of patients and collection of clinical variables

In the present case-control study, we included additional patient cohorts (training and validation cohort) previously recruited in the frame of ASPIRE study (Aspergillosis – Individual Risk Estimation). All patients were recruited between 2008 and 2013, suffered from haematological malignancies and underwent alloSCT at the University Hospital of Würzburg. Patients were categorized as probable IPA cases and controls according to that time actual EORTC/MSG criteria (De Pauw *et al*., 2008). Investigated patient cohorts were balanced according to sex, age and underlying disease as best as possible. The training cohort consisted of 36 probable IPA cases and 36 matched controls (without *Aspergillus* infection) (Table 12). IPA was diagnosed on average 105 days after alloSCT.

Clinical variables significantly associated with IPA diagnosis in the training cohort were evaluated further in an additional patient cohort, consisting of 23 IPA cases and 25 controls suffering from haematological malignancies, receiving alloSCT between 2007 and 2015. The main underlying disease was acute myeloid leukaemia (AML, n=28), followed by multiple myeloma (MM, n=5). The average age of the patients was 56 years (range: 26–72 years) and the average time of IPA diagnosis after alloSCT was 101 days. In the case of the validation cohort, only the clinical variables significantly associated with IPA diagnosis were collected. Set of clinical variables consisted of static (n=96) and dynamic variables (n=7). Static variables were collected twice weekly, whenever feasible (Suppl. Table S4). Dynamic variables (blood counts) were collected weekly, four weeks prior to the diagnosis of IPA.

Table 12: Clinical characteristics of investigated IPA cases (IPA cases) and their matched controls (controls). The table is modified after Zoran *et al*., 2019.

	controls	IPA Cases	all patients
total number	36	36	72
age (median, range)	54 (21-72)	56 (20-69)	55 (20-72)
male	24	23	47
female	12	13	25
underlying disease			
acute myeloid leukaemia	7	13	20
myelodysplastic syndrome	4	4	8
acute lymphoblastic leukaemia	2	5	7
chronic lymphocytic leukaemia	2	3	5
multiple myeloma	11	4	15
other diseases	10	7	17
donor source			
matched unrelated donor	26	21	47
matched related donor	10	15	25
mould-active therapy	17	30	47
voriconazole	10	17	27
posaconazole	8	13	21
caspofungin	6	7	13
anidulafungin	4	2	6
mmphotericin B	3	8	11
fluconazole	34	29	63

2.3.2 *In vitro* study: Effects of etanercept on the immune response to *A. fumigatus* infection

2.3.2.1 Generation of monocyte-derived macrophages

PBMCs and monocytes were isolated as described previously (see chapters 2.1.2.1 and 2.1.2.2) with exception of added 1 % FCS (Sigma-Aldrich, USA) in HBBS solution. Monocytes were differentiated into monocyte-derived macrophages (MDM) in 24 well plates (Sarstedt, Germany) at a density 10^6 / mL in RPMI-1640 supplemented with 120 µg/ml Refobacin, 10 % heat-inactivated FCS, and 25 ng/ml GM-CSF (Sanofi-Aventis, France) at 37 °C and 5 % CO_2 atmosphere. The medium was changed every second to the third day and MDM were used for further experiments on day six.

2.3.2.2 Co-cultures with A. fumigatus and etanercept

Live germ tubes were prepared as described previously (see chapter 2.1.1.1) and used for infection at MOI 0.5. The potential effects of etanercept (Enbrel®, Pfizer, Germany) on gene expression and cytokine response of infected MDM, were investigated at a concentration of 2 µg/ml, which is comparable to the concentration in plasma of arthritic patients (Keystone *et al*., 2004; Obeng *et al*., 2016). Co-cultures with *A. fumigatus* in the presence or absence of etanercept were performed in 12-well plates at a density of 10^6 MDM / ml in RPMI1640 supplemented with 10 % heat-inactivated FCS and 120 µg/ml Refobacin. MDM were challenged with etanercept and *A. fumigatus* for 6 hours at 37°C and 5 % CO_2 atmosphere.

2.3.2.3 RNA isolation

MDM were harvested and resuspended in 400 µl of RNAprotect Cell Reagent and stored at -20 °C or used immediately. RNA was isolated using RNeasy mini kit (Qiagen, Germany) according to the manufacturer's protocol. RNeasy mini kit allows the purification of RNA longer than 200 nucleotides. RNA was eluted in 20-30 µl of RNase-free water and the RNA purity and concentration were determined with NanoDrop 1000. Samples were frozen for a short term at -80 °C.

2.3.2.4 RNA- seq and data processing

Before the sequencing, the integrity of RNA was investigated with Agilent 2100 BioAnalyzer. Determined RIN values of investigated samples were above 8.5. Removal of rRNA, library preparation and RNA–seq were performed at IMGM Laboratories (Munich, Germany). RNA-seq library pool was prepared from the RNA-seq libraries generated with the Illumina TruSeq® Stranded mRNA HT technology. RNA-seq was performed on the Illumina Next® 500 next-generation sequencing system (75 bp, single-end reads).

Generated raw reads were kindly processed by Dr. Jörg Linde, in collaboration with Leibniz Institute for Natural Product Research and Infection Biology–Hans Knöll Institut, as previously described by Bolger *et al.* (2014) and deposited at Gene Expression Omnibus (GSE113254). Trimmed reads were mapped to the human reference genome (GRCh38) as described by Kim and colleagues (2014). Raw counts were normalized using RPKM values and were identified by DESeq with a log2FC cut-off of at least 0.5 and an adjusted p-value of ≤ 0.05. Gene regulatory network consisting of BCL3 (ENSG00000069399), BIRC3 (ENSG00000023445), CXCL10 (ENSG00000169245), ICAM1 (ENSG00000090339), NFKB1

(ENSG00000109320), and RELB (ENSG00000104856) was kindly generated by Dr. Michael Weber, using Pathway Studio V9.

2.3.2.5 Protein quantification

Protein levels in cell supernatants were determined by multiplex immunoassays, which were kindly performed by Dr. Kerstin Hünniger in collaboration with Fungal Septomics, Leibniz Institute for Natural Product Research and Infection Biology–Hans Knöll Institut (Jena, Germany). Cytokine profiles were investigated using Bio-Plex Pro Human Cytokine 27-plex Assay (Bio-Rad, Germany), according to the manufacturer protocol. Serum levels of CXCL10 in 80 samples of probable IPA cases (N=8), were determined by Human CXCL10 (IP-10) ELISA MAX™ Deluxe Set (BioLegend, USA) following manufacturer protocol.

2.3.2.6 Statistics and modeling

Univariate logistic regression models were employed to identify associations between collected clinical variables and diagnosis of IA in probable IPA cases and their matched controls as described previously (Zoran *et al*., 2019). Significant differences were tested with the likelihood-ratio test (LRT, $p \leq 0.05$). Differences in cytokines levels among investigated groups were detected using Wilcoxon-Mann-Whitney tests applying a p-value ≤ 0.05.

Logistic regression modelling and statistical analysis were kindly performed by Dr. Michael Weber in collaboration with Leibniz Institute for Natural Product Research and Infection Biology–Hans Knöll Institut (Jena, Germany).

2.3.3 Ethics approval

As requested by the Ethics Committee of the University Hospital of Würzburg, Germany (#173/11), informed consent has been obtained for study participation and publication.

3. Results

3.1 *In vitro* investigation of human transcriptome profiles in response to *A. fumigatus* infection

In response to *A. fumigatus* infection, increased levels of transcripts from genes linked to inflammatory processes (e.g., cytokine and TLR signalling, phagocytosis) have been demonstrated in various experimental models (Cortez *et al*., 2006; Bruno *et al*., 2020). Although in the last decade host transcriptome has been commonly studied, there is limited information available on non-coding RNAs in the context of *Aspergillus* spp. infections (Croston *et al*., 2018). MiRNAs, small non-coding RNAs, are post-transcriptional regulators of gene expression and their potential as host biomarkers have been studied in multiple research fields (Lee *et al*., 1993; Moldovan *et al.*, 2014). Few authors have reported dysregulation of hsa-miR-132 upon *A. fumigatus* infection in myeloid cells and suggested hsa-miR-132 is a relevant regulator of the immune response against *A. fumigatus* (Das Gupta *et al.*, 2014; Dix *et al.*, 2017). Several studies highlighted the potential of host transcriptome biomarkers as promising diagnostic aids in the diagnosis of respiratory infections, hence continuous research in this field is encouraged (Zaas *et al*., 2009; Ashkenazi-Hoffnung *et al*., 2018).

3.1.1 Study design and workflow

The incidence of IPA among alloSCT patients is relatively low which presents a challenge for studies characterizing host transcriptome during IPA and biomarker research due to the limited number of recruited patients and investigated samples (Ribaud, 2006). In this chapter, we characterized the host transcriptome response to *A. fumigatus* infection by a standardized *in vitro* approach using moDCs. We explored genes and miRNAs signatures indicating *A. fumigatus* infection, promising for further evaluation in collected blood samples of alloSCT patients (see chapter 3.2). Additionally, we investigated the potential to discriminate between fungal (*A. fumigatus*) and bacterial (*E. coli*) infection based on obtained transcriptome profiles and evaluated the feasibility of miRNA investigation in the context of host biomarkers for *A. fumigatus* infection (Figure 3).

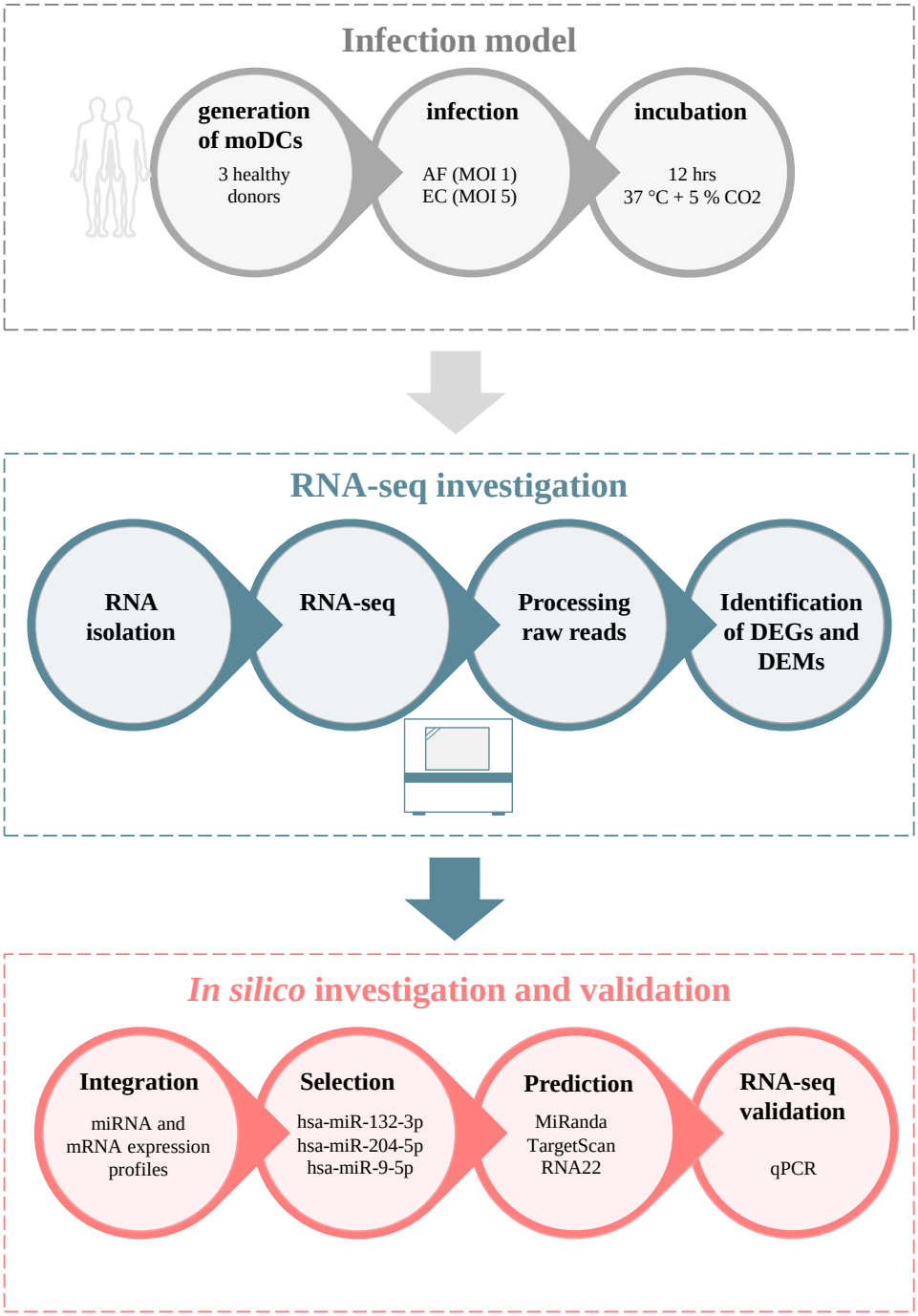

Figure 3: Workflow and study design of *in vitro* study characterizing host transcriptome response to *A. fumigatus*. MoDCs were generated from monocytes isolated from three healthy donors and infected on day six with inactivated *A. fumigatus* (AF) germ tubes or *E. coli* (EC) and incubated for 12 hours. Transcriptome profiles were investigated by RNA-seq. After processing raw reads and identification of DEGs and DEMs, we investigated potential characteristic signatures for each type of infection. We focused on *A. fumigatus* specific host transcriptome signatures, integrated miRNA-mRNA expression profiles and validated selected DEMs and their predicted target genes in additional donors by an independent method, qPCR.

3.1.2 Gene expression profiles in response to *A. fumigatus* infection

RNA-seq of moDCs infected with either *A. fumigatus* or *E. coli* revealed more than 5000 significant DEGs (Log2FC 2; adjusted p-value < 0.01) in response to infection (Figure 4 a). In detail, our analysis indicated 6182 DEGs in response to *A. fumigatus* and 5658 DEGs in response to *E. coli* infection. We further screened for pathogen-characteristic DEGs and identified 2716 DEGs in response to *A. fumigatus* exposure only. Among these, 1667 DEGs (61.4 %) were induced and 1049 DEGs (38.6 %) were downregulated. *E. coli*-infected moDCs demonstrated 2192 DEGs, among these 1315 DEGs (59.9 %) were induced and 878 DEGs (40.1 %) were downregulated. Overall, we observed 3466 DEGs common in response to *A. fumigatus* and *E. coli* infection (Figure 4 a). RNA-seq analysis indicated four characteristic gene clusters, which were further investigated by performing gene ontology (GO) enrichment analysis (Figure 4 b). Significantly enriched GO categories of the identified gene clusters common in response to both types of infections, were mainly linked to metabolic processes (downregulated genes) and immune system processes, response to cytokines and stress (induced genes) (Figure 4 b). Among the top significantly induced genes in *A. fumigatus*- and *E. coli*-infected moDCs (log2FC > 9) were genes encoding matrix metallopeptidases (*MMP1, MMP10, MMP3*) and cytokines (e.g., *CXCL3, CXCL8, IL1B*).

We further investigated genes specifically dysregulated after *E. coli* infection and observed among others enrichment of categories related to inflammatory response, response to stress and IFN-γ (induced genes) as well as regulation of cell death, MAPK cascade and cell motility (downregulated genes) (Figure 4 b). Some of these identified immune-related DEGs were, for example, *CXCL10*, *MMP8*, *ITGB5*, and *CASP3* (Table 13).

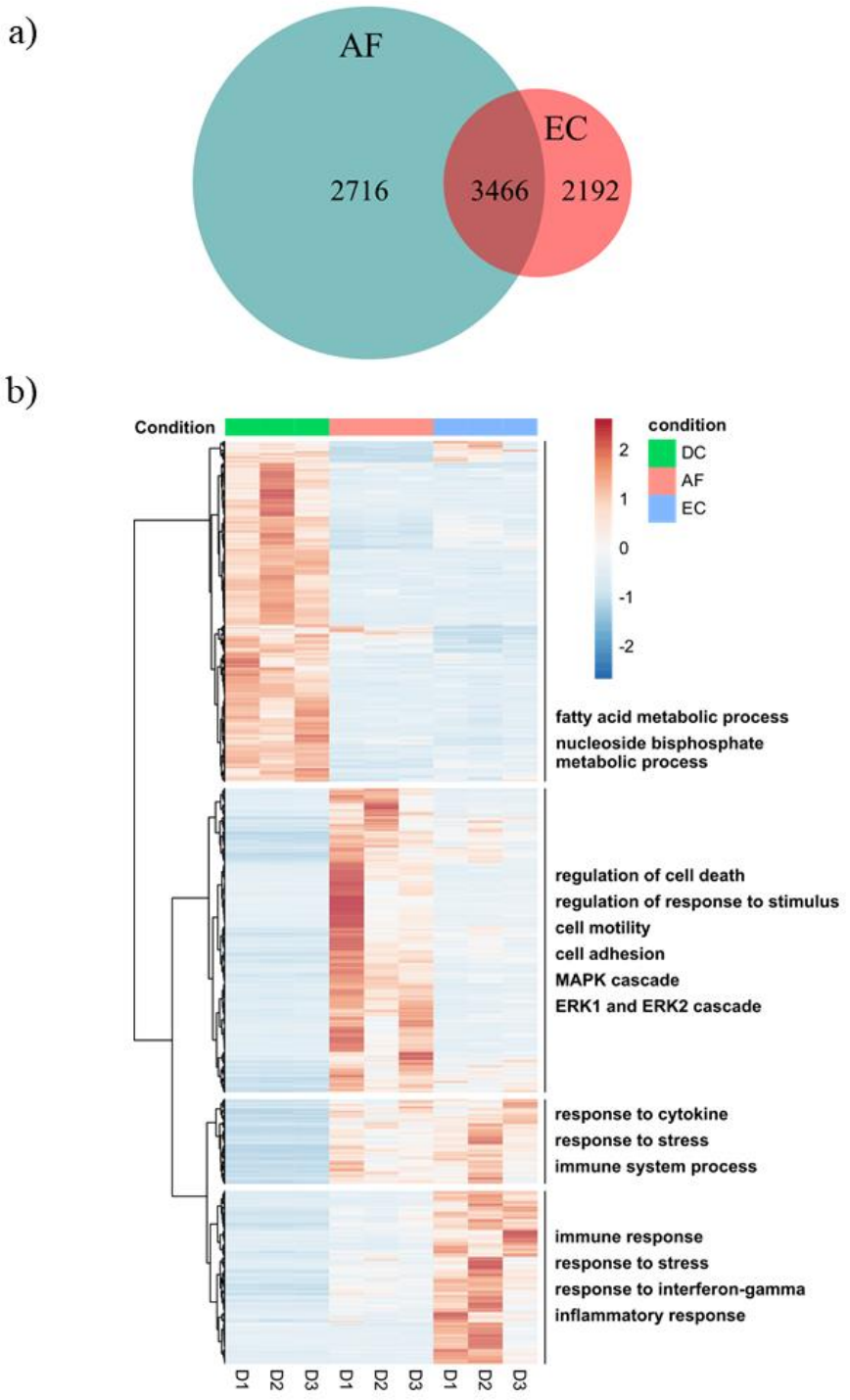

Figure 4: Investigation of host gene expression profiles in response to *A. fumigatus* or *E. coli* infection. a) Venn diagram demonstrating number of DEGs in *A. fumigatus*-infected (AF) or *E. coli*-infected moDCs (EC). **b)** Gene expression profiles of uninfected moDCs (DC), *A. fumigatus*-infected moDCs and *E. coli*- infected moDCs (EC). Data were obtained by RNA-seq of three biological replicates. DEGs were identified by applying adjusted $p < 0.01$ and log2FC of at least 2.

Table 13: Immunity-related DEGs that are characteristic in response to *A. fumigatus* or *E. coli* exposure. Data were obtained by RNA-seq of three biological replicates. DEGs were identified by applying Log2FC of at least 2 and adjusted p-value < 0.01.

A. fumigatus			***E. coli***		
gene ID	**log2FC**	**p-value (adj)**	**gene ID**	**log2FC**	**p-value (adj.)**
CLEC7A	-2.96	1.65×10^{-13}	*IL27*	9.34	7.61×10^{-17}
TLR3	3.04	3.89×10^{-36}	*CXCL10*	9.27	5.18×10^{-13}
CCL13	-4.15	2.91×10^{-17}	*CCL8*	8.49	2.88×10^{-16}
CCL22	2.92	5.36×10^{-8}	*IFN-γ*	7.82	1.04×10^{-7}
CCL23	-2.47	1.46×10^{-8}	*CCL19*	6.73	3.69×10^{-25}
CCR5	2.25	9.06×10^{-14}	*CLEC5A*	5.03	7.12×10^{-19}
CXCL9	2.47	1.78×10^{-3}	*MMP8*	4.46	3.29×10^{-6}
ITGAL	-2.10	5.68×10^{-12}	*IL15*	4.29	2.35×10^{-16}
MMP9	4.21	5.21×10^{-17}	*SIGLEC9*	3.24	1.68×10^{-19}
MMP25	-2.80	8.05×10^{-7}	*STAT1*	2.97	1.84×10^{-09}
SIGLEC1	6.30	6.80×10^{-29}	*SIGLEC14*	2.91	9.48×10^{-12}
LGALSL	3.12	9.84×10^{-9}	*STAT3*	2.46	8.08×10^{-27}
LGALS2	-3.51	2.24×10^{-4}	*ITGB5*	-2.25	2.99×10^{-6}
CXCL14	5.07	3.25×10^{-7}	*TLR5*	-3.59	1.51×10^{-11}
ITGBL1	3.96	1.19×10^{-4}	*CASP3*	2.61	2.30×10^{-27}

GO enrichment analysis of the genes specifically induced after infection with *A. fumigatus* revealed among others, categories related to cell adhesion, MAPK cascade as well as regulation of cell death and response to a stimulus. Specifically downregulated genes after infection with *A. fumigatus* were linked to inflammatory responses, response to stress and IFN-γ (Figure 4 b). Among immune-related DEGs characteristic for *A. fumigatus*-infected moDCs, we thus observed *CLEC7A*, *TLR3*, *MMP9*, *LGALS2* and others (Table 13).

Taken together, our study revealed common and distinctive gene expression signatures in *A. fumigatus*- and *E. coli*-infected moDCs and indicated the potential to discriminate *A. fumigatus* from *E. coli* infection based on obtained gene expression profiles in the investigated experimental model.

3.1.3 MiRNA expression profiles in response to *A. fumigatus* infection

MiRNA profiling revealed common and distinctive miRNA expression profiles in response to *A. fumigatus* and *E. coli* infection. As overall response to infection we identified 32 differentially expressed miRNAs (DEMs) (Log2FC 2; adjusted p-value < 0.01) (Figure 5, Table 14). Common miRNA expression signature identified in *A. fumigatus*- and *E. coli*-infected moDCs consisted of hsa-miR-9-5p, hsa-miR-155-3p and hsa-miR-155-5p induction along with hsa-miR-1303 downregulation (Figure 5).

In response to *E. coli* infection, we identified eight dysregulated miRNAs (Figure 5). Among these, hsa-miR-155-5p, hsa-miR-9-3p, hsa-miR-146a-5p, hsa-miR-155-3p, hsa-miR-1303, hsa-miR-27a-3p and hsa-miR-187-3p were induced, while hsa-miR-1303 was downregulated. Furthermore, observed induction of hsa-miR-9-3p, hsa-miR-146a-5p, hsa-miR-27a-3p, and hsa-miR-187-3p was characteristic in response to *E. coli* infection only (Figure 5; Table 14).

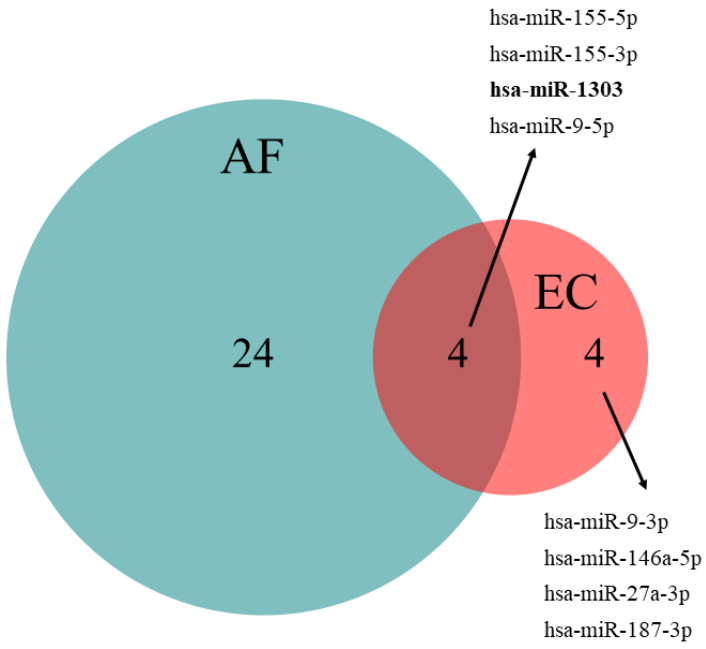

Figure 5: Venn diagram of significantly dysregulated miRNAs in response to *A. fumigatus* (AF) and *E. coli* (EC) infection. Downregulated miRNAs are shown in bold. Data were obtained by small RNA-seq of three biological replicates and significantly dysregulated miRNAs were identified by applying log2FC of 1 and adjusted p-value < 0.05.

Table 14: Significantly dysregulated miRNAs in response to *A. fumigatus* and *E. coli* infection. MiRNA expression was investigated by small RNA-seq and DEMs were identified by applying log2FC of 1 and adjusted p-value <0.05. Data are shown for three biological replicates.

miRNA	log2FC	p-value (adj.)
A. fumigatus		
hsa-miR-132-3p	2.86	2.63×10^{-15}
hsa-miR-27a-5p	3.07	9.31×10^{-9}
hsa-miR-155-5p	3.34	2.71×10^{-8}
hsa-miR-132-5p	2.44	4.74×10^{-8}
hsa-miR-222-5p	3.86	4.74×10^{-8}
hsa-miR-212-3p	2.72	7.48×10^{-8}
hsa-miR-6087	3.66	2.56×10^{-7}
hsa-miR-155-3p	4.98	5.01×10^{-7}
hsa-miR-4792	2.98	9.75×10^{-7}
hsa-miR-212-5p	2.18	4.99×10^{-6}
hsa-miR-29b-1-5p	2.95	4.93×10^{-5}
hsa-miR-1303	-1.78	5.32×10^{-5}
hsa-miR-6126	6.96	1.35×10^{-4}
hsa-miR-9-5p	1.66	2.63×10^{-4}
hsa-miR-1-3p	2.71	9.85×10^{-4}
hsa-miR-3187-3p	-3.10	2.68×10^{-3}
hsa-miR-129-5p	2.11	2.84×10^{-3}
hsa-miR-549a	4.28	2.84×10^{-3}
hsa-miR-877-5p	-1.53	2.35×10^{-2}
hsa-miR-6763-5p	-2.98	2.98×10^{-2}
hsa-miR-197-5p	-1.82	3.26×10^{-2}
hsa-miR-204-5p	-1.64	3.26×10^{-2}
hsa-miR-221-5p	1.13	3.25×10^{-2}
hsa-miR-1307-3p	-1.06	3.54×10^{-2}
hsa-miR-3195	2.65	3.54×10^{-2}
hsa-miR-671-3p	-1.45	3.64×10^{-2}
hsa-miR-1227-3p	-5.35	4.60×10^{-2}
hsa-miR-1908-5p	-1.65	4.75×10^{-2}
E. coli		
hsa-miR-9-5p	3.35	3.19×10^{-15}
hsa-miR-155-5p	4.14	5.12×10^{-2}
hsa-miR-9-3p	2.78	3.56×10^{-8}
hsa-miR-146a-5p	2.14	5.48×10^{-8}
hsa-miR-155-3p	4.11	2.28×10^{-4}
hsa-miR-1303	-1.51	3.54×10^{-3}
hsa-miR-27a-3p	1.65	1.84×10^{-2}
hsa-miR-187-3p	2.89	2.82×10^{-2}

In response to *A. fumigatus* infection, we identified overall 28 DEMs. Among these, 24 miRNAs were characteristic in *A. fumigatus*-infected moDCs (Figure 5, Table 14). In particular, we observed induction of 15 DEMs (e. g., hsa-mir-132-3p, hsa-miR-129-5p, hsa-miR-6126) and repression of nine DEMs (e.g., hsa-miR-204-5p, hsa-miR-1307-3p, hsa-miR-671-3p) in *A. fumigatus*-infected moDCs (Table 14).

Taken together, our *in vitro* model revealed distinctive miRNA signatures associated with *A. fumigatus* or *E. coli* infection and thus showed the potential of miRNA expression profiles to discriminate between *A. fumigatus* from *E. coli*-infected moDCs.

3.1.4 Integration of miRNA and mRNA expression profiles

In the next step, we integrated obtained miRNA and mRNA expression profiles to identify potential characteristic miRNA-mRNA signatures indicating *A. fumigatus* infection, therefore we focused on the DEMs in response to *A. fumigatus* infection only. Predictions of mRNA targets for dysregulated miRNAs were performed using miRWalk 2.0, an archive with a large collection of predicted and experimentally verified miRNA–target interactions (Dweep and Gretz, 2015).

While one miRNA can regulate numerous genes, one gene can be regulated by several miRNAs. (Xu *et al*., 2020). The complexity of miRNA-mRNA interactions was observed also in our *in silico* analysis, which revealed large and complex networks of predicted miRNA-mRNA interactions. Thus, in the next step, we focused on inverse correlations between miRNA-mRNA only and filtered the interactions according to the Pearson correlation coefficient – 0.6 or less. Using combined analysis of experimentally validated miRNA-mRNA predictions and correlation analysis, we identified characteristic miRNA-mRNA signature indicating *A. fumigatus* infected moDCs, consisting of the following nine dysregulated miRNAs: hsa-miR-1227-3p, hsa-miR-129-5p, hsa-miR-1307-3p, hsa-miR-132-3p, hsa-miR-1908-5p, hsa-miR-204-5p, hsa-miR-212-3p, hsa-miR-671-3p and hsa-miR-877-5p (Figure 6).

Identified miRNA-mRNA signature consisting of nine DEMs and 61 target genes enable discrimination between uninfected moDCs, *A. fumigatus*-infected moDCs and *E. coli*-infected moDCs (Figure 6).

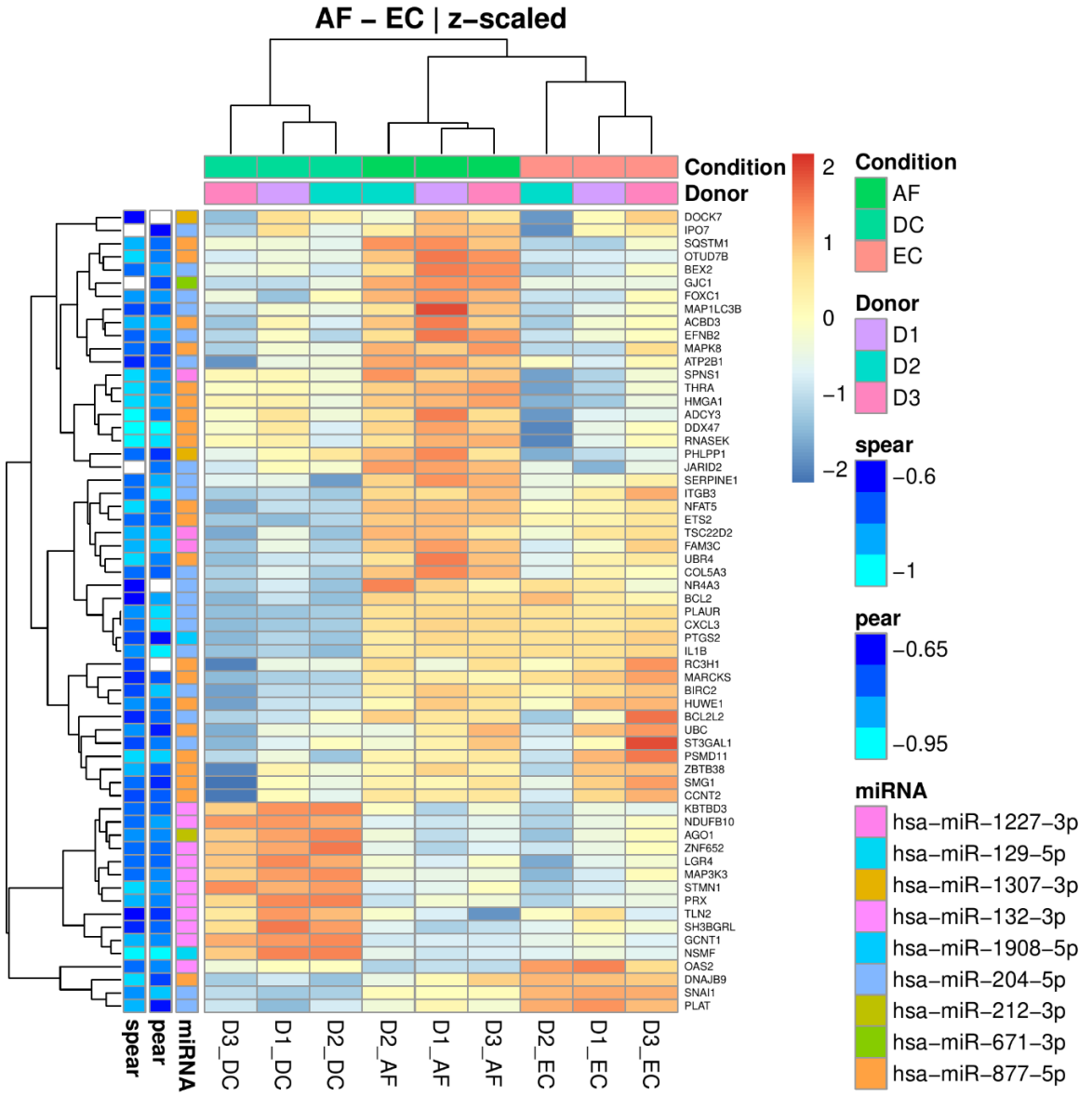

Figure 6: Heatmap demonstrating characteristic miRNA-mRNA profiles after *A. fumigatus* (dark green) and *E. coli* infection (light green). MiRNAs specifically altered after *A. fumigatus* infection and their predicted target genes were used for the investigation of potential characteristic signatures. Integrated expression profiles are shown for three biological replicates and reported for uninfected moDCs (DC), *A. fumigatus*-infected moDCs (AF), and *E. coli*-infected moDCs (EC). Spear, Spearman correlation coefficient; pear, Pearson correlation coefficient.

We additionally investigated whether we can discriminate between *A. fumigatus* and *E. coli*-infected moDCs based on miRNA-mRNA signatures consisting of only one miRNA and predicted negatively correlated mRNA targets. For further investigation, we selected hsa-miR-132-3p (induced) and hsa-miR-204-5p (downregulated), which were differentially expressed following *A. fumigatus* exposure only. While induction of hsa-mir-132-3 has already been reported following *A. fumigatus* exposure, little is known about hsa-miR-204-5p expression in the context of *Aspergillus* spp. infections (Croston *et al*., 2018). In addition, we further investigated hsa-miR-9-5p, dysregulated in both, *A. fumigatus*- and *E. coli*-infected moDCs, to investigate whether we can observe distinctive patterns based on the expression of predicted target genes.

While all three generated miRNA-mRNA signatures showed discrimination between uninfected and infected moDCs, strong differentiation between *A. fumigatus*- and *E. coli*-infected moDCs, based on predicted target genes was not observed in the case of hsa-miR-132-3p and hsa-miR-9-5p (Figure 7 a, b). Hence, these predicted target genes could be part of the common mRNA response to both types of infection. In contrast, an integrated signature based on the of hsa- miR-204-5p and its target genes revealed a distinctive signature for *A. fumigatus*-infected moDCs (Figure 7 c). Strong induction of known immune response-related genes (e.g., *BCL2*, *ITGB3*, *IL1B* and *CXCL3*) was observed in both types of infection, while genes such as *BEX2*, *EFNB2*, *MAP1LC38*, *JARID2* and others showed strong induction only in *A. fumigatus*-infected moDCs.

Next, we selected two predicted target genes per miRNA according to generated miRNA-mRNA profiles along with available literature in the context of the immune response, and follow up further: *IL1B*, *ITGB3*, *LGR4*, *TLN2*, *MAP3K3* and *RAB34* (Zhang and Wang, 2012; Du *et al.*, 2013; Prashar *et al*., 2017; Harjunpaa *et al.*, 2019). We next investigated the binding sites of hsa-miR-204-5p, hsa-miR-132-3p and hsa-miR-9-5p and their target genes, using the following three tools: MiRanda, TargetScan and RNA22 (Oliveira *et al*., 2017). These algorithms predict the probability of a functional miRNA interaction site within investigated mRNA target (Kuhn *et al.*, 2008).

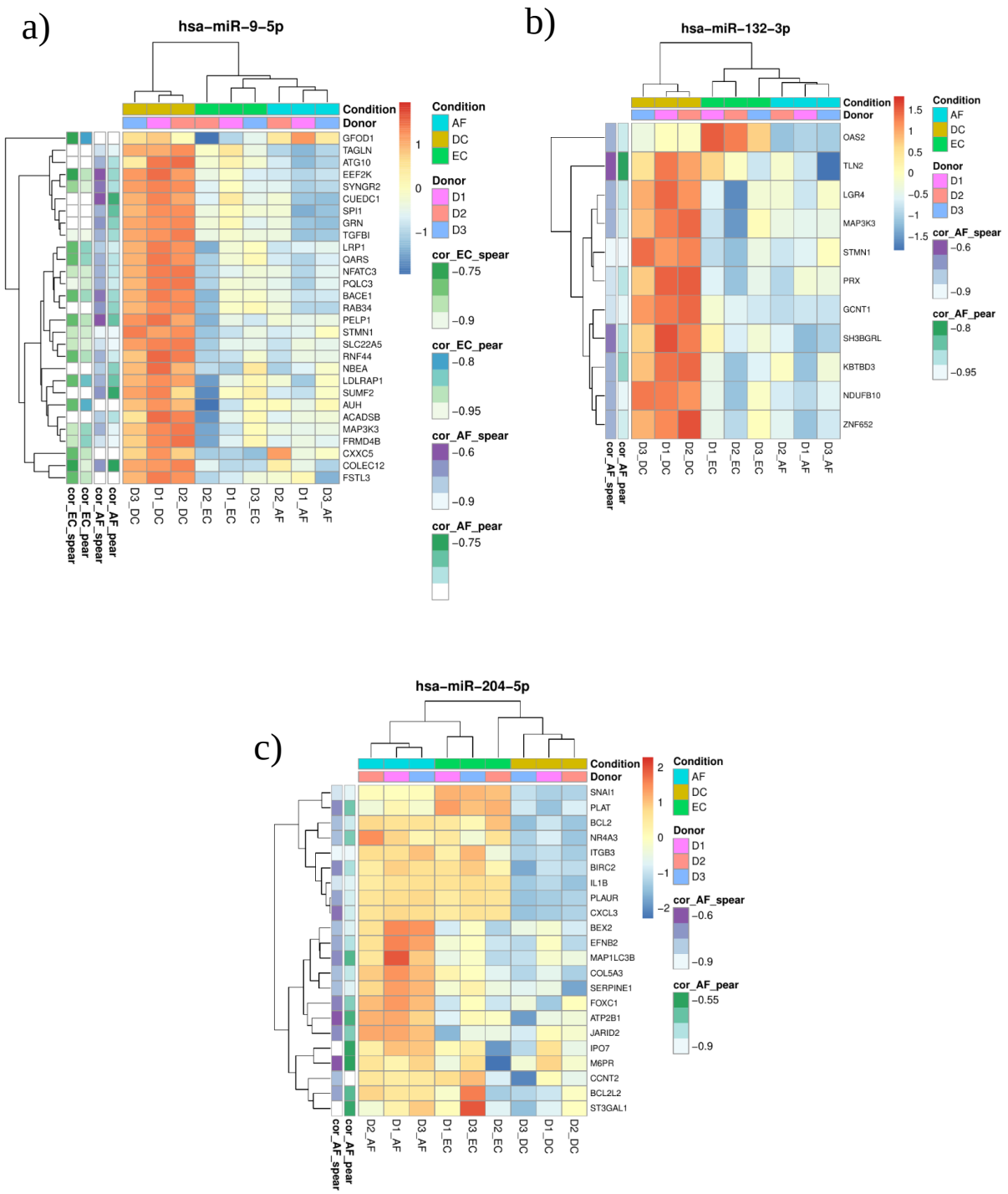

Figure 7: Selected integrated miRNA-mRNA expression profiles for a) hsa-mir-9-5p b) hsa-miR-132-3p and c) hsa-miR-204-5p. Data are shown for three biological replicates: uninfected moDCs (DC), *A. fumigatus*-infected moDCs (AF) and *E. coli*-infected moDCs (EC). Target genes were filtered according to the inverse correlation and the strength of correlation (Pearson coefficient of 0.6 or less). Integrated miRNA-mRNA signatures for A. fuimaguts infected moDCs are marked in blue (AF).

In most cases miRNAs induce mRNA degradation and translational repression by binding to the 3' UTR of the target mRNAs, thus we investigated interaction sites of selected miRNAs only within 3' UTR regions of their target mRNAs (Kuhn *et al*., 2008).

For each investigated miRNA-mRNA pair, we identified an interaction site with at least one of the used tools (Table 15). All tools predicted interaction sites for hsa-miR-132-3p-*TLN2* and hsa-miR-9-5p-*MAPK3K* (Table 15).

Table 15: Investigation of interaction sites for selected miRNA-mRNA predicted pairs. Binding sites were investigated by three tools MiRanda, TargetScan and RNA22 (Oliveira *et al*., 2017).

miRNA	gene	MiRanda	TargetScan	RNA22	nr. of predicted seq	union	Pearson coefficient
hsa-miR-204-5p	*IL1β*	F	F	T	1 (1)	T	-0.963
	ITGB3	T	F	T; T	3 (3)	T	-0.951
has-miR-132-3p	*LGR4*	T	F	F	1 (1)	T	-0.767
	TLN2	T	T	T; T	3 (4)	T	-0.683
hsa-miR-9-5p	*MAP3K3*	T	T; T	T	3 (4)	T	-0.714
	RAB34	T	T	F	1 (1)	T	-0.771

F, not significant; T, significant (multiple T for multiple significant results – multiple predicted binding sites), nr., number

Predicted binding sites of investigated miRNA within their target mRNA are shown in Figure 8. Used algorithms might predict several putative miRNA binding sites on a specific mRNA target (Kuhn *et al.*, 2008). Hence, it is required to experimentally evaluate which predicted interaction sites are functional, by employing a reporter system (e.g., luciferase assay). Our investigation revealed different binding sites within target 3' UTR and selected miRNAs for the following pairs: hsa-miR-204-5p – *ITGB3*, hsa-miR-132-3p – *TLN2* and hsa-miR-9-5p– *MAP3K3* (Figure 8). It is suggested that at least two algorithms predict the same miRNA interaction site before additional validation experiments are performed (Kuhn *et al*., 2008). In our study, the same binding sites were predicted using RNA22 and TargetScan for miR-132-3p – *TLN2*, hsa-miR-9-5p – *MAP3K3* and hsa-miR-9-5p – *RAB34*, suggesting these putative predictions could be promising for further experimental validation.

Figure 8: Predicted binding sites of hsa-miR-204-5p a), hsa-miR-132-3p b) and hsa-miR-9-5p c) within the 3'UTR region of investigated target mRNAs. Binding sites were investigated using three tools: MiRanda, TargetScan and RNA22 (Oliveira *et al.*, 2017). Identical 3'UTR sequences of the target gene are shown in yellow.

If miRNA regulates the expression of its mRNA target, they both have to be co-expressed. Co-expression can be demonstrated simply by qPCR using total RNA isolated from a specific sample, detecting miRNA and mRNA of interest (Kuhn *et al.*, 2008). Thus, we next validated our RNA-seq results and correlation analysis and investigated the expression levels of selected miRNAs and their targets in *A. fumigatus*- and *E. coli*-infected moDCs by qPCR (Figure 9 a, b). We demonstrated induction of hsa-miR-9-5p and downregulation of its targets *MAP3K3* and *RAB34* in response to *A. fumigatus* and *E. coli* infection. Additionally, we showed induction of hsa-miR-132-3p and downregulation of *LGR4* and *TLN2* following *A. fumigatus* and *E. coli* exposure. Previous RNA-seq investigation did not indicate hsa-miR-132-3p dysregulated in response to *E. coli* infection. Interestingly, we observed a significant difference ($p < 0.05$) in hsa-miR-204-5p expression between *A. fumigatus*- (downregulation) and *E. coli*-infected (induction) moDCs and further demonstrated induction of *IL1B* and *ITGB3* after *A. fumigatus* and *E. coli* infection (Figure 9 a, b). Elevated levels of *IL1B* in response to *A. fumigatus* and *E. coli* infection were demonstrated also on the protein level, which further suggests the interaction of hsa-miR-204-5p and *IL1B* (Figure 9 c).

Since direct experimental validation of predicted binding sites of selected miRNA and their target mRNA was outside of the scope of this study, we encourage future studies to experimentally validate predicted miRNA-mRNA interactions in this chapter.

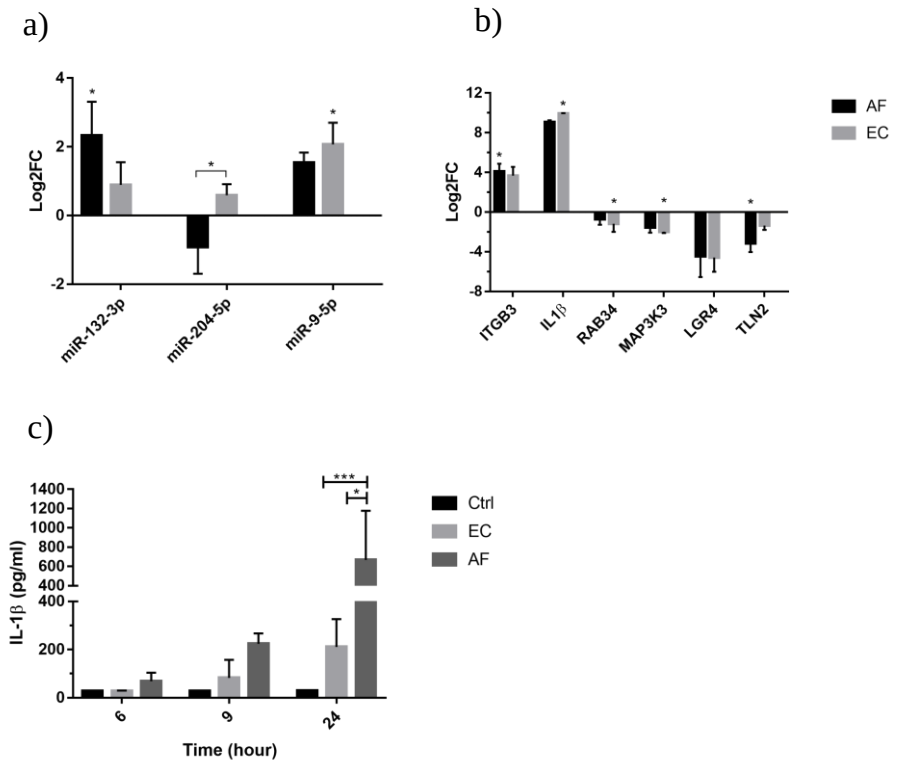

Figure 9: Indirect validation of selected miRNAs and their predicted target genes. RNA-seq and *in silico* results were validated further by qPCR. **a)** Expression of hsa-miR-132-3p, hsa-miR-204-5p, hsa-miR-9-5p and **b)** their selected target genes in *A. fumigatus*-infected (black) or *E. coli*-infected moDCs (grey) are shown relative to the control, uninfected moDCs. **c)** IL-1β levels were determined in uninfected moDCs (black), *A. fumigatus*-infected moDCs (dark grey) and *E. coli*-infected moDCs (light grey). MoDCs were infected with either *A. fumigatus* or *E. coli* for 12 hrs. Data are shown for three biological replicates as mean with SD. Significant differences are shown as: *, $p < 0.05$; ***, $p < 0.001$.

Parts of the results presented in the following chapter have been published in:

Zoran T, Seelbinder B, White PL*, et al.* 2022. Molecular Profiling Reveals Characteristic and Decisive Signatures in Patients after Allogeneic Stem Cell Transplantation Suffering from Invasive Pulmonary Aspergillosis. J Fungi (Basel) **8**. doi.org/10.3390/jof8020171.

Reprinted with the permission of the Journal of Fungi.

3.2 Investigation of characteristic molecular signatures indicating IPA in patients post alloSCT

Despite the advances in the field of IPA diagnostics and recently updated EORTC/MSGERC criteria for the management of fungal infections, the diagnosis of IPA remains challenging (Donnelly *et al*., 2020). As a result of often unspecific symptoms and challenging diagnosis, emerging new risk groups and antifungal resistance, IPA is associated with poor outcomes (Nedel *et al*., 2009; Garcia-Vidal *et al*., 2015; Lass-Flörl, 2019). Considering the complex pathobiology of IPA as well as haematological malignancies and alloSCT, continuous research not only on improving diagnostics but also on characterizing the host immune response during IPA is important for better understanding this multifactorial disease and improving the outcome. Compared to fungal biomarkers such as *Aspergillus* DNA and galactomannan which are already implemented in diagnostic laboratories, host biomarkers are not well-characterized noir in clinical use (Donnelly *et al*., 2020). Among the most investigated host biomarkers for IPA have been single-nucleotide polymorphism (SNPs) and cytokine profiles (Cunha *et al.*, 2013; Thammasit *et al*., 2021). As omics technologies continue to advance, studying host response became faster and less expensive. Hence, assays based on host response may in the future, as diagnostic aids support the diagnosis of respiratory infections and help to improve the management of respiratory infections in alloSCT patients (Ross *et al*., 2019; Astashchanka *et al*., 2021).

The present pilot, longitudinal, case-control study was conducted to characterize the host response of alloSCT patients during IPA in a multilevel manner. We aimed to investigate characteristic IPA signatures and identify potential molecular candidates indicating IPA promising for further evaluation in larger and multicenter studies.

3.2.1 Study design and workflow

To characterize the host response of alloSCT patients during IPA and identify potential characteristic signatures, we prospectively collected blood samples from patients undergoing alloSCT at the University Hospital of Würzburg, between March 2017 and December 2019 (Würzburg cohort). Serum and whole blood samples were collected twice-weekly until 100 days post alloSCT, whenever feasible. Overall, we recruited 90 patients with at least four time points and collected overall 2000 blood samples. According to the EORTC/MSGERC criteria, we identified three probable IPA cases with a sufficient amount of collected blood samples appropriate for the profiling (Donnelly *et al*., 2020). Control patients did now show any signs of *Aspergillus* spp. infection and were matched to cases by the same sex and underlying disease (AML), similar age and past time since receiving alloSCT (similar collected time points after alloSCT). As investigated alloSCT patients developed IPA at different times post alloSCT, we established relative time for the onset of probable IPA. Day 0 represented the day of positive mycology (detection of galactomannan or *Aspergillus* DNA in serum or BAL) along with positive radiology (CT-scan).

The workflow of the present longitudinal, case-control study is shown in Figure 10. To identify characteristic IPA signatures post alloSCT, we used an integrated approach based on transcriptome profiling of selected three probable IPA cases and their matched controls combined with an investigation of seven gene expression datasets obtained from six relevant, publicly available *in vitro* studies, characterizing gene expression in myeloid cells in response to *A. fumigatus* infection. Selected potential molecular candidates were further quantified in patient sera using immunoassays. We further assessed the protein levels of potential molecular candidates in possible IPA cases and their controls obtained from the Würzburg and Cardiff medical centre (Suppl. Table S1). The specificity of potential molecular candidates was assessed in an additional independent cohort (Cardiff II) consisting of CAPA patients (aspergillosis as secondary infection) and appropriate COVID-19 controls (Suppl. Table S2). In addition, we evaluated the potential effect of GvHD on the identified characteristic IPA signature by assessing the gene expression and protein levels of investigated molecular candidates in GvHD patients. Finally, the identified IPA characteristic signature was evaluated *in vitro,* using moDCs infected with inactivated *A. fumigatus* germ tubes.

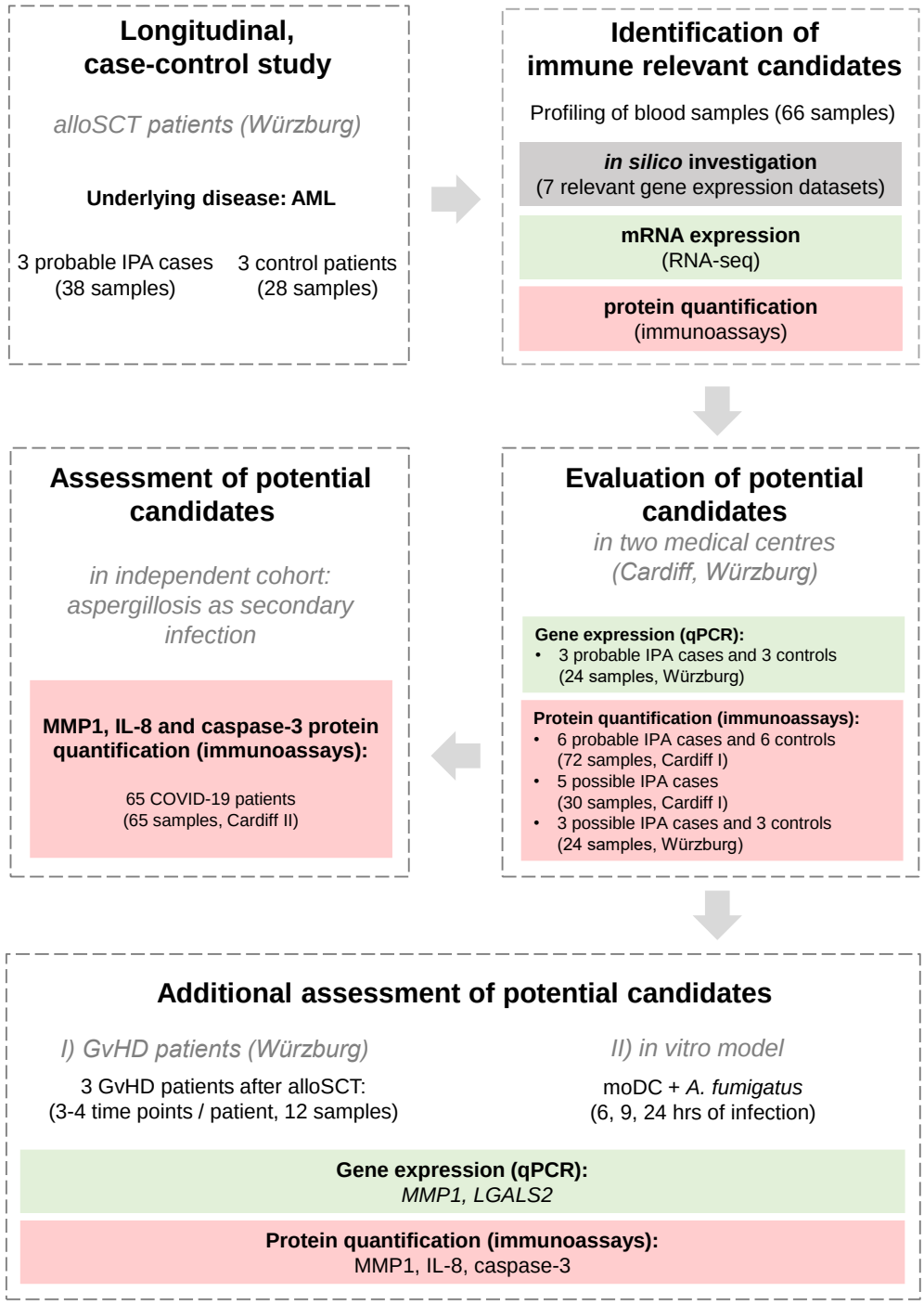

Figure 10: Workflow and study design of the pilot, case-control study investigating host response of IPA patients post alloSCT. Adapted and modified from Zoran *et al*., 2022. Characteristic host signatures indicating IPA in alloSCT patients (Würzburg) were identified by combining transcriptome profiling, literature search and gene expression analysis of publicly available, relevant *in vitro* studies characterizing host response to *A. fumigatus*. Potential molecular candidates were evaluated in additional alloSCT patients categorized as possible and probable IPA cases and their matched controls (Cardiff I, Würzburg cohort). The specificity of identified potential molecular candidates was evaluated in an additional COVID-19 cohort. Finally, characteristic IPA molecular candidates were further evaluated in GvHD patients and *in vitro* in *A. fumigatus*-infected moDCs.

3.2.2 Identification of host transcriptome signatures indicating IPA post alloSCT

As shown in Figure 11, whole blood RNA-seq revealed variability in gene expression due to the clinical heterogeneity of investigated patients (e.g., other diseases or infections, different treatments). Nevertheless, we observed characteristic and robust gene expression patterns indicating IPA in profiled alloSCT patients (Figure 11 a). Irrespective of investigated time (across all 66 investigated samples), we identified 1131 DEGs ($q < 0.05$; log2FC cutoff 0.8) in probable IPA cases compared to their matched controls. GO enrichment analysis of identified DEGs revealed metabolic processes (e.g., long-chain fatty acids, vitamin K) together with immune response processes such as neutrophils mediated immunity, response to fungi, positive regulation of NF-κβ transcription activity, immune cell activation and immunoglobulin production (Figure 11 a). Altogether, these data demonstrate the potential to differentiate between probable IPA cases and controls, according to the host blood-based gene expression profiles. Next, we selected nine immune-relevant molecular candidates for further evaluation: *CASP3*, *CD40*, *CXCL8*, *ITGB3*, *LGALS2*, *MMP1*, *MMP9*, *SERPINE1* and *VEGFA*. These candidates were selected using an integrated approach combining our RNA-seq results, literature search and additional gene expression analysis of publicly available datasets obtained from six relevant *in vitro* studies (Gibson *et al*., 2003; Stanzani *et al*., 2005; Weiss *et al*., 2005; Cortez *et al.*, 2006; Ben-Ami *et al.*, 2009; Heldt *et al.*, 2017; Gonçalves *et al*., 2017).

The risk of developing IPA is highest within the first four weeks post alloSCT (Cadena *et al*., 2021). As early diagnosis and treatment of IPA are crucial for a successful outcome of the disease, we analysed our data within the first five weeks (up to 35 days) after IPA onset if not stated otherwise (Jenks and Hoenigl, 2018). Moreover, to avoid bias from individual patients, we balanced the total number of investigated samples per patient ($n = 4$). Investigation of mean gene expression within the first five weeks after IPA onset (balanced dataset), indicated significant induction of *ITGB3*, *MMP1* and *MMP9* and repression of *CD40*, *CXCL8* and *LGALS2* in probable IPA cases compared to their controls (Figure 11 b).

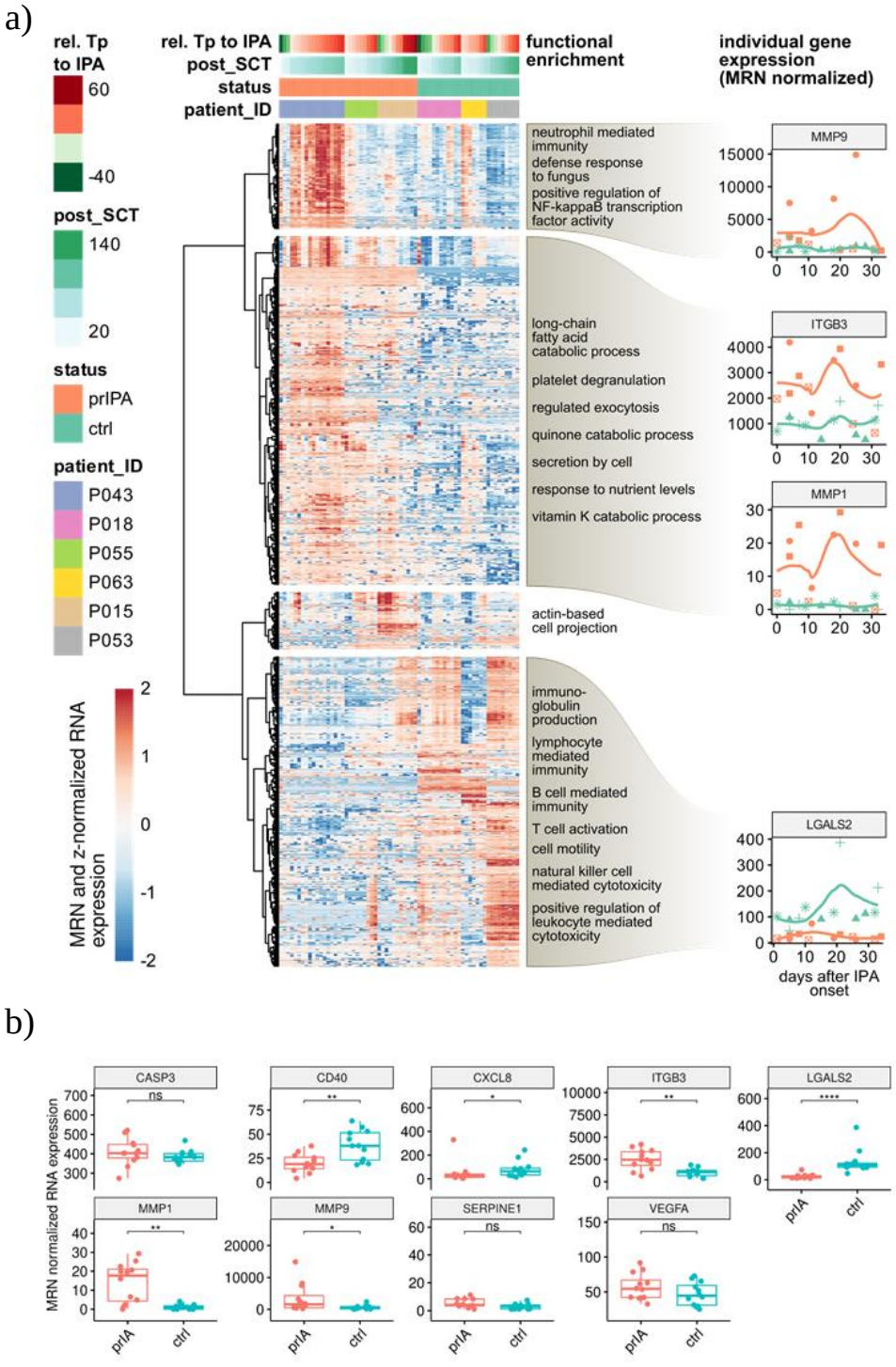

Figure 11: Whole blood transcriptome profiles obtained by RNA-seq of investigated three probable IPA cases and their matched controls. Taken from Zoran *et al*., 2022. **a)** Hierarchical clustering and GO enrichment analysis of identified DEGs in IPA cases (red) compared to their matched controls (blue) across all investigated blood samples ($p < 0.05$; log2FC 0.8). **b)** Median ratio normalized RNA expression of selected potential molecular candidates within the first five weeks after IPA onset (balanced dataset). Data are shown as mean MRN normalized RNA expression values with 95% confidence intervals. Significant differences were investigated by the Wilcoxon test (ns, not significant; *, $p < 0.05$; **, $p < 0.01$; ****, $p < 0.0001$).

Overall, regardless of investigated time frame (across all 66 profiled samples or balanced dataset), our datasets indicated matrix metallopeptidases, integrins and galectins as potential characteristic candidates indicating IPA. Therefore, we further validated our RNA-seq data and investigated the expression of *MMP1*, *MMP9*, *ITGB3* and *LGALS2* by an independent method, qPCR (Figure 11 a, right column).

We confirmed significant induction of *MMP1* ($p < 0.0001$), *MMP9* ($p < 0.0173$) and *ITGB3* ($p < 0.0009$) as well as repression of *LGALS2* ($p < 0.0001$) in IPA cases compared to their matched controls (Figure 12 a). In addition, we investigated gene expression of molecular candidates over a longer time frame (up to 56 days after IPA onset) using all available profiled samples (Figure 9 b). We observed downregulation of *LGALS2* expression in all IPA cases compared to their matched controls across all investigated time points. In the first two weeks, *MMP1* induction was observed in all probable IPA cases compared to matched controls. One matched case-control pair (P15-P53) demonstrated downregulation of *MMP1* expression after two weeks of IPA onset. In contrast, *MMP9* and *ITGB3* expression in IPA cases compared to their matched controls was not consistent across investigated 56 days after IPA onset, demonstrating patient-specific variance (Figure 12 b). Taken together, our findings indicated *MMP1* and *LGALS2* as potential molecular candidates indicating IPA among investigated alloSCT patients, especially in the early time of IPA.

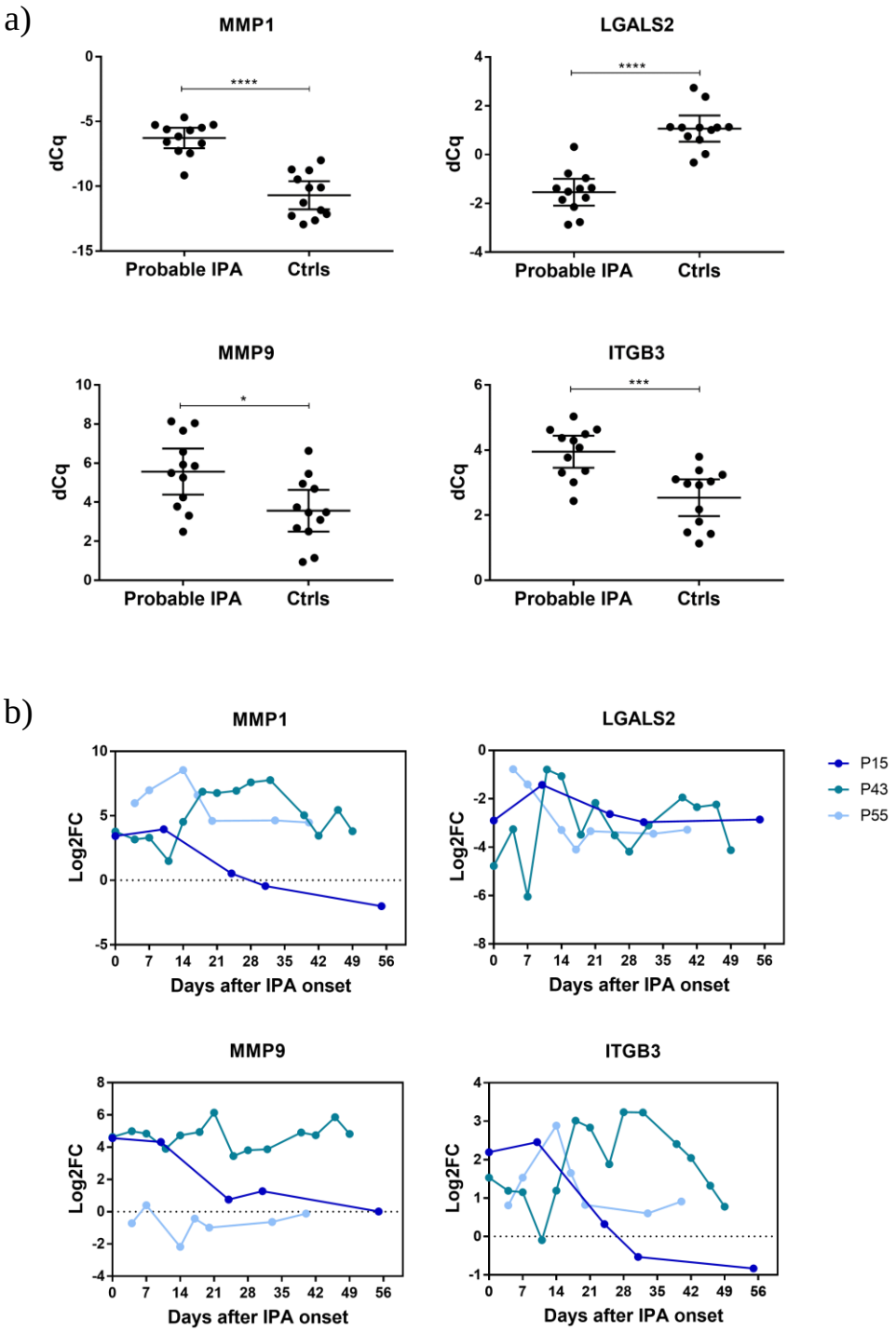

Figure 12: Validation of RNA-seq results of selected potential candidates by qPCR. Modified from Zoran *et al*., 2022. **a)** Mean expression of molecular candidates in investigated three probable IPA cases and their controls within the first five weeks after IPA onset (balanced dataset). Data are shown as mean ΔCq values with 95% confidence intervals. **b)** Expression levels (Log2FC) of molecular candidates across all investigated time (up to 56 days after IPA onset) in probable IPA cases relative to their matched controls. Mann-Whitney test was used to determine significant differences between cases and controls (*, $p < 0.05$; ***, $p < 0.001$).

Next to the gene expression profiling of selected probable IPA cases and controls, we additionally evaluated six publicly available *in vitro* studies investigating myeloid cells infected with *A. fumigatus* by RNA-seq or microarrays (Figure 10). We investigated the expression of previously selected nine candidates in seven datasets, consisting of at least 1000 DEGs (Cortez *et al*., 2006; GSE174827, GSE60729, GSE69723, GSE174827, GSE134344, GSE177040). All nine investigated molecular candidates were found as DEGs in at least one study (Table 16). Induction of *CXCL8*, *MMP1* and *CD40* gene expression was demonstrated in all seven investigated datasets. Observed induction of *MMP1* in all investigated datasets and *LGALS2* repression in two datasets further supported our transcriptome profiling results, suggesting these two genes as promising candidates for further studies.

Table 16: Selected molecular candidates investigated in six relevant publicly available *in vitro* studies elucidating host response to *A. fumigatus* using myeloid cells. Taken from Zoran *et al*., 2022. Investigated gene expression datasets were generated by microarrays or RNA-seq and consisted of at least 1000 DEGs. Reported are gene symbols (symbol), encoded proteins (protein), the number of datasets (nr. of datasets), Ensembl annotation and the trend of expression (+, induction; -, downregulation).

protein	Ensembl annotation	symbol	nr. of datasets	expression
Caspase-3	ENSG00000164305	*CASP3*	1	+
CD40	ENSG00000101017	*CD40*	7	+
IL-8 (CXCL8)	ENSG00000169429	*CXCL8*	7	+
ITGB3	ENSG00000259207	*ITGB3*	3	+
Galectin-2	ENSG00000100079	*LGALS2*	2	-
MMP-1	ENSG00000196611	*MMP1*	7	+
MMP-9	ENSG00000100985	*MMP9*	5	+
PAI-1	ENSG00000106366	*SERPINE1*	6	+
VEGF-A	ENSG00000112715	*VEGFA*	6	+

3.2.3 Protein quantification of selected molecular candidates

Using immunoassays, we further investigated if previously selected nine molecular candidates (Figure 11 b, Table 16) show characteristic patterns also on the protein level. As previously, we investigated molecular candidates in patient sera across all collected samples and within the first five weeks after IPA onset.

We observed significantly elevated ITGB3 ($p < 0.0154$) and Serpine-1 ($p < 0.0004$) serum levels in probable IPA cases compared to controls, yet these differences were not clinically relevant and observed only when we analysed all collected samples (unbalanced dataset) (Figure 13 a, b). Interestingly, irrespective of the analysed time, no significant differences between cases and controls were found in galectin-2 serum levels. Galectin-2 is encoded by *LGALS2*, which was one the strongest molecular candidates indicating IPA in investigated alloSCT patients on the transcriptome level. Furthermore, CD40 was not detected across the majority of the investigated serum samples, therefore we excluded these four molecular candidates from further evaluation.

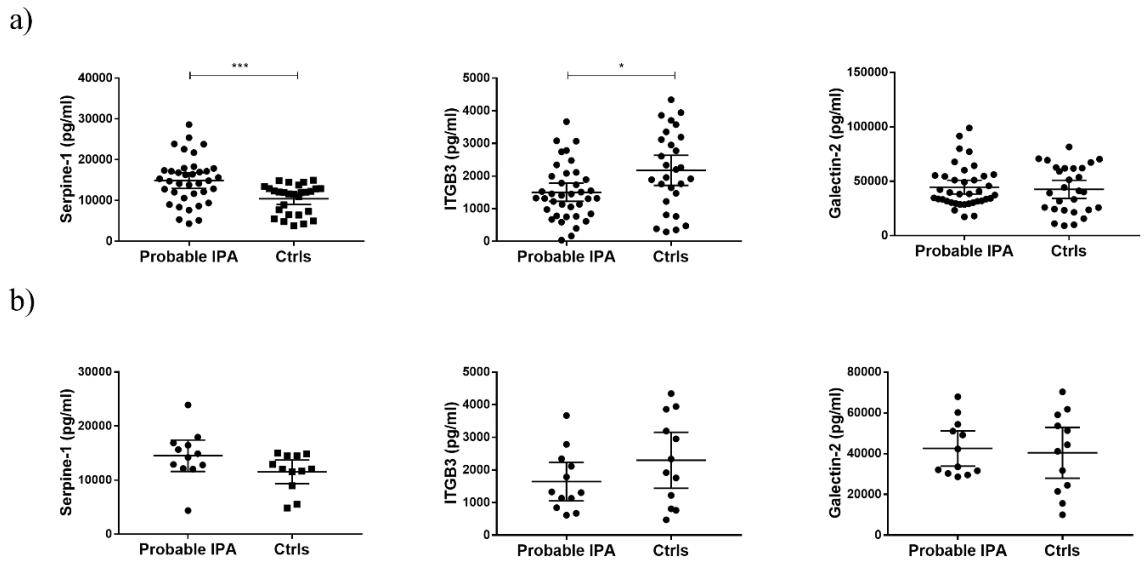

Figure 13: Serpine-1, ITGB3 and galectin-2 serum levels investigated in profiled probable IPA cases and their matched controls. a) Protein levels of selected molecular candidates were investigated in all collected samples and **b)** within the first five weeks after IPA onset (balanced dataset). Data are shown for cases and three controls as mean protein levels with 95% confidence intervals. Significant differences were determined by the Mann-Whitney test (*, $p < 0.05$; ***, $p < 0.001$).

To investigate the robustness of our findings, we evaluated MMP1, MMP9, IL-8, caspase-3 and VEGFA serum levels in alloSCT patients obtained from two independent medical centres: University hospital of Würzburg (original, profiled cohort) and Public Health Wales Microbiology Cardiff medical centre (Cardiff I cohort) (Figure 10). Cardiff I cohort consisted of six probable IPA cases and their six matched controls without any signs of *Aspergillus* spp. infection. From these patients, we investigated six time points per patient, altogether 72 serum samples.

VEGFA serum levels in cases compared to controls were significantly elevated ($p < 0.0172$) in the Würzburg cohort (Figure 14 a, all collected samples), whereas Cardiff I cohort demonstrated significantly lower VEGFA levels ($p < 0.0473$) (Figure 14 c). These observed differences in both cohorts were without clinical importance (Figure 14). Significantly higher MMP9 serum levels ($p < 0.05$, irrespective of the analysed time) in cases compared to controls, were observed in the Würzburg cohort only, yet without clinical importance (Figure 14 a, b).

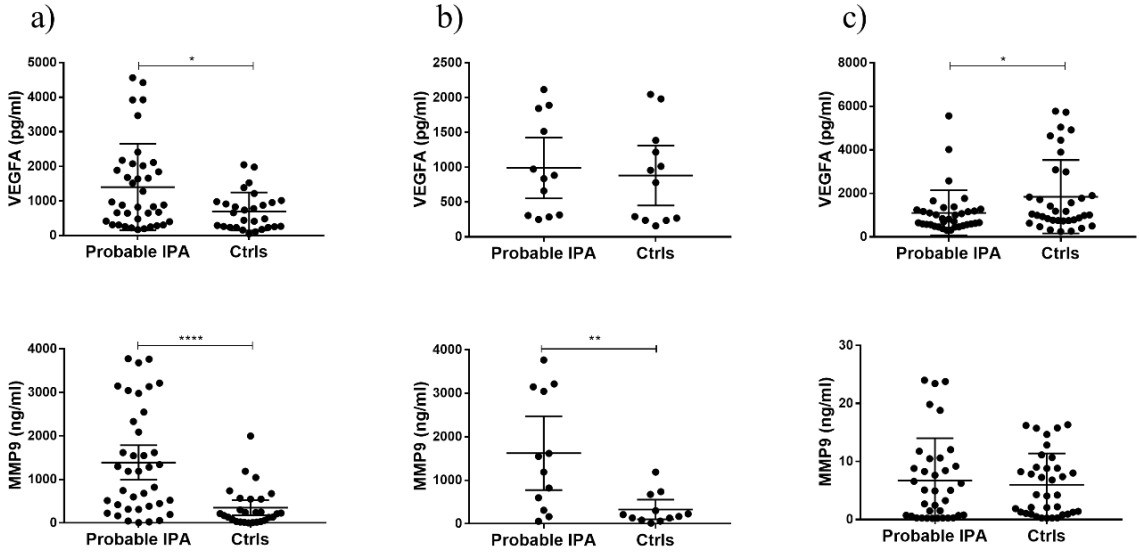

Figure 14: VEGFA and MMP9 serum levels investigated in probable IPA cases and their matched controls. Adapted from Zoran *et al.*, 2022. Protein levels were determined **a**) in all collected samples obtained from the original Würzburg cohort (N=6), **b)** within five weeks after IPA onset in the original Würzburg cohort (balanced dataset; N=6) and **c)** in Cardiff I cohort obtained from Public Health Wales Microbiology (N=12). Data are presented as mean protein levels with 95% confidence intervals. P-values were generated by the Mann-Whitney test (* $p < 0.05$, ** $p < 0.01$, **** $p < 0.0001$). N, number of patients.

The most promising candidates indicating IPA on the protein level were MMP1, IL-8 and Caspase-3 (Figure 15). MMP1 serum levels were significantly elevated in cases compared to controls in the Würzburg cohort ($p = 0.0001$) (Figure 15 a). A similar trend was observed also in the Cardiff I cohort, yet, without the significance ($p = 0.088$) (Figure 15 b). Both investigated cohorts demonstrated significantly elevated IL-8 (Cardiff I, $p < 0.000$; Würzburg, $p = 0.0165$) and caspase-3 serum levels (Cardiff I, $p < 0.0001$; Würzburg, $p = 0.0029$) in cases compared to controls.

Next, we investigated these candidates across all collected samples on the individual patient level in probable IPA cases and controls obtained from the Würzburg cohort (Figure 15 c). Elevated MMP1 levels in probable IPA cases compared to controls were observed in almost all investigated time points, whereas IL-8 and caspase-3 serum levels did not demonstrate distinct day to day separation, indicating patient and sex-specific patterns (Figure 15 c). In particular, a female case (P43) demonstrated elevated IL-8 and caspase-3 levels compared to male cases, which was observed to some extent as well for the matched control (P18). The observed trend was not confirmed in Cardiff I cohort (data not shown).

Despite observed differences as a result of patient origin and clinical heterogeneity, our findings demonstrated MMP1, IL-8 and caspase-3 as potential candidates for IPA in investigated alloSCT patients and were evaluated further.

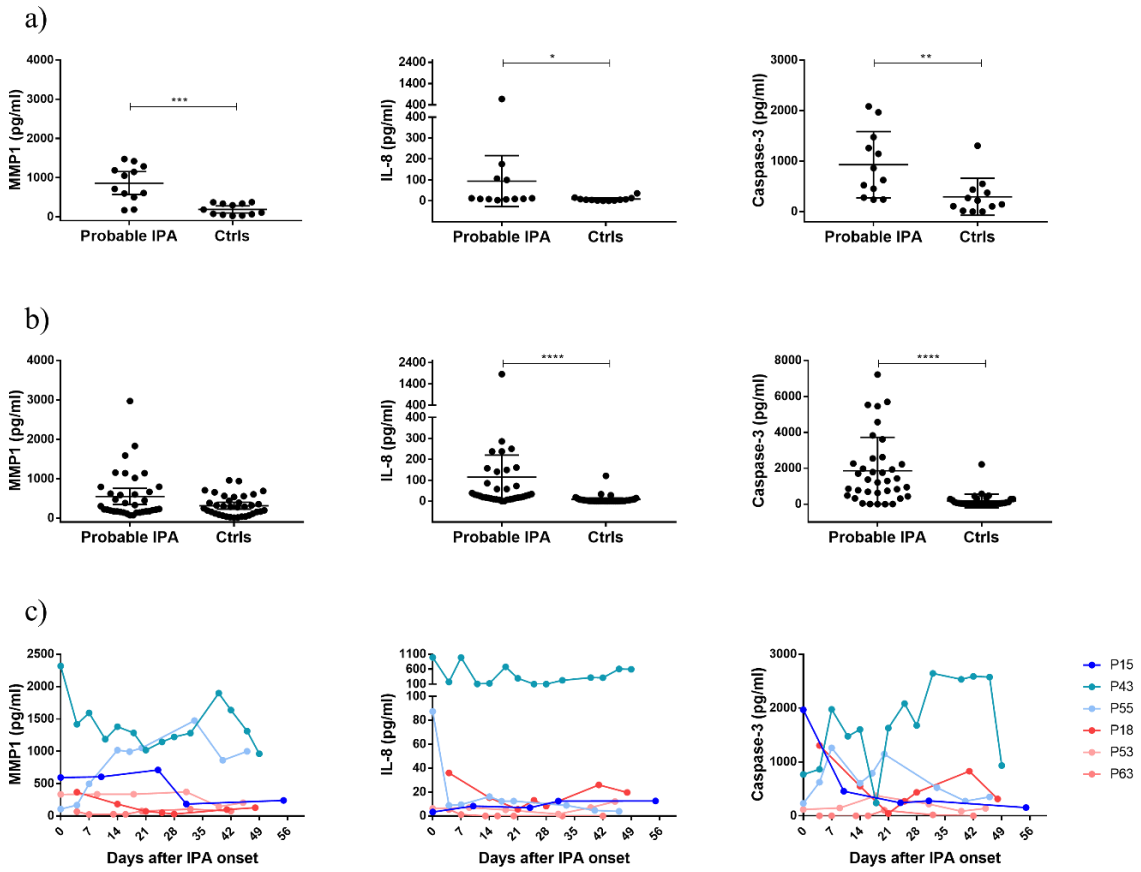

Figure 15: MMP1, IL-8 and caspase-3 serum levels in probable IPA cases and their matched controls. Adapted from Zoran *et al*., 2022. Protein levels were determined in probable IPA cases and their matched controls, obtained from **a)** the original, Würzburg cohort (N=6, balanced dataset) **b)** the Cardiff I cohort from Public Health Wales Microbiology (N=12) and **c)** across all collected samples from the original profiled cohort (Würzburg). Protein levels are shown as mean with 95% confidence intervals. Significant differences between cases and controls were investigated by Mann-Whitney test (* $p < 0.05$, ** $p < 0.01$, *** $p < 0.001$, **** $p < 0.0001$). N, number of investigated alloSCT patients.

3.2.4 Follow up assessment of selected potential molecular candidates

3.2.4.1 Evaluation of MMP1, IL-8 and caspase-3 in possible IPA cases

The category of possible IPA presents challenges not only due to vague classification and the limitations of currently used diagnostics assays but also due to underrepresented studies elucidating host response in possible IPA patients (Donnelly *et al.*, 2020). Thus, we next evaluated serum levels of MMP1, IL-8 and caspase-3 in possible IPA cases obtained from the Würzburg and Cardiff I cohort.

No significant differences in MMP1 serum levels were found between possible IPA cases and controls (Figure 16). We observed significantly elevated IL-8 ($p < 0.0001$) and caspase-3 ($p < 0.0001$) serum levels in possible IPA cases compared to controls in Cardiff I cohort only. This indicates clinical heterogeneity in investigated patients together with centre-specific differences due to the ambiguity of possible IPA and therefore necessitates further investigation.

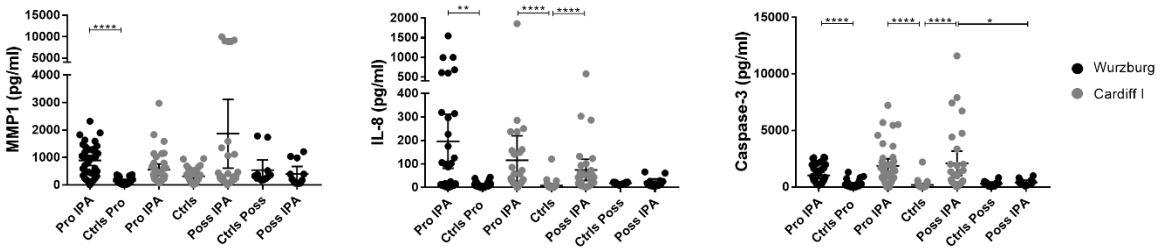

Figure 16: MMP1, IL-8 and caspase-3 serum levels in investigated possible IPA patients obtained from Würzburg and Cardiff (Cardiff I). Adapted from Zoran *et al.*, 2022. Possible IPA cases (Poss IPA) and controls (Ctrls) were obtained from the original, Würzburg cohort (black, N=6, n=24) and Cardiff I cohort from Public Health Wales Microbiology (grey, N= 11, n=66). Previously investigated probable IPA cases (Pro IPA) and controls (Ctrls) are added for comparison. Results are shown as mean serum levels with 95 % confidence intervals. Mann-Whitney test was used to determine significant differences between cases and controls (* $p < 0.05$, ** $p < 0.01$, *** $p < 0.001$, **** $p < 0.0001$). n, number of samples; N, number of investigated alloSCT patients.

3.2.4.2 Assessment of MMP1, IL-8 and caspase-3 in independent COVID-19 cohort

Next, we assessed serum levels of potential molecular candidates for IPA identified in alloSCT patients in an additional, non-classical patient cohort (Cardiff II). This independent COVID-19 cohort consisted of 20 CAPA patients suffering from aspergillosis as a secondary infection and 45 COVID-19 control patients (Suppl. Table S2). One time point per patient, altogether 65 samples were investigated by immunoassays.

No significant differences were observed in MMP1 serum levels among investigated patients (Figure 17). Furthermore, CAPA cases compared to COVID-19 controls demonstrated significantly decreased IL-8 ($p < 0.0001$) and caspase-3 ($p < 0.0001$) serum levels (Figure 17 a). Interestingly, our data revealed sex-specific differences in IL-8 and caspase-3 serum levels. In detail, higher IL-8 and caspase-3 levels were detected in male compared to female COVID-19 controls (Figure 17 b, c). Male CAPA patients demonstrated significantly decreased IL-8 ($p = 0.0001$) and caspase-3 ($p = 0.0004$) serum levels compared to COVID-19 controls. Female CAPA patients compared to COVID-19 controls demonstrated significantly lower serum levels of IL-8 ($p = 0.0409$) only. Considering the lower number of investigated samples obtained from female ($N = 19$) compared to male ($N = 46$) patients, further studies are encouraged to confirm our observations. Taken together, our data indicated a distinctive profile of investigated molecular candidates in the COVID-19 patient cohort compared to alloSCT patients, highlighted by lower serum levels in cases compared to controls.

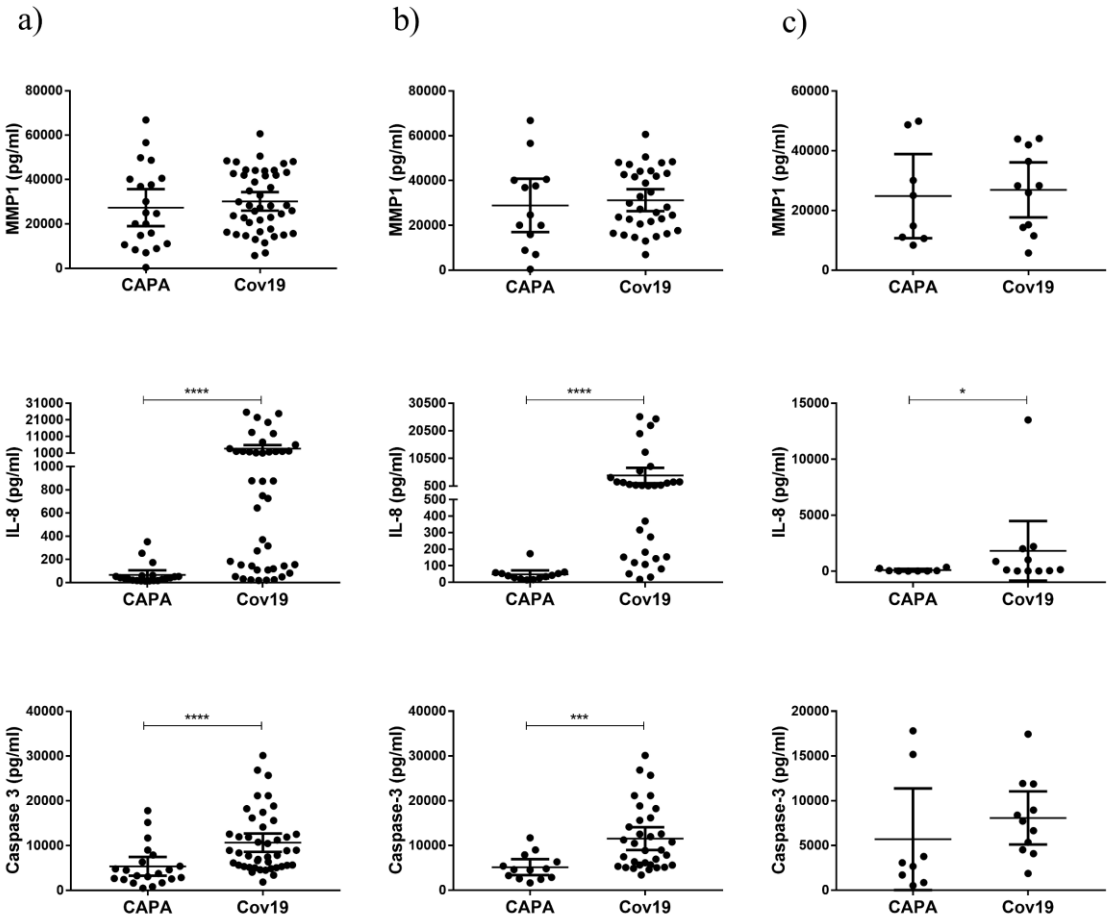

Figure 17: MMP1, IL-8 and caspase-3 serum levels assessed in an independent COVID-19 patient cohort (Cardiff II) comprised of CAPA cases (CAPA) and COVID-19 controls (Cov19). Adapted from Zoran *et al*., 2022. Levels of investigated molecular candidates are shown as mean with 95% confidence intervals **a)** across all COVID-19 patients (N=65; CAPA, N=20; Cov19, N=45), **b)** in male COVID-19 patients (N=46) and **c)** in female COVID-19 patients (N=19). Significant differences between CAPA cases and COVID-19 controls were determined by the Mann-Whitney test (* $p < 0.05$, *** $p < 0.001$, **** $p < 0.0001$). N, number of investigated patients.

3.2.4.3 Assessment of potential molecular candidates in the GvHD patient cohort

Considering alloSCT patients often develop GvHD, which induces a complex immune response, we investigated whether GvHD has an impact on identified characteristic IPA signature (Jaglowski *et al*., 2014; Ganapule *et al*., 2017). Thus, we investigated *LGALS2* and *MMP1* gene expression by qPCR and quantified MMP1, IL-8 and caspase-3 serum levels by immunoassays. The levels of selected molecular candidates were assessed in three patients suffering from severe GvHD (grade>2) and were compared to three previously profiled probable IPA cases. All investigated patients were obtained from the University Hospital of Würzburg (Würzburg cohort; Suppl. Table S1). In total, we investigated three to five samples per patient, collected closest to the time of GvHD diagnosis. Significantly higher MMP1 ($p < 0.0001$) and lower LGALS2 ($p < 0.0011$) expression was demonstrated in IPA compared to GvHD patients (Figure 18 a). IPA compared to GvHD patient cohort demonstrated significantly higher caspase-3 serum levels ($p < 0.0242$). A similar trend was observed in MMP1 serum levels, yet without significance. No significant differences between IPA and GvHD patient cohorts were observed in IL-8 serum levels (Figure 18 b). Taken together, in investigated patients *MMP1*, *LGALS2* and caspase-3 levels are significantly different between IPA and GvHD patient cohorts. Further studies, using larger patient cohorts are necessary to confirm these observations.

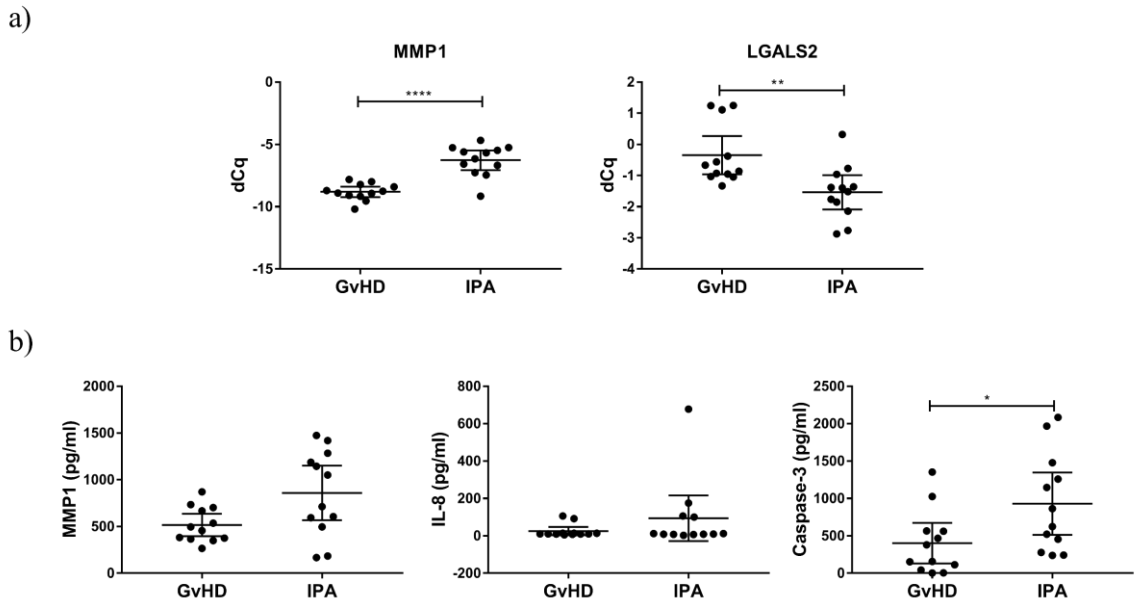

Figure 18: Assessment of potential molecular candidates indicating IPA in GvHD patient cohort. a) Gene expression and **b)** protein levels of potential molecular candidates are shown as mean levels with 95 % confidence intervals. Significant differences between GvHD (GvHD, N=3) and probable IPA patient (IPA, N=3) cohorts were investigated by Mann-Whitney test (* $p < 0.05$, ** $p < 0.01$, **** $p < 0.0001$). N, number of investigated patients.

3.2.4.4 Assessment of potential molecular candidates in A. fumigatus-infected moDCs

To further support our profiling results, we evaluated previously identified molecular candidates indicating IPA *in vitro*, using moDCs infected with inactivated *A. fumigatus* germ tubes or *E. coli*. Since investigated candidates might be involved in immune response at different stages, we performed a time-course experiment (3, 6, 9 and 24 hrs). *A. fumigatus*-infected moDCs demonstrated *MMP1* induction and *LGALS2* repression which supports our previous observations in probable IPA cases (Figure 19 a). Despite a similar expression trend upon both infections, we observed significant differences between *A. fumigatus* and *E. coli*-infected moDCs in early time points for *MMP1* ($p < 0.0001$) and the latest time points for *LGALS2* ($p < 0.001$). Furthermore, we confirmed elevated MMP1, IL-8 and caspase-3 levels in response to *A. fumigatus* infection (Figure 19 b). While MMP1 and IL-8 showed increased levels also in *E. coli*-infected moDCs, this was not observed for caspase-3, where we observed a significant difference between *A. fumigatus* and *E. coli*-infected moDCs ($p < 0.01$). To summarize, our *in vitro* findings further support the characteristic IPA signature identified in alloSCT patients.

a)

b)

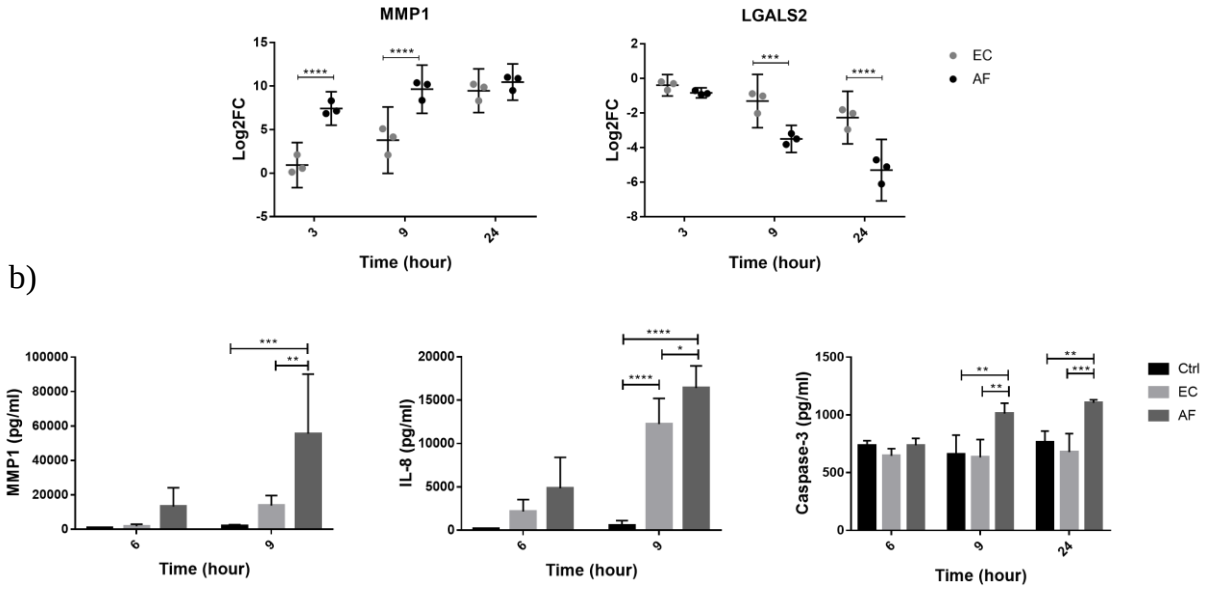

Figure 19: *In vitro* assessment of potential molecular candidates in moDCs infected with *A. fumigatus* (AF) and *E. coli* (EC). a) Gene expression (Log2FC) of *MMP1* and *LGALS2* relative to uninfected moDCs **b)** Protein levels of MMP1, IL-8 and caspase-3 quantified in cell supernatants. MoDCs were infected with inactivated *A. fumigatus* or *E. coli* for 3, 6, 9 and 24 hours. Gene expression was investigated by qPCR and protein levels were determined by ELISA. Data are shown for three biological replicates as mean with 95 % confidence intervals. Significant differences between investigated groups were determined by 2-way ANOVA, followed by Bonferroni's multiple comparison test.

Parts of the results presented in the following chapter have been published in:

Zoran T, Weber M, Springer J, *et al.* 2019. Treatment with etanercept and low monocyte concentration contribute to the risk of invasive aspergillosis in patients post allogeneic stem cell transplantation. Sci Rep **9**, 17231. doi:10.1038/s41598-019-53504-8.

Reproduced with permission from Springer Nature

3.3 Investigation of human risk factors contributing to the risk of invasive pulmonary aspergillosis in patients post alloSCT

The epidemiology of aspergillosis is evolving and new risk groups without traditional risk factors are emerging (Nedel *et al.*, 2009). Besides major risk factor, immunodeficiency, several studies are reporting severe influenza, CMV and recently COVID-19 disease as risk factors for aspergillosis (Garcia-Vidal, 2008; Schauwvlieghe *et al*., 2008; Armstrong *et al*., 2020). Due to new therapies in the last years, cases of aspergillosis have been reported in patients receiving monoclonal antibodies, agents for autoimmune disorders, small-molecule protein kinases and novel immunotherapies (Nedel *et al.*, 2009; Dunbar *et al*., 2019; Wudhikarn *et al*., 2020). However, little is known about the mechanisms of action of the above-mentioned drugs in association with *Aspergillus* spp. infection. Identification of high-risk patients in combination with diagnostic assays (e.g., galactomannan and *Aspergillus* DNA detection) may allow earlier recognition of IPA as well as prompt and targeted antifungal treatment (Kaya *et al*., 2017).

The following longitudinal case-control study was conducted by including additional alloSCT patients categorized as probable IPA cases and controls, part of the previous ASPIRE study. We investigated associations between collected clinical variables and IPA diagnosis promising for further multicentre studies. Identified novel risk factors might together with already known risk factors and currently used fungal biomarkers allow risk stratification and consequently allow earlier IPA diagnosis in high-risk alloSCT patients.

3.3.1 Study design and workflow

To investigate potential factors predicting the risk of IPA in alloSCT recipients, we retrospectively collected clinical information from 36 probable IPA patients and their 36 matched controls without *Aspergillus* infection (Training cohort). Dynamic and static clinical variables were collected after alloSCT, twice-weekly whenever feasible. Overall, we collected seven dynamic (continuous) variables comprised of blood cell counts and 96 binary (static) variables such as e. g. sex, age, underlying disease, and drug treatments (antibiotics, antifungals, antiviral and immunosuppressive agents).

The study design and main identified clinical variables significantly associated with IPA are shown in Figure 20.

By applying logistic regression, we first investigated associations between collected clinical variables and IPA diagnosis in the training cohort. Next, the most promising results and the predictive power of our model were further investigated in an additional validation cohort consisting of 23 probable IPA cases and 25 controls without *Aspergillus* infection. We further investigated the combined effect of the selected significant variables from the univariate models and evaluated *in vitro* the effect of the TNF inhibitor, etanercept, on monocyte-derived macrophages in the presence or absence of *A. fumigatus*.

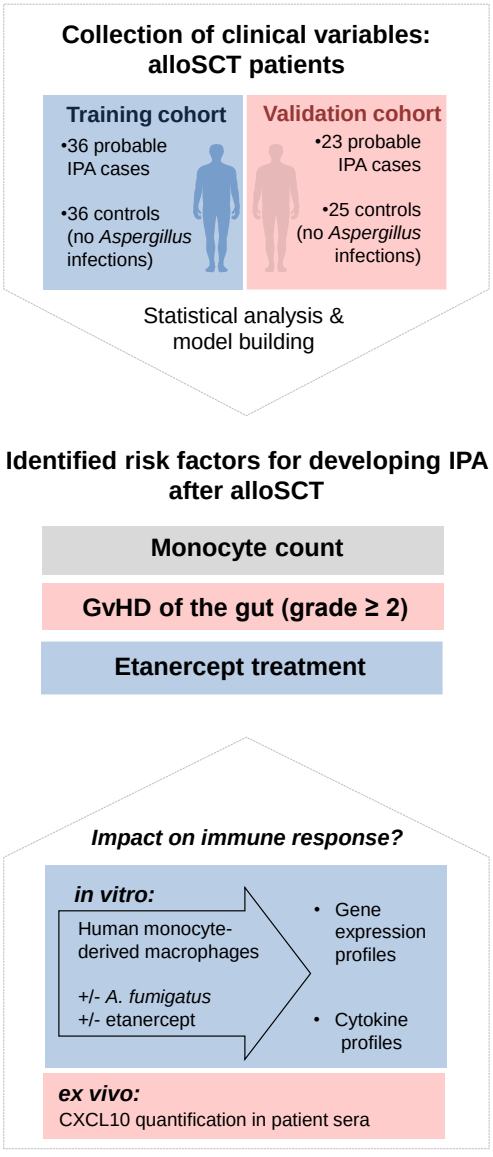

Figure 20: Study design and workflow. Modified from Zoran *et al*., 2019. Associations between collected clinical variables and diagnosis of IPA were first investigated in the training cohort and identified significant clinical variables were evaluated further in the validation cohort. Additionally, we investigated *in vitro* effects of etanercept on gene expression and cytokine profiles of monocyte-derived macrophages infected with *A. fumigatus*.

3.3.2 Dynamic clinical variables

Dynamic clinical variables included blood counts of different types of leukocytes and were collected weekly, four weeks prior to the IPA diagnosis. We performed time-dependent case-control matching, where cell counts of a case were compared to the closest time point of matched IPA control.

Monocyte, leukocyte and granulocyte counts were significantly lower ($p \leq 0.05$) in cases compared to controls, one week before IPA diagnosis (Table 17). In detail, granulocyte concentration in cases was significantly lower ($p = 0.0041$) with an average of 354 cells/µl compared to 648 cells/µl in controls, while, leukocyte concentration was significantly decreased ($p = 0.0014$) in cases with an average of 611 cells/µl compared to 1101 cells/µl in control patients. Monocyte concentration in cases was significantly reduced to an average of 44 cells/µl compared to control patients with 162 cells/µl ($p = 4.8 \times 10^{-6}$) (Table 17).

Table 17: Blood cell counts of IPA (case) and control patients (control) for four weeks prior to IPA diagnosis. Adapted from Zoran *et al.*, 2019. Reported are average concentration (x 10^2 / µl), odds ratio (OR) and likelihood ratio p-value.

cell type	week before IPA	case	control	OR (95% CI)	p-value
monocytes	1	0.44	1.62	13.3 (3.3 to 80.2)	4.8×10^{-06}
	2	0.44	1.14	3.9 (1.4 to 18.9)	6.2×10^{-03}
	3	0.32	0.88	11.9 (2 to 134)	2.7×10^{-03}
	4	0.24	1.62	589.0 (31 to 52497)	1.1×10^{-09}
leukocytes	1	6.11	11.01	1.1 (1.1 to 1.3)	1.4×10^{-03}
	2	5.18	9.61	1.0 (1.02 to 1.2)	1.1×10^{-02}
	3	4.53	9.03	1.1 (1 to 1.2)	8.7×10^{-03}
	4	6.71	11.8	1.1 (1 to 1.15)	4.0×10^{-02}
granulocytes	1	3.54	6.48	1.3 (1.1 to 1.7)	4.1×10^{-03}
	2	3.11	5.77	1.2 (0.98 to 1.65)	0.1
	3	2.44	5.90	1.3 (0.99 to 2)	5.5×10^{-02}
	4	1.09	26.78	6.4 (2.2 to 49)	2.2×10^{-07}

Overall, average granulocyte counts were significantly lower in cases compared to controls in the first ($p = 4.1 \times 10^{-03}$) and fourth week ($p = 2.2 \times 10^{-07}$) prior to IPA diagnosis. Leukocyte and monocyte counts showed significantly lower levels in cases compared to controls in all four weeks before IPA diagnosis (Table 17). Nevertheless, compared to leukocyte and granulocyte counts, decreased monocyte counts in IPA cases compared to controls, showed stronger significance in most of the investigated weeks prior to IPA diagnosis (Table 17, Figure 21). Furthermore, we confirmed significantly lower monocyte counts in cases compared to controls

also in the validation cohort, starting from the second week prior to IPA diagnosis (p = 0.018). However, no significant differences in monocyte levels between cases and controls were found in the first week before IPA diagnosis.

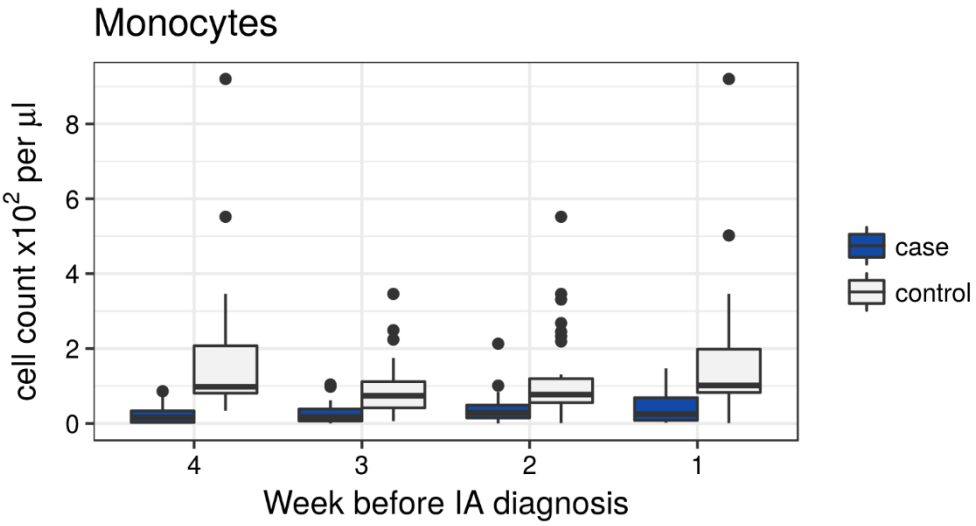

Figure 21: Monocyte concentrations of investigated cases and controls four weeks prior to the diagnosis of IPA. Taken from Zoran *et al*., 2019. Monocyte concentrations were significantly decreased in IPA cases (blue boxplots) compared to control patients (white boxplots) in all four weeks.

3.3.3 Static clinical variables

Among investigated static clinical variables, seven were significantly ($p < 0.05$) associated with the diagnosis of IPA (Table 18): positive *Aspergillus* PCR and galactomannan ELISA, treatment with dexamethasone, nitroimidazole, etanercept, positive *Enterococcus faecalis* blood culture and severe GvHD of the gut (grade ≥ 2). Positive *Aspergillus* PCR and galactomannan ELISA are directly connected to the diagnosis of IPA and do not represent independent variables. Furthermore, corticosteroid treatment with dexamethasone, antibiotic treatment with nitroimidazole and the presence of *E. faecalis* in the blood culture could not be confirmed as independent risk factors in the validation cohort. Thus, we excluded these five variables from further analysis. GvHD of the gut (grade ≥ 2) and administration of etanercept were significantly associated with the risk of IPA, confirmed also in the validation cohort and therefore evaluated further (Figure 20).

Table 18: Identified clinical variables significantly associated with the IPA. Adapted from Zoran *et al*., 2019. Reported are the number of cases and controls (nr.), the proportion of males and females (m:f), odds ratio (OR) and likelihood ratio p-value.

clinical variable	nr. of cases (m:f)	nr. of controls (m:f)	OR (95% CI)	p-value
galactomannan	28 (11:17)	3 (0:3)	38.5 (10.5 to 192.8)	3.10×10^{-10}
Enterococcus faecalis	11 (5:6)	1 (0:1)	15.4 (2.7 to 290.6)	7.20×10^{-04}
etanercept	13 (6:7)	3 (2:1)	6.2 (1.8 to 29.4)	3.50×10^{-03}
dexamethasone	17 (8:9)	6 (3:3)	4.5 (1.6 to 14.3)	4.70×10^{-03}
GvHD of the gut (grade ≥ 2)	13 (5:8)	4 (3:1)	4.5 (1.4 to 17.7)	1.08×10^{-02}
nitroimidazole	22 (8:14)	12 (3:9)	3.1 (1.2 to 8.5)	1.70×10^{-02}
***Aspergillus* PCR**	15 (6:9)	8 (3:5)	4.0 (1.2 to 14)	2.00×10^{-02}

While we observed a significant association of severe GvHD of the gut (grade ≥ 2) with IPA diagnosis ($p = 1.08 \times 10^{-02}$), the general GvHD variable, which included less severe types and GvHD affecting other organs such as skin, was not significantly associated with the IPA. Our results demonstrated, that are IPA cases at increased risk of developing GvHD (36 %) compared to controls (11 %). In detail, 13/36 IPA patients developed GvHD, while in the control group 4/36 patients. Significant association of GvHD of the gut (grade ≥ 2) with IPA diagnosis was confirmed as well in the validation cohort (OR = 6.92, 95 % CI= 1.51 to 50.24, $p = 1.1 \times 10^{-02}$).

Among investigated drug treatments, etanercept was the only one significantly associated with IPA diagnosis ($p = 3.5 \times 10^{-03}$) and confirmed in the additional validation cohort. We observed that alloSCT patients receiving etanercept treatment have a higher probability of developing IPA (36%) compared to control patients (8 %). In detail, among investigated alloSCT patients, etanercept was administered to 13/36 IPA cases and 3/36 control patients. Similar trend was observed also in the validation cohort, where 80 % (8/10) of patients under etanercept treatment developed IPA (OR = 6.13, 95 % CI = 1.32 to 44.5, p = 0.019).

Next, we added etanercept as a new variable to the GvHD model. As expected, the predictive power of our model significantly increased (p = 0.015). Our results showed that patients with severe GvHD of the gut (grade ≥ 2) under etanercept treatment showed the highest risk to develop IPA (100 %, 10/10), in contrast to patients with severe GvHD of the gut (grade ≥ 2) not receiving etanercept treatment (43%, 3/7).

3.3.4 Combination of identified clinical variables associated with IPA

A multiple logistic regression model was used to investigate a combination of previously identified risk factors: severe GvHD of the gut (grade ≥ 2), etanercept administration and low monocyte concentration. The model for all three variables was established for four weeks prior to IPA diagnosis due to previously observed low monocyte counts. To evaluate the performance of the model, we used receiver operating characteristic (ROC) analysis and investigated selected three variables for original and validation data for each week separately. We estimated the area under the ROC curve (AUC) as a measure of the predictive accuracy of our model. Statistical estimates of the area under the ROC curve (AUC) are shown in Figure 22. While our model performed a good classification in the first (AUC = 0.62, 95 % CI = 0.31 to 0.88) and fourth week (AUC = 0.68, 95 % CI = 0.31 to 0.89), performance was exceptionally well in week two (AUC = 0.85, 95 % CI= 0.73 to 1) and week three (AUC = 0.78, 95 % CI = 0.54 to 1). Observed lower performance in the first week might be due to the elevated monocyte counts in several cases, which lowered the sensitivity of our model.

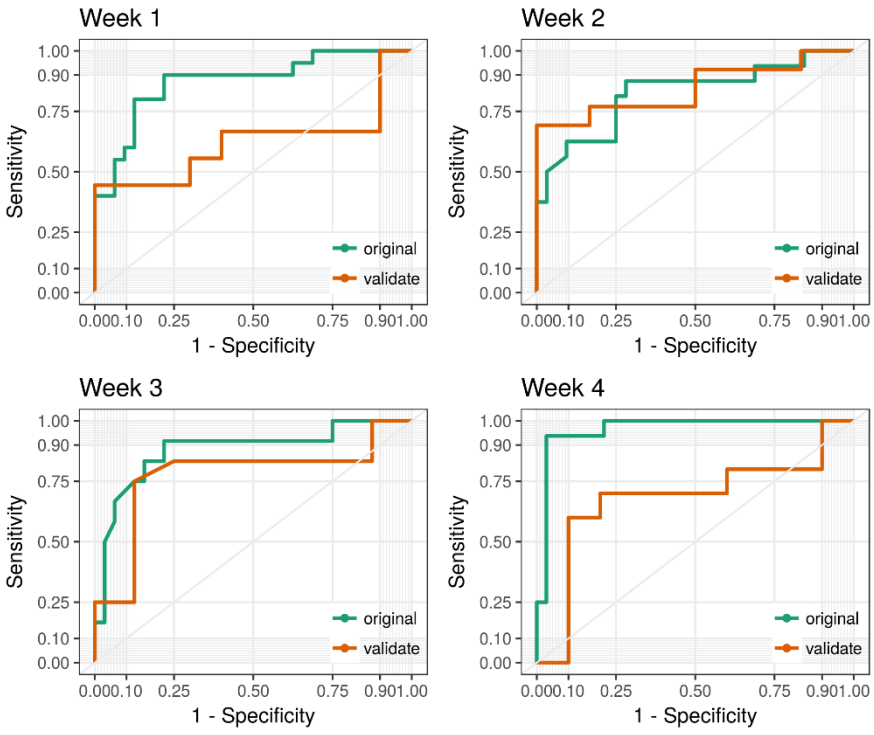

Figure 22: Performance of multivariable logistic regression models for training and validation dataset shown by ROC curves. Taken from Zoran *et al.*, 2019. A combination of previously identified clinical variables significantly associated with IPA diagnosis: severe GvHD of the gut (grade ≥ 2), etanercept administration and low monocyte concentration were investigated in the training and validation cohort.

3.3.5 Effects of etanercept on MDM infected with *A. fumigatus*

To investigate the effect of etanercept (TNF inhibitor) on the immune response during *A. fumigatus* infection we used MDM, one of the main TNF-α producing immune cells, pivotal in response to *A. fumigatus* infection (Dagenais and Keller, 2009). To get a comprehensive insight, we combined transcriptome and cytokine profiling using RNA-seq and immunoassays. MDM were confronted with live *A. fumigatus* germ tubes in the presence or absence of etanercept (Figure 20). Unstimulated MDM, as well as MDM co-cultured with etanercept only, were used as a control.

3.3.5.1 Transcriptome profiling

RNA-seq revealed the highest number of DEGs in MDM infected with *A. fumigatus*, indicating a strong immune response following *A. fumigatus* exposure in absence of etanercept (Figure 23). We identified 388 DEGs in MDM infected with *A. fumigatus* compared to control, uninfected MDM. From these, 382 DEGs were induced while only 6 genes were repressed (*LRRC25, HOXA1, HHEX, RASL11B, ID3, AL034397.3*).

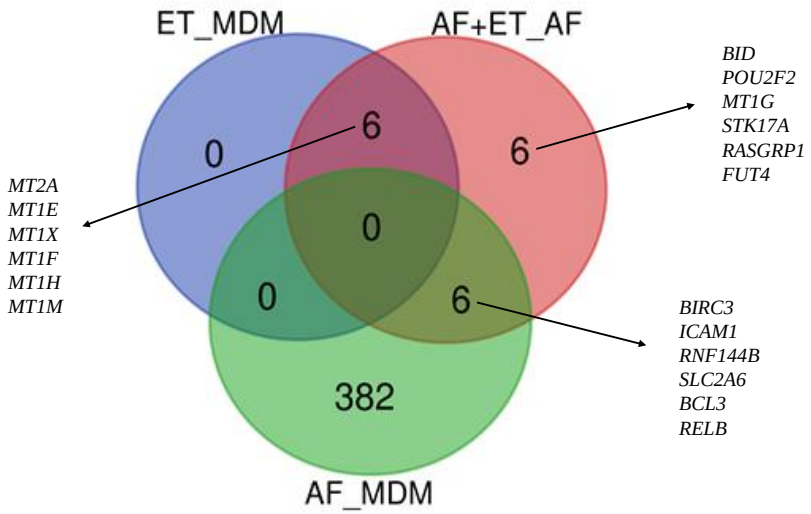

Figure 23: RNA-seq of MDM infected with *A. fumigatus* in the presence or absence of etanercept. MDM were infected with live *A. fumigatus* germ tubes (MOI 0.5) in the presence or absence of etanercept for six hours and investigated by RNA-seq. Venn diagram presents the number of identified DEGs in MDM infected with *A. fumigatus* in presence of etanercept (AF+ET_AF), in MDM co-cultured with etanercept (ET_MDM) and MDM infected with *A. fumigatus* (AF_MDM).

We observed more than 40-fold induction of expression in genes encoding interleukins and chemokines (e.g., *IL-6*, *CXCL1*, *CXCL2*, *CXCL3*, *CXCL3*, *CCL4*) as well as other immunity-related genes such as *TNF*, *MMP1* and others (Suppl. Table S5). In contrast, etanercept itself did not significantly induce the expression of any gene, yet 6 genes encoding metallothioneins were significantly repressed (*MT2A*, *MT1E*, *MT1X*, *MT1F*, *MT1H*, *MT1M*) (Figure 23).

Next, we compared gene expression of *A. fumigatus*-infected MDM in the presence of etanercept to MDM infected with *A. fumigatus* only. We identified 18 significantly DEGs in MDM infected with *A. fumigatus* in presence of etanercept (Table 19, Figure 23). Again, we observed repression in genes encoding metallothioneins: *MT1G MT2A*, *MT1E*, *MT1X*, *MT1F*, *MT1H* and *MT1M*. Additionally, we observed repression of genes involved in the antimicrobial humoral response, apoptotic processes and NFkB signalling (*BID*, *BIRC3*, *POU2F2*, *BCL3*, *ICAM1*, *RELB*, *RNF144B*, *SLC2A6*, *STK17A*, *RASGRP1*, *FUT4*) (Table 19, Figure 23). While TNF-α expression was not significantly altered, other genes involved in TNF-α signalling were significantly downregulated: *RELB*, *ICAM1*, *BCL3*, *BIRC3* (Table 19). These genes together with TNF-α were in absence of etanercept in MDM infected with *A. fumigatus*, induced.

Table 19: DEGs identified in MDM infected with *A. fumigatus* in presence of etanercept compared to MDM infected with *A. fumigatus* only. Adapted from Zoran *et al*., 2019. MDM were infected with live *A. fumigatus* germ tubes (MOI 0.5) in the presence or absence of etanercept (6 hrs) and investigated by RNA-seq. DEGs were identified by DESeq, applying a cut-off of at least 0.5 and an adjusted p-value of 0.05.

gene	fold change	log2FC	p-value (adj.)	description
BID	0.673	-0.572	3.493×10^{-2}	BH3 interacting domain death agonist
BIRC3	0.415	-1.269	3.925×10^{-4}	baculoviral IAP repeat containing 3
POU2F2	0.516	-0.955	1.562×10^{-3}	POU class 2 homeobox 2
BCL3	0.388	-1.366	4.835×10^{-2}	B-cell CLL/lymphoma 3
ICAM1	0.693	-0.530	4.835×10^{-2}	intercellular adhesion molecule 1
RELB	0.613	-0.706	6.490×10^{-3}	RELB proto-oncogene, NF-κB subunit
MT1G	0.059	-4.095	2.087×10^{-30}	metallothionein 1G
MT2A	0.239	-2.062	5.005×10^{-17}	metallothionein 2A
RNF144B	0.542	-0.885	5.383×10^{-8}	ring finger protein 144B
SLC2A6	0.392	-1.350	1.588×10^{-10}	solute carrier family 2 member 6
STK17A	0.722	-0.469	4.276×10^{-2}	serine/threonine kinase 17a
MT1E	0.199	-2.327	3.336×10^{-20}	metallothionein 1E
RASGRP1	0.557	-0.844	4.276×10^{-2}	RAS guanyl releasing protein 1
MT1X	0.105	-3.250	2.980×10^{-17}	metallothionein 1X
FUT4	0.640	-0.644	1.128×10^{-4}	fucosyltransferase 4
MT1F	0.197	-2.344	8.881×10^{-16}	metallothionein 1F
MT1H	0.049	-4.357	2.368×10^{-9}	metallothionein 1H
MT1M	0.000	-Inf	1.611×10^{-4}	metallothionein 1M

3.3.5.2 Cytokine profiling

Using immunoassays, we investigated the potential effects of etanercept on the immune relevant proteins during *A. fumigatus* infection. Significantly altered ($p < 0.05$) protein levels of investigated cytokines, quantified in cell supernatants are shown in Table 20. *A. fumigatus*-infected MDM compared to unstimulated MDM (control), demonstrated significantly elevated levels of FGF, IL-9, IFN-γ, eotaxin, IL-17, IL-6, TNF-α, MIP1beta, IL-8 and CXCL10. On the contrary, MDM stimulated with etanercept compared to unstimulated MDM, demonstrated significantly elevated levels of MCP1 and IL1RA. As hypothesized, MDM infected with *A. fumigatus* in presence of etanercept compared to MDM infected with *A. fumigatus* only, showed significantly decreased levels of TNF-α (Figure 24 a). Interestingly, the presence of etanercept led also to significantly decreased levels of GCSF and CXCL10 in *A. fumigatus*-infected MDM (Table 20, Figure 24 a).

Table 20: Protein quantification of immune relevant proteins in cell supernatants MDM infected for six hours with live *A. fumigatus* germ tubes (MOI 0.05) in the presence (AF_ET) or absence of etanercept (AF). Taken from Zoran *et al.*, 2019. Cell supernatants of three donors were investigated by immunoassays and significant differences were investigated by Wilcoxon-Mann-Whitney tests ($p < 0.05$).

protein	concentration (pg/ml)		p-value
	MDM	**AF**	
FGF	0.00	63.38	1.16×10^{-2}
IL9	28.86	474.92	1.36×10^{-2}
IFN-γ	17.27	144.11	1.66×10^{-2}
Eotaxin	0.00	84.71	1.98×10^{-2}
IL17	0.00	171.34	2.06×10^{-2}
IL6	10.32	580.14	2.33×10^{-2}
TNF-α	14.75	1365.21	2.86×10^{-2}
MIP1beta	267.19	8614.88	3.31×10^{-2}
IL8	523.67	13425.00	4.16×10^{-2}
CXCL10	61.90	1624.30	4.52×10^{-2}
	MDM	**ET**	
MCP1	284.47	374.50	7.88×10^{-3}
IL1RA	9850.40	12335.72	4.24×10^{-2}
	AF	**AF_ET**	
CXCL10	1624.28	248.23	3.69×10^{-4}
TNF-α	1365.21	440.78	1.04×10^{-2}
GCSF	19.16	15.30	3.50×10^{-2}

We further investigated CXCL10 serum levels in four IPA patients under etanercept treatment and compared them to four IPA patients without etanercept treatment (altogether 80 samples). We observed significantly lower CXCL10 serum levels ($p = 0.017$) in IPA patients receiving etanercept compared to IPA patients without etanercept treatment (Figure 24 b).

The main findings of our *in vitro* study are summarized in Figure 24 c-d. To sum up, we demonstrated etanercept treatment represses genes located downstream of the TNF-α signalling pathway as well as lowers TNF-α and CXCL10 secretion *in-vitro* and *ex-vivo*. Although in MDM infected with *A. fumigatus* in the presence of etanercept, *CXCL10* and *TNF-α* were not significantly altered, we observed their repression.

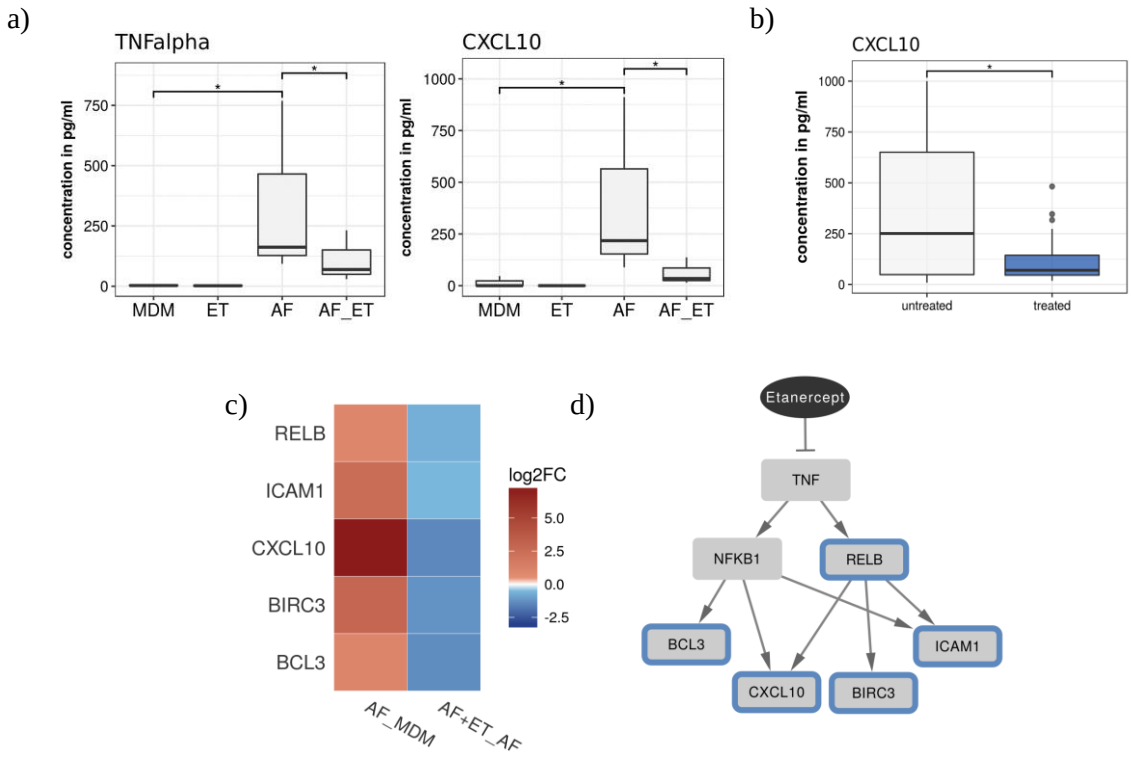

Figure 24: Summarized main findings of the effects of etanercept on MDM during *A. fumigatus* infection. Adapted from Zoran *et al*., 2019. **a)** TNF-α and CXCL10 levels in supernatants of MDM infected with *A. fumigatus* in the presence (AF_ET) or absence of etanercept (AF) detected by immunoassays. Unstimulated MDM (MDM) and MDM stimulated with etanercept only (ET) were used as control. Infection was performed with MDM generated from three donors and live *A. fumigatus* germ tubes (MOI 0.5) and/or etanercept, for six hours. **b)** Mean serum CXCL10 levels of four IPA patients under etanercept treatment (treated) and four IPA patients without treatment (untreated). **c)** Downregulated genes during *A. fumigatus* infection in presence of etanercept (AF+ET_AF) **d)** Network summarizing the effect of etanercept on the NF-κβ target genes. Data are shown as mean with SD (a, b) and significant differences are highlighted by * ($p \leq 0.05$, Wilcoxon-Mann-Whitney test).

4. Discussion

4.1 *In vitro* investigation of human transcriptome profiles in response to *A. fumigatus* infection

Patient recruitment and obtaining an appropriate sample size, due to the low incidence of IPA among alloSCT patients, are some of the common challenges in conducting clinical studies. In addition, many IPA cases might be missed or diagnosed post mortem (Ribaud, 2006). Until now human transcriptome response to *A. fumigatus* has been mostly studied using *in vitro* and *in vivo* models (Bruno *et al*., 2020; Pakshir *et al.*, 2020; Steinbrink *et al*., 2020). Although these models cannot fully reflect the complexity and dynamics of the human body, they are a good starting point to characterize host response in reproducible and standardized experimental conditions (Bruno *et al*., 2020). Therefore, before the profiling of selected IPA cases (chapter 3.2), we conducted *in vitro* study to investigate the potential distinctive host miRNA and mRNA signatures indicating *A. fumigatus* infection and explore the feasibility of miRNA investigation as well as the potential of miRNAs as host biomarkers.

Host transcriptome responses to *A. fumigatus* were characterized using primary moDCs. These immune cells are linking innate and adaptive immunity and are crucial for the development and maintenance of Th1 cell response to *A. fumigatus* infection (Palucka and Bancherau, 1999; Cenci *et al*., 1997). Overall, our *in vitro* model indicated a higher number of DEGs compared to DEMs following *A. fumigatus* or *E. coli* exposure, which was previously observed by Dix *et al.* (2017). Hence, in the context of biomarker screening, mRNA profiling might provide a higher number of potential biomarker candidates or distinctive signatures for further evaluation, which was observed also in other research fields (Li and Li, 2020; Katiyar *et al*., 2021).

4.1.1 Characteristic genes expression signatures in response to *A. fumigatus* infection

Recently, it has been demonstrated that blood-based gene expression signatures enable discrimination between different fungal species such as *A. fumigatus*, *Candida albicans* and *Rhizopus oryzae* (Bruno *et al*., 2020). Gene expression profiles enable also a differentiation between viral from bacterial acute respiratory infection (Zaas *et al.*, 2009). Considering respiratory infections are common complications post alloSCT and the importance of timely diagnosis and prompt treatment, host blood transcriptome signatures may present a non-invasive approach to support the diagnosis of respiratory infections (Cordonnier *et al.*, 1986; Astashchanka *et al*., 2021).

Our *in vitro* study indicated common as well as distinct transcriptome signatures in *A. fumigatus*- and *E. coli*-infected moDCs, which is consistent with the previous research (Dix *et al*., 2015; Dix *et al*., 2017). Among top induced immune-related DEGs in response to *A. fumigatus* and *E. coli* infection were genes encoding matrix metallopeptidases (e.g., *MMP1*, *MMP3*), cytokines (e.g., *CXCL8, IL6, IL1B*) and others (e.g., *SERPINB2, PTGS2*), suggesting these genes as universal markers of infection in our model. Within groups mentioned above, we observed also genes altered in response to *A. fumigatus* infection only (e.g., *MMP9,* C*XCL9)*. Among other dysregulated genes identified in *A. fumigatus*-infected moDCs only, were genes encoding integrins (e.g., *ITGAL, ITGBL1*), pattern recognition receptors (e.g., *CLEC7A, TLR3*) and galectins (e.g., *LGALS2*), suggesting these as interesting candidates for further studies.

Recognition of *A. fumigatus* by pattern recognition receptors such as TLRs and C-type lectin receptors (e.g., Dectin-1) is a pivotal step in the activation of antifungal response (Bourgeois and Kuchler, 2012). Dectin-1 (encoded by *CLEC7A),* is one of the key receptors, recognizing fungal *β-1,*3 glucans on the surface of *A. fumigatus* and has been extensively studied (Brown, 2006). The exact role of galectins, in particular, galectin-2 (encoded by *LGALS2*) in response to *A. fumigatus* infections, has not been fully elucidated. These β-galactosidase-binding lectins are expressed by several immune cells in response to infection (Barondes *et al*., 1994). It has been reported that galectins are involved in the recognition of fungal glycans, the interaction between immune cells, recruitment of neutrophils and regulation of cytokines (Vasta *et al*., 2009; Snarr *et al*., 2020). Integrins are important in communication between the lung epithelial cells and immune cells, lung homeostasis and their involvement in response to respiratory infections have already been reported (Meliopoulos *et al*., 2016). Matrix-metallopeptidases (MMPs), the family of proteolytic enzymes degrading matrix and non-matrix proteins, play an important role during respiratory infections (Gross and Lapiere, 1962; Elkington *et al*., 2005). MMPs process cytokines and chemokines, facilitate leukocyte recruitment and are crucial in the tissue remodelling in the lungs (Elkington *et al*., 2005). MMP9 (gelatinase B) is suggested as an indicator of lung injury and its secretion is associated with IL-8 (Gibson *et al*., 2006). Altered expression of *MMP1* and *MMP2* in response to *A. fumigatus* infection was previously demonstrated in monocytes, moDCs and bronchial epithelial cells (Cortez *et al.,* 2006; Mezger *et al*., 2008a; Gomez *et al*., 2010). Cytokines are crucial regulators of the immune response to infection and are secreted from various cell types (Tisoncik *et al*., 2012). Their dysregulation

in response to *A. fumigatus* was demonstrated in various *in vitro* and *in vivo* models (Cortez *et al*., 2006; Gomez *et al*., 2010; Bruno *et al*., 2020; Steinbrink *et al*., 2020).

4.1.2 Dysregulated miRNA in response to *A. fumigatus* and feasibility of miRNA expression profiling

Identified dysregulated miRNAs (hsa-miR-155-5p, hsa-miR-155-3p, hsa-miR-9-5p and hsa-miR-1303) in response to both, *A. fumigatus* and *E. coli* infections are known regulators of immune response to infections (Bazzoni *et al*., 2009; Vigorito *et al*., 2013; Au *et al*., 2016). Induction of hsa-miR-155 and hsa-miR-9 in response to LPS and *A. fumigatus* has been previously demonstrated in monocytes and moDCs (Das Gupta *et al*., 2014; Dix *et al.* 2017). In contrast, dysregulation of hsa-miR-1303 expression to our knowledge has not been yet reported in the context of *A. fumigatus* infection and its role during fungal infections is poorly understood (Pakshir *et al*., 2020).

Among specifically induced miRNAs after infection with *A. fumigatus*, were hsa-miR-129, hsa-miR-132 and hsa-miR-212, which is in line with the previous research (Das Gupta *et al*., 2014; Dix *et al*., 2017). To date, these miRNAs are one of the most commonly reported miRNAs in response to *A. fumigatus* infection (Pakshir *et al*., 2020). Recently Lin *et al*. (2021) demonstrated hsa-miR-129-5p induction in a keratitis mouse model infected with *Fusarium solani*. Induction of hsa-miR-132/212 in moDCs has been previously reported during *C. albicans* infection (Dix *et al.* 2017). Hsa-miR-132/212 are well-known regulators of TLR signalling and are therefore important in pathogen recognition (Nahid *et al.*, 2013; Pakshir *et al*., 2020). This might explain hsa-miR-132-3p induction in *A. fumigatus*- and *E. coli*-infected moDCs in the follow-up experiments (Figure 9). Furthermore, RNA-seq validation by qPCR showed downregulation of hsa-miR-204-5p in *A. fumigatus*-infected and weak induction in *E. coli*-infected moDCs. Interestingly this miRNA was identified as DEM only in *A. fumigatus*-infected moDCs. The exact role of hsa-miR-204-5p during respiratory infections in particular *A. fumigatus* infection is not well understood. Recently, downregulation of hsa-miR-204-5p has been demonstrated in sepsis and acute lung injury, leading to activation of the NF-κB pathway and proinflammatory cytokine release (Li *et al*., 2021b). Downregulation of hsa-miR-204-5p has been reported in fungal keratitis corneas infected with *A. flavus* and it has been linked to corneal epithelial cell proliferation and migration during wound healing (Boomiraj *et al*., 2015). Hsa-miR-204-5p repression has also been demonstrated in the response to *C. albicans* and bacterial infections (Matsushima *et al*., 2011; Li *et al*., 2014). Discussed above indicates the

complexity of miRNAs and their involvement in the regulation of immune response to various pathogens as well as highlights the limitations of using simple *in vitro* models for screening of characteristic miRNA expression signatures.

One miRNA can regulate numerous genes and is involved in various biological processes, which together with a lack of consistency and standardization in miRNA research, presents a methodological challenge for the validation of reported miRNAs (Kuhn *et al*., 2008; Moldovan *et al*., 2014). Challenges related to the validation of reported miRNAs have been observed in various fields. For instance, proposed miRNA biomarkers in cancer research were not consistent even in a specific investigated cancer (Kirschner *et al*., 2013; Miotto *et al*., 2014). Furthermore, induction of hsa-miR-21 has been demonstrated in patients with prostate, liver, lung, breast, colorectal and endometrial cancer (Saliminejad *et al*., 2019). However, the specificity of miRNAs as host biomarkers could be increased by using a combination of miRNAs or integrated miRNA-mRNA signatures.

The present study demonstrated distinctive signatures associated with *A. fumigatus*-infected moDCs, consisting of nine miRNAs and their 61 negatively correlated target genes (Figure 6). In addition, we showed the potential to discriminate between *A. fumigatus*- and *E. coli*-infected moDCs based on hsa-miR-204-5p and its predicted negatively correlated target genes. Moreover, further investigation by qPCR suggested hsa-miR-204-5p might in response to *A. fumigatus* have a role in *IL1B* and *ITGB3* regulation. *In silico* prediction of miRNA-mRNA interactions requires experimental validation. The establishment of reporter systems for direct validation of miRNA-mRNA interaction is labour intense and it was out of the scope of the present study (Kuhn *et al*., 2008). Hence, the experimental validation of reported *in silico* predicted miRNA-mRNAs interactions is encouraged. As we used an *in vitro* model based on moDCs and well-standardized conditions, it would be useful to extend the current findings by validating the proposed host transcriptome signatures in other myeloid immune cell types or biofluids. Our *in vitro* model does not assess to what extent the identified transcriptome signatures allow to differentiate aspergillosis from other respiratory infections and does not account for differences in inter-host variability or host immune response to different fungal strains. Thus, validation of these signatures in human material (e.g., detection in biofluids) is encouraged. Despite the limitations, the present study provided valuable insights into the host transcriptome in particular miRNA profiles in response to *A. fumigatus* infection, highlighted the complexity of miRNA biomarker research and suggested potential miRNAs and their targets promising for further investigation.

4.2 Investigation of characteristic molecular signatures indicating IPA in patients post alloSCT

To investigate potential host molecular candidates indicating IPA, we next conducted a pilot, longitudinal, case-control study. As alloSCT patients are severely ill and immunocompromised, we screened for blood-based molecular candidates, which is compared to obtaining BAL specimens less invasive approach (Lass-Flörl, 2019; Feinstein *et al*., 2021). Profiling on transcriptome and protein levels provides a broader spectrum of potential biomarker candidates and characteristic signatures as well as offers deeper insights into complex diseases (Quezada *et al*., 2017). Our study highlighted that not all investigated molecular candidates showed the same potential on transcriptome and protein levels (e.g., *LGALS2* encoding galectin-2), further supporting the used multilevel approach. Alterations in gene expression might enable faster detection of pathophysiological changes compared to proteins that might undergo posttranslational modifications. Yet, proteins are directly connected to pathophysiological processes and have usually better biological stability (Xi *et al*., 2017; Shao *et al*., 2019). After initial broad transcriptome profiling of investigated IPA cases and their matched controls by RNA-seq, we further evaluated selected potential molecular candidates by qPCR and immunoassays. While qPCR presents a sensitive thus labour-intense method that requires a certain level of expertise and the need for standardization, immunoassays such as ELISA in case of characterized proteins might be a more straightforward method to implement in diagnostic laboratories. As these methods are frequently used in laboratories and commercially available, further evaluation of identified molecular candidates in larger, multicentre studies is encouraged (Quezada *et al*., 2017).

4.2.1 Suggested potential molecular candidates indicating IPA

Our study revealed characteristic IPA signature in investigated alloSCT patients, consisting of *LGALS2* repression and *MMP1* induction along with elevated IL-8 and caspase-3 protein levels. Considering the low IPA incidence during the timeframe of this PhD project and consequently a low number of profiled patients, we performed additional follow up investigations to further evaluate our profiling results. Investigation of six relevant *in vitro* studies, focusing on gene expression of myeloid cells following *A. fumigatus* exposure further supported our transcriptome results obtained by RNA-seq. While we observed repression of *LGALS2* in two investigated studies, MMP1 induction was found in all six studies. Investigated *in vitro* studies used different experimental setups such as time of infections, cell type, *A. fumigatus*

morphology, MOI and readouts (RNA-seq, microarrays). Furthermore, *in vitro* models present simplified and more standardized models compared to patient blood samples which might explain observed *LGALS2* downregulation in two studies only. In addition, we confirmed the identified characteristic IPA signature (*MMP1*-*LGALS2*-IL8-caspase-3) in our *in vitro* model using *A. fumigatus*-infected moDCs.

MMP1 encodes matrix metallopeptidase 1 (MMP1), collagenase which degrades also IL-1β, TNF-α and several chemokines (Hatfield *et al.*, 2010; Herrera *et al.*, 2013). Excess of MMP1 activity might lead to tissue destruction and consequently, help *A. fumigatus* to invade blood vessels and disseminate to other organs. Up to date, clinical studies investigating MMP1 levels in patients suffering from aspergillosis are rare. Recently, elevated MMP1 levels in the blood have been associated with the severity of CPA (Huang *et al.*, 2021), suggesting a potential to investigate this candidate also in other clinical manifestations of aspergillosis. The exact role of galectins during *A. fumigatus* infection is not well characterized. Recently, Snarr *et al.* (2020) demonstrated elevated galectin-3 serum levels in *A. fumigatus*-infected mice and increased susceptibility of galectin-3 deficient mice to *A. fumigatus* infection. Increased galectin-3 serum levels were reported also in patients suffering from aspergillosis (IPA and CPA) compared to healthy individuals (Snarr *et al.*, 2020). While our data demonstrated *LGALS2* (encoding galectin-2) as the most promising biomarker candidate on the gene expression level, no differences in galectin-2 protein levels were observed between cases and controls. Galectin-2 remains one of the least characterized members of the galectin family and its role during *Aspergillus* spp. infection is not known. Current research indicates galectin-2 acts as an inducer of T-cell apoptosis and modulates inflammation through binding proinflammatory cytokine, lymphotoxin-α (Ozaki *et al.*, 2004; Sturm *et al.*, 2004). Further research is encouraged to understand the exact role of galectin-2 in the context of *Aspergillus* spp. infections.

IL-8, a chemotactic factor attracting neutrophils, basophils, and T-cells, is an important mediator of an inflammatory response (Baggiolini *et al.*, 1989; Heinekamp *et al.*, 2015). Several studies reported elevated IL-8 serum or BAL levels in patients suffering from aspergillosis and this cytokine has already been suggested as a biomarker candidate for IPA in patients at risk (Gonçalves *et al.*, 2017; Heldt *et al.*, 2018). As part of the host immune responses to *Aspergillus* spp., pro-caspases are induced via TLRs and dectin-1 (Tomalka and Hise, 2015). Recently, Gayathri *et al.* (2020) demonstrated that mycotoxins, gliotoxin and fumagillin secreted by *A. fumigatus*, induce an intrinsic pathway of apoptosis through induction of caspase-3. Furthermore, suppression of host apoptosis by caspase-3 inhibition has been suggested as *A.*

fumigatus strategy to reduce the efficient host response (Volling *et al*., 2007; Féménia *et al.*, 2009).

Taken together, according to our results, the biological role of the identified potential molecular candidates along with the previous research, suggested molecular candidates for IPA seem to be promising for further evaluation in a larger patient cohort.

4.2.2 Additional assessment of identified potential molecular candidates

Challenges in the diagnosis and management of fungal infections led to the establishment of EORTC/MSGERC criteria, which categorize patients according to the certainty of the diagnosis into possible, probable and proven cases. Despite the recently updated EORTC/MSGERC criteria, patient stratification remains challenging (Donnelly *et al*., 2020). Identification of possible IPA cases, which are common in clinical reality is ambiguous and often subjective. The present study highlighted centre-specific differences in IL-8 and caspase-3 levels in investigated possible IPA cases, which might be explained by subjective categorization and clinical heterogeneity. While possible cases from Würzburg might reflect false positive radiology, possible cases from Cardiff might be actual IPA cases with false-negative mycology. This highlights the need for host biomarkers, which may in the future provide additional information about host response and disease status and thus improve patient stratification.

As GvHD is a common complication after alloSCT, causing dynamic changes in the immune response, we assessed the suggested IPA characteristic signature in the GvHD cohort (Paczesny *et al*., 2009). *MMP1* and *LGALS2* gene expression along with caspase-3 protein levels were significantly different between GvHD and probable IPA patients, suggesting these molecular candidates are not affected by GvHD in our investigated alloSCT patients. IL-8 is secreted by various immune cells in response to infection as well as inflammation and is therefore a universal marker (Baggiolini *et al*., 1989; Shahzad *et al*., 2001). Increased levels of IL-8 have been already reported in GvHD patients and this cytokine has been suggested as a potential GvHD biomarker (Paczesny *et al*., 2009). This might explain why no significant differences in IL-8 serum levels were found between investigated probable IPA and GvHD patients and suggest using IL-8 rather in combination with other molecular candidates and not as an individual marker. Due to the small number of investigated patients, further studies are necessary to confirm these observations in a larger patient cohort.

Recent studies reported emerging CAPA as a secondary infection complicating COVID-19 disease (Armstrong-James *et al*., 2020; White *et al*., 2020). We additionally assessed the

specificity of identified molecular candidates in an independent patient cohort consisting of CAPA cases and COVID-19 controls. Interestingly, CAPA cases demonstrated lower levels of investigated candidates compared to COVID-19 control patients, indicating a distinctive signature compared to the alloSCT cohort. As levels of these candidates increased in alloSCT patients suffering from IPA, further research is encouraged to investigate whether low IL-8 and caspase-3 levels might indicate CAPA among COVID-19 patients. Strong immune response in COVID-19 patients has been reported previously (Guo *et al*., 2021). High IL-8 levels in severe COVID-19 patients have already been demonstrated and the potential role of this cytokine as a biomarker for COVID-19 is under discussion (Li *et al*., 2021a; Ma *et al*., 2021). Strong caspase response in COVID-19 patients and therapeutic potential of caspase inhibitors have been recently reported by Plassmeyer *et al.* (2021). Several studies reported stronger host response during COVID-19, higher mortality and more often severe outcomes in males compared to female patients (Gebhard *et al*., 2020; Takahashi *et al*., 2020; Jacobsen and Klein, 2021). This is in line with our findings that highlighted sex-specific differences in IL-8 and caspase-3 levels among COVID-19 controls.

4.2.3 Limitations of the pilot, longitudinal case-control study

One of the major limitations of our pilot, longitudinal case-control study is the low number of investigated IPA cases. From March 2017 to December 2019, we identified three probable IPA cases, which fulfilled EORTC/MSGERC and our criteria (> 20 years, > 4 collected time-points, sufficient RNA yield, matching control patients) (Donnelly *et al.*, 2020). To address this challenge, we used an integrated approach to identify potential molecular candidates indicating IPA in investigated alloSCT patients. Furthermore, we performed an additional assessment of identified candidates in our *in vitro* model and included additional patients from an independent medical centre (Figure 10). The used *in vitro* model does not reflect the complexity of alloSCT patients, therefore further clinical studies are encouraged to evaluate identified signature indicating IPA post alloSCT. The selection and matching of case-control patients present another challenge in clinical studies. Due to the low incidence and the complexity of alloSCT and multifactorial IPA disease, additionally included and investigated alloSCT patients suffered from different underlying diseases (Suppl. Table S1).

Despite these limitations, the present work has provided new insights into host response during IPA in alloSCT patients. Clinical studies elucidating the immune response of IPA patients in a

multilevel manner are rare and validation of suggested characteristic IPA signature is a necessary next step.

4.3 Investigation of human risk factors contributing to the risk of invasive pulmonary aspergillosis in patients post alloSCT

Despite well studied classical risk factors associated with IPA such as neutropenia, GvHD, viral infections and corticosteroid treatments, IPA is still associated with a poor outcome (Baddley, 2011; Donnelly *et al*., 2020). The introduction of new therapeutic modalities in patients with hematologic malignancies improved the outcome, yet lead to emerging new risk factors for developing IPA (Girmenia, 2019). In the last decade, several studies are reporting cases of IPA in patients with haematological malignancies, receiving new targeted treatment in particular monoclonal antibodies, kinase inhibitors, agents targeting cell-surface antigens and chimeric antigen receptor-modified T-cells, agents (Nedel *et al*., 2009; Girmenia, 2019). Since most of the clinical symptoms indicating IPA in alloSCT patients are unspecific, risk stratification for IPA is crucial to identify patients at risk and may provide clinicians additional information to design individual treatment strategies focusing on either intensive monitoring of the patient or antifungal prophylaxis (Bonnet *et al*., 2017).

4.3.1 GvHD of the gut (grade ≥ 2)

It is well known that GvHD presents a risk for subsequent infections, not only due to immunosuppressive treatment but also because of an intrinsic immunosuppressive effect of GVHD and following defects in cutaneous and mucosal barriers (Rashidi *et al*., 2017). GvHD and its corticosteroid treatment are already known as risk factors for invasive fungal infections among alloSCT patients (Jantunen *et al*., 1997; Fukuda *et al*., 2003). In fact, GvHD is also included in the EORTC/MSGERC criteria as one of the host factors indicating invasive fungal infection in high-risk patients (Donnelly *et al*., 2020). Several studies reported IPA as the most common invasive mould disease in GvHD patients (Labbe *et al*., 2007; Garcia-Cadenas *et al*., 2017; Jin *et al*., 2019). Our results, indicating GvHD of the gut (grade ≥ 2) is significantly associated with IPA diagnosis are hence in line with the previously published studies.

4.3.2 Low monocyte concentrations

Monocytes circulate in the blood and migrate into the tissue where they differentiate into dendritic cells and macrophages (Serbina *et al*., 2009; Heung, 2020). It has been demonstrated monocytes are recruited to the site of *Aspergillus* spp. infection and are among essential immune cells preventing the formation of invasive *Aspergillus* hyphae and consequently IPA in the murine lung (Serbina *et al.*, 2009; Espinosa *et al.*, 2014). Furthermore, Hohl *et al.* (2009) demonstrated that monocyte-deficient mice are more susceptible to infection with *A. fumigatus*. Therefore, it is not surprising monocytopenia might lead to an improper immune response during IPA. Clinical evidence suggesting monocytopenia as a risk factor for developing IPA in patients with haematological malignancies has already been reported (Weinberger *et al*., 1992; Garcia-Vidal *et al*., 2008). Our results are hence in line with previous clinical studies, suggesting low monocyte counts should be considered as an important risk factor for developing IPA after alloSCT.

4.3.3 Etanercept administration

TNF-α blockade has been used to treat autoimmune inflammatory diseases such as rheumatoid arthritis, psoriasis and inflammatory bowel disease (Gottlieb, 2007). Since TNF-α is a fundamental mediator of GvHD, biological agents targeting this cytokine have been used also for corticosteroid-refractory GvHD in patients post alloSCT (Tsiodras *et al*., 2008). TNF-α inhibitors have been associated with an increased risk for bacterial, viral and fungal infections (Scott, 2014; Downey, 2016;). In the past decade, several studies have reported the occurrence of fungal infections in patients receiving TNF-α blockers such as infliximab, adalimumab and etanercept (Tsiodras *et al*., 2008; Nedel *et al*., 2009; Scott, 2014). Fungal infections associated with TNF-α blockade have been mostly reported sporadically. Tsiodras *et al*. (2008) investigated cases of invasive fungal infections linked to the use of TNF-α inhibitors between 1966 and 2007 and reported about 281 cases associated with adalimumab, infliximab and etanercept treatment. Histoplasmosis was the most common reported IFI (30 %) followed by candidiasis and aspergillosis (23 %). Overall, among 64 reports of aspergillosis associated with TNF-α inhibitors, 75 % (48) were associated with infliximab, 22 % (14) with etanercept and 3% (2) with adalimumab (Tsiodras *et al*., 2008). More recently, Garcia-Cadenas *et al.* (2017) reported aspergillosis as the most common fungal infection in patients with steroid-refractory GvHD receiving TNF-α inhibitors. Although fungal infections associated with etanercept administration have already been reported, the exact mechanism of action during IPA is not well elucidated.

4.3.3.1 Effects of etanercept on MDM infected with A. fumigatus

Etanercept is a fusion protein consisting of two TNFR2 (75kD) receptors both linked to the human IgG1 Fc domain. The drug acts as a soluble receptor for TNF and binds TNF-α as well as TNF-β (also known as lymphotoxin-α, LTA), while not depleting cells expressing both cytokines. By binding TNF-α and LTA, etanercept prevents their interaction with cell receptors and thus antagonizes TNF-induced proinflammatory activity (Gottlieb, 2007). TNF-α is a central proinflammatory cytokine, expressed by several immune cells such as activated monocytes, macrophages, neutrophils, NK and T cells, and has an essential role in the immune response to fungal infections (Roilides *et al*., 1998; Sedger and McDermott, 2014). It is well established, that in response to *A. fumigatus* infection TNF-α levels increase. *In vivo* depletion of TNF-α leads to reduced lung neutrophil influx and consequently increased fungal burden (Mehrad *et al*., 1999). During infection, TNF-α promotes activation and recruitment of immune cells for intracellular killing and granuloma formation, which helps to prevent the dissemination of fungal pathogens (Tsiodras *et al*., 2008). While TNF blockade by etanercept has been widely studied in the context of autoimmune inflammatory diseases (e.g., rheumatoid arthritis), the exact effect of this biological agent during *A. fumigatus* infections remain vague.

We showed that etanercept in uninfected and *A. fumigatus*-infected MDM represses genes encoding metallothioneins (Table 19, Figure 23). These metal-binding proteins maintain zinc and copper homeostasis and are important in essential biological and cellular processes (Vignesh and Deepe, 2017). For example, while an excess of zinc can exert toxic effects on immune cells, zinc deficiency can cause increased susceptibility to infections. Induction in gene expression of different metallothionein isoforms has been reported in response to viral, bacterial and fungal infections (Vignesh and Deepe, 2017). Moreover, it is known that TNF-α induces the expression of metallothioneins (Sato *et al*., 1994). Hence, etanercept might through TNF-α inhibition and repression of genes encoding metallothioneins disrupt zinc and copper homeostasis and consequently affect crucial processes involved in immune response and cell survival during *Aspergillus* infection.

A. fumigatus-infected MDM in presence of etanercept demonstrated the downregulation of genes involved in the antimicrobial humoral response, NF-Kβ signalling and apoptotic processes. Repression in genes involved in NF-Kβ signalling was observed for *RELB* (RELB Proto-Oncogene, NF-κB Subunit), *ICAM1* (Intercellular Adhesion Molecule 1) and *BCL3* (B-Cell Lymphoma 3 Protein). TNF-α is one of the proinflammatory cytokines involved in the activation of the NF-Kβ transcription family which is essential in the regulation of inflammation

and immunity (Liu *et al*., 2017). RELB is one of the NF-Kβ family members, mediating transcription of target genes and can be activated by dectin-1 (Gringhuis *et al*., 2009; Oeckinghaus and Ghosh, 2009). BCL3 is an atypical NF-Kβ family member, modulating the transcription of NF-Kβ targets (Oeckinghaus and Ghosh, 2009). ICAM1 is a member of the immunoglobulin superfamily and is important for cell adhesion, leukocyte activation and trafficking to the site of inflammation (Ruetten *et al*., 1999). Extrinsic apoptosis, activated by TNF-α is one of the key defence mechanisms in response to infection and is important for *Aspergillus spp.* clearance as well as preventing dissemination to other organs (Féménia *et al*., 2009; Camili *et al*., 2021). Repression of genes involved in apoptosis might therefore affect cell death and favour pathogen dissemination to other organs.

Finally, we demonstrated the presence of etanercept during *A. fumigatus* infection significantly decreases CXCL10 levels *in vitro* and *ex vivo*. CXCL10 is chemokine activated by TNF-α, recruiting immune cells that secrete or respond to IFN-γ, such as activated NK-cells, monocytes and T-cells (Taub *et al*., 1996). CXCL10 secretion in response to *A. fumigatus* infection has been previously demonstrated *in vitro*, and it was observed also in our study (Guo *et al*., 2020). Elevated CXCL10 serum levels have been also reported in alloSCT patients suffering from IPA compared to control patients without fungal infections (Mezger *et al*., 2008b). Moreover, CXCL10 polymorphism has been recently associated with a higher risk of developing IPA in alloSCT patients (Fisher *et al*., 2017). Altogether, these findings suggest etanercept might by inhibition of TNF-α and lowering CXC10 levels prevent the presence of various immune cells essential for the successful defence against *A. fumigatus*.

5. Conclusions and outlook

As a result of the nonspecific clinical presentation of IPA, the diagnosis and antifungal treatment are often delayed, leading to poor outcomes in alloSCT patients (Garcia-Vidal *et al*., 2015; Lass-Flörl, 2017). Despite the advancements in the last years, currently used diagnostic tools lack specificity and sensitivity, highlighting a necessity for improving the IPA diagnosis and overall management of this life-threatening disease (Cadena *et al*., 2021). Considering aspergillosis is a multifactorial disease, investigating different aspects (e.g., fungal pathogens, host immune response, environment) might help to overcome current challenges in the management of IPA.

The present PhD project indicated that host molecular signatures may have the potential as diagnostic aids to support the diagnosis of IPA. Using *in vitro* model, we identified 24 specifically dysregulated miRNAs in *A. fumigatus*-infected moDCs and demonstrated distinctive miRNA-mRNA signatures associated with *A. fumigatus* infection. As detailed knowledge about predicted miRNA-mRNA interactions could not be provided, further studies are encouraged to evaluate the suggested miRNA-mRNA distinctive signatures and elucidate the role of hsa-miR-204-5p and its predicted targets in response to *A. fumigatus* infection. We showed host transcriptome signatures enable discrimination between *A. fumigatus*- and *E. coli*-infected moDCs. Both conducted studies, *in vitro* (chapter 3.1) and a pilot case-control study, (chapter 3.2), highlighted the involvement of cytokines, matrix metallopeptidases and galectins among others in the response to *A. fumigatus*. We further demonstrated characteristic IPA signature in investigated alloSCT patients, consisting of *MMP1* induction, *LGALS2* repression and elevated IL-8 and caspase-3 levels, which was further confirmed *in vitro* in *A. fumigatus*-infected moDCs. Since identified potential molecular candidates for IPA may be involved in various biological processes and dysregulated in response to several pathogens, a combination of proposed candidates in a characteristic signature (*LGALS2*-*MMP1*-IL-8-caspase-3) could increase diagnostic accuracy.

Apart from the suggested molecular candidates in the present study, there might be other interesting candidates indicating IPA, promising for further evaluation. For instance, elevated levels of IL-1β, IL-6, IL-17A, IL-23, and TNF-α in BAL in IPA patients have been reported by Gonçalves *et al*. (2017). Chai *et al*. (2010) suggested a combination of CRP together with IL-6 and IL-8 levels as useful markers for the early identification of patients with a poor response to antifungal treatment. Elevated IL-8 and MMP9 (matrix metallopeptidase 9) levels in sputum

have been demonstrated in ABPA patients (Gibson *et al*., 2003). Moreover, in non-neutropenic patients, elevated PTX3 (Pentraxin 3) levels in BALF and plasma have been suggested to discriminate aspergillosis from lung cancer and pulmonary cryptococcosis (Li *et al.*, 2019). Recently, Machata *et al.* (2020), reported a characteristic IPA signature consisting of 172 proteins detected in BALs of IPA patients suffering from different underlying diseases. Among the most abundant proteins enriched in IPA patients were CRP, TLR2, CD177 antigen (protein of neutrophils) and others (Machata *et al*., 2020). Clinical studies elucidating miRNA expression profiles during IPA are rare (Pakshir *et al.*, 2020). In a preliminary study, Gohir *et al.* (2019), reported dysregulation of hsa-miR-101-3p, hsa-miR-1285-5p, hsa-miR-99b-5p and hsa-miR-877-5p in patients with haematological malignancies suffering from IPA compared to healthy controls. Recently, Tolnai *et al*. (2020) reported miRNA TetramiR panel indicating IPA in patients with haematological malignancies, consisting of overexpression of hsa-miR-142-3p, hsa-miR-142-5p, hsa-miR-26-5p and hsa-miR-21-5p. Although miRNAs showed good potential as non-invasive biomarkers, due to their detection and stability in various biofluids, there are several methodological difficulties associated with standardization of miRNA processing, normalization and discrimination between closely related miRNAs (Saliminejad *et al*., 2019).

Identification of risk factors for developing IPA in alloSCT patients enables early treatment and might prevent the development of the disease (Kaya *et al*., 2017). We showed severe GvHD of the gut, low monocyte counts and administration of etanercept are significantly associated with IPA diagnosis in patients post alloSCT. Additionally, we demonstrated that etanercept affects antifungal immune response through repression of genes involved in NF-κB as well as TNF-α signalling and decreases CXCL10 release. With the use of new therapeutic agents and emerging infections (e.g., SARS-CoV-2), the epidemiology of aspergillosis is changing (Nedel *et al*., 2009; Armstrong-James *et al*., 2020). Investigation of risk factors and changes in the epidemiology of aspergillosis is important for developing therapeutic strategies and may help to improve the prognosis of immunosuppressed patients (Kaya *et al*., 2017).

Lastly, we propose an individual patient-specific strategy based on identified potential biomarker candidates (*LGALS2*, *MMP1*, IL-8, caspase-3) and risk factors (e.g., monocytopenia, etanercept administration) (Figure 25). Together with diagnostic assays and collected clinical information of investigated IPA cases, this integrative approach has the potential to improve diagnosis, the establishment of appropriate patient-specific therapy and monitoring treatment response. Albeit, combined features showed similar profiles among investigated IPA patients,

patient-specific profiles demonstrate the overall complexity of IPA and alloSCT patients often met in clinical reality (Figure 25 a). Observed clinical heterogeneity is a common challenge in biomarker research for infectious diseases. Treatment of IPA patients is established based on the collected clinical, radiological and mycological evidence (Lass-Flörl, 2019). However, clinicians are regularly faced with patients either having supporting mycology but lacking typical radiology or patients with typical radiology for IPA but the absence of mycological evidence of *Aspergillus* (possible IPA). Late mycology often leads to empirical antifungal therapy in patients with refractory fever. Considering the side effects linked to antifungal therapy, associated costs, as well as emerging azole resistance, establishing appropriate antifungal therapy, is critical. Characteristic IPA host biomarkers could increase the confidence in the diagnosis of possible IPA patients or not well-defined IPA cases with mycological evidence and might help to strengthen the current patient classification (Donnelly *et al*., 2020). Until now, fungal biomarkers currently used in the IPA diagnosis did not demonstrate strong evidence in determining patient prognosis. Hence monitoring of characteristic IPA host biomarkers in combination with clinical parameters could play an important role in determining the prognosis of IPA patients.

Altogether, this PhD work may pave the way for further host biomarker and risk factor research in the IPA field. Potential molecular candidates indicating IPA in alloSCT patients may be evaluated further in larger multicentre studies by using broadly available methods such as qPCR and immunoassays (ELISA). Considering the present study characterized host response after IPA onset only, the prognostic potential of these candidates and their performance in other clinical manifestations of aspergillosis may be investigated. We encourage future research to evaluate the proposed integrative approach for the diagnosis of IPA, based on identified molecular candidates for IPA, patient-specific factors and currently used fungal biomarkers (Figure 25 b). To conclude, due to new therapies and emerging non-traditional patient risk groups developing IPA along with emerging azole resistance, continuous research on risk factors and host response to *A. fumigatus* is an essential step towards improved IPA management.

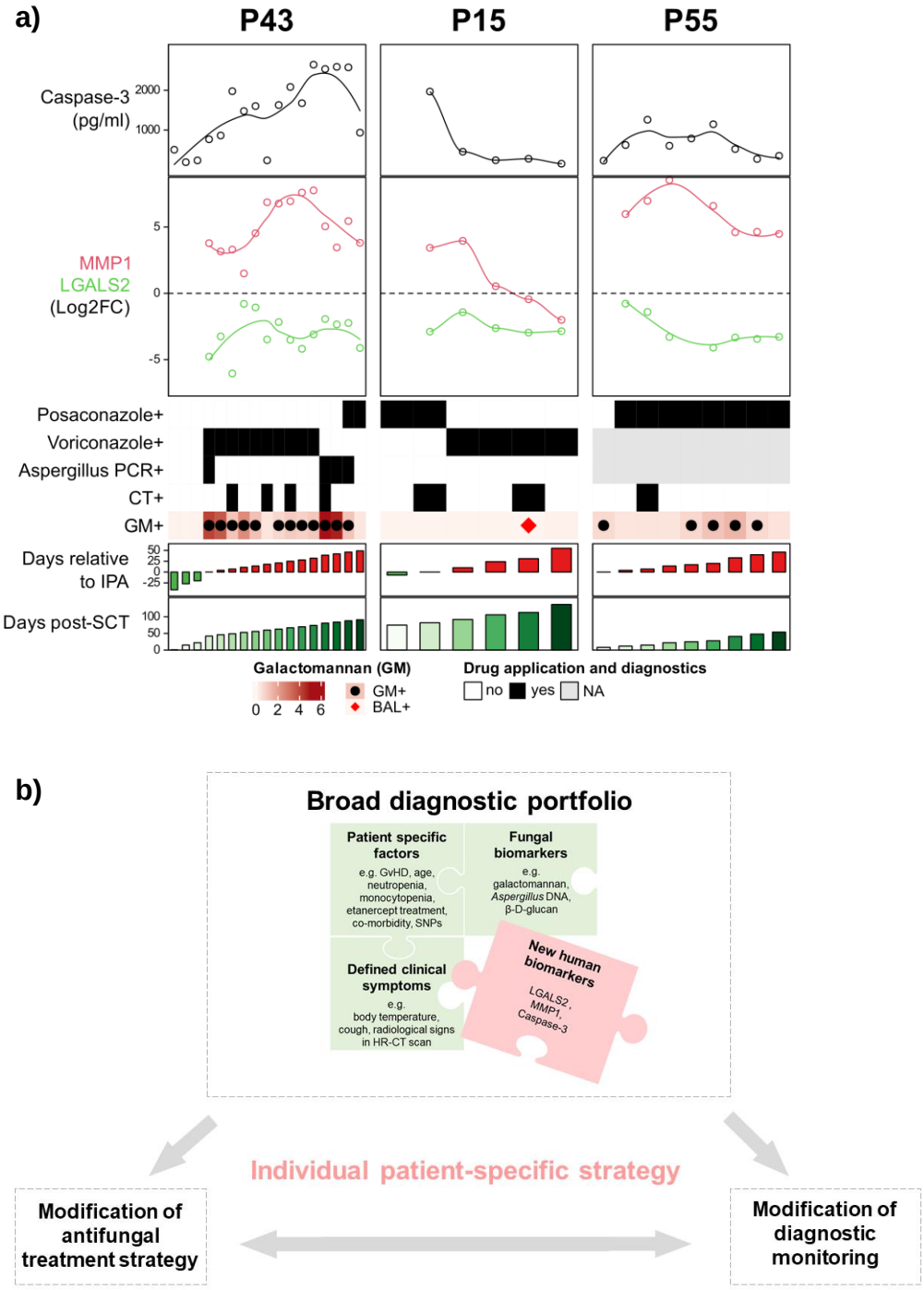

Figure 25: Clinical utility of suggested molecular candidates and risk factors for IPA in alloSCT patients investigated in the present PhD project. a) Integrated patient-specific profile based on the most promising molecular candidates (*LGALS2*, *MMP1*, caspase-3), performed diagnostic assays (CT-scan, *Aspergillus* DNA and galactomannan) and clinical information (antifungal treatment). Time (days) post alloSCT is marked in green and days relative to IPA in red. Timepoints with positive diagnostics assay and potential antifungal treatments are marked in black. Results for positive CT-scan are shown closest to the time point of blood drawing, in case, If CT investigation was not performed on the exact day of blood draw. **b)** Suggested individual patient-specific strategy for diagnosis of IPA in alloSCT patients. The approach combines suggested molecular candidates for IPA and risk factors along with well-established fungal biomarkers, clinical and patient-specific factors (e.g., neutropenia, clinical symptoms). Taken from Zoran *et al*., 2022.

6. References

Aguado JM, Vazquez L, Fernandez-Ruiz M, *et al.* 2015. Serum galactomannan versus a combination of galactomannan and polymerase chain reaction-based Aspergillus DNA detection for early therapy of invasive aspergillosis in high-risk hematological patients: a randomized controlled trial. Clin Infect Dis **60**, 405-414.

Ahmed W, Zheng K, Liu ZF. 2016. Small Non-Coding RNAs: New Insights in Modulation of Host Immune Response by Intracellular Bacterial Pathogens. Front Immunol **7**, 431.

Alkharabsheh O, Alsayed A, Morlote DM, *et al.* 2021. Cerebral Invasive Aspergillosis in a Case of Chronic Lymphocytic Leukemia with Bruton Tyrosine Kinase Inhibitor. Curr Oncol **28**, 837-841.

Anders S, Huber W. 2010. Differential expression analysis for sequence count data. Genome Biol **11**, R106.

Andersen CL, Jensen JL, Orntoft TF. 2004. Normalization of real-time quantitative reverse transcription-PCR data: a model-based variance estimation approach to identify genes suited for normalization, applied to bladder and colon cancer data sets. Cancer Res **64**, 5245-5250.

Arastehfar A, Carvalho A, Houbraken J, *et al.* 2021. Aspergillus fumigatus and aspergillosis: From basics to clinics. Stud Mycol **100**, 100115.

Armstrong-James D, Youngs J, Bicanic T, *et al.* 2020. Confronting and mitigating the risk of COVID-19 associated pulmonary aspergillosis. Eur Respir J **56**.

Ashkenazi-Hoffnung L, Oved K, Navon R, *et al.* 2018. A host-protein signature is superior to other biomarkers for differentiating between bacterial and viral disease in patients with respiratory infection and fever without source: a prospective observational study. Eur J Clin Microbiol Infect Dis **37**, 1361-1371.

Astashchanka A, Ryan J, Lin E, *et al.* 2021. Pulmonary Complications in Hematopoietic Stem Cell Transplant Recipients-A Clinician Primer. J Clin Med **10**.

Au KY, Pong JC, Ling WL, *et al.* 2016. MiR-1303 Regulates Mycobacteria Induced Autophagy by Targeting Atg2B. PLoS One **11**, e0146770.

Ayona D, Fournier PE, Henrissat B, *et al.* 2020. Utilization of Galectins by Pathogens for Infection. Front Immunol **11**, 1877.

Bacher P, Steinbach A, Kniemeyer O, *et al.* 2015. Fungus-specific CD4(+) T cells for rapid identification of invasive pulmonary mold infection. Am J Respir Crit Care Med **191**, 348-352.

Baddley JW. 2011. Clinical risk factors for invasive aspergillosis. Med Mycol **49 Suppl 1**, S7-S12.

Baggiolini M, Walz A, Kunkel SL. 1989. Neutrophil-activating peptide-1/interleukin 8, a novel cytokine that activates neutrophils. J Clin Invest **84**, 1045-1049.

Bandyopadhyay S, Mitra R, Maulik U, *et al.* 2010. Development of the human cancer microRNA network. Silence **1**, 6.

Barondes SH, Castronovo V, Cooper DN, *et al.* 1994. Galectins: a family of animal beta-galactoside-binding lectins. Cell **76**, 597-598.

Barrett T, Wilhite SE, Ledoux P, *et al.* 2013. NCBI GEO: archive for functional genomics data sets--update. Nucleic Acids Res **41**, D991-995.

Bazzoni F, Rossato M, Fabbri M, *et al.* 2009. Induction and regulatory function of miR-9 in human monocytes and neutrophils exposed to proinflammatory signals. Proc Natl Acad Sci U S A **106**, 5282-5287.

Ben-Ami R, Lewis RE, Leventakos K, *et al.* 2009. Aspergillus fumigatus inhibits angiogenesis through the production of gliotoxin and other secondary metabolites. Blood **114**, 5393-5399.

Bhatia S, Fei M, Yarlagadda M, *et al.* 2011. Rapid host defense against Aspergillus fumigatus involves alveolar macrophages with a predominance of alternatively activated phenotype. PLoS One **6**, e15943.

Bhattacharya S, Rosenberg AF, Peterson DR, *et al.* 2017. Transcriptomic Biomarkers to Discriminate Bacterial from Nonbacterial Infection in Adults Hospitalized with Respiratory Illness. Sci Rep **7**, 6548.

Biomarkers Definitions Working G. 2001. Biomarkers and surrogate endpoints: preferred definitions and conceptual framework. Clin Pharmacol Ther **69**, 89-95.

Bolger AM, Lohse M, Usadel B. 2014. Trimmomatic: a flexible trimmer for Illumina sequence data. Bioinformatics **30**, 2114-2120.

Bonnet S, Dulery R, Regany K, *et al.* 2017. Long-term follow up of invasive aspergillosis in allogeneic stem cell transplantation recipients and leukemia patients: Differences in risk factors and outcomes. Curr Res Transl Med **65**, 77-81.

Boomiraj H, Mohankumar V, Lalitha P, *et al.* 2015. Human Corneal MicroRNA Expression Profile in Fungal Keratitis. Invest Ophthalmol Vis Sci **56**, 7939-7946.

Bourgeois C, Kuchler K. 2012. Fungal pathogens-a sweet and sour treat for toll-like receptors. Front Cell Infect Microbiol **2**, 142.

Bretagne S, Marmorat-Khuong A, Kuentz M, *et al.* 1997. Serum Aspergillus galactomannan antigen testing by sandwich ELISA: practical use in neutropenic patients. J Infect **35**, 7-15.

Brown GD. 2006. Dectin-1: a signalling non-TLR pattern-recognition receptor. Nat Rev Immunol **6**, 33-43.

Bruno M, Dewi IMW, Matzaraki V, *et al.* 2021. Comparative host transcriptome in response to pathogenic fungi identifies common and species-specific transcriptional antifungal host response pathways. Comput Struct Biotechnol J **19**, 647-663.

Burska A, Boissinot M, Ponchel F. 2014. Cytokines as biomarkers in rheumatoid arthritis. Mediators Inflamm **2014**, 545493.

Cadena J, Thompson GR, 3rd, Patterson TF. 2021. Aspergillosis: Epidemiology, Diagnosis, and Treatment. Infect Dis Clin North Am **35**, 415-434.

Caillot D, Couaillier JF, Bernard A, *et al.* 2001. Increasing volume and changing characteristics of invasive pulmonary aspergillosis on sequential thoracic computed tomography scans in patients with neutropenia. J Clin Oncol **19**, 253-259.

Camilli G, Blagojevic M, Naglik JR, *et al.* 2021. Programmed Cell Death: Central Player in Fungal Infections. Trends Cell Biol **31**, 179-196.

Cenci E, Perito S, Enssle KH, *et al.* 1997. Th1 and Th2 cytokines in mice with invasive aspergillosis. Infect Immun **65**, 564-570.

Chai L, Netea MG, Teerenstra S, *et al.* 2010. Early proinflammatory cytokines and C-reactive protein trends as predictors of outcome in invasive Aspergillosis. J Infect Dis **202**, 1454-1462.

Challa S. 2018. Pathogenesis and Pathology of Invasive Aspergillosis. Curr Fungal Infect Rep **12**, 23-32.

Chen CZ, Li L, Lodish HF, *et al.* 2004. MicroRNAs modulate hematopoietic lineage differentiation. Science **303**, 83-86.

Chen F, Xu XY, Zhang M, *et al.* 2019. Deep sequencing profiles MicroRNAs related to Aspergillus fumigatus infection in lung tissues of mice. J Microbiol Immunol Infect **52**, 90-99.

Chowdhary A, Kathuria S, Xu J, *et al.* 2013. Emergence of azole-resistant aspergillus fumigatus strains due to agricultural azole use creates an increasing threat to human health. PLoS Pathog **9**, e1003633.

Cordonnier C, Bernaudin JF, Bierling P, *et al.* 1986. Pulmonary complications occurring after allogeneic bone marrow transplantation. A study of 130 consecutive transplanted patients. Cancer **58**, 1047-1054.

Cortez KJ, Lyman CA, Kottilil S, *et al.* 2006. Functional genomics of innate host defense molecules in normal human monocytes in response to Aspergillus fumigatus. Infect Immun **74**, 2353-2365.

Croston TL, Nayak AP, Lemons AR, *et al.* 2016. Influence of Aspergillus fumigatus conidia viability on murine pulmonary microRNA and mRNA expression following subchronic inhalation exposure. Clin Exp Allergy **46**, 1315-1327.

Cruciani M, Mengoli C, Barnes R, *et al.* 2019. Polymerase chain reaction blood tests for the diagnosis of invasive aspergillosis in immunocompromised people. Cochrane Database Syst Rev **9**, CD009551.

Cunha C, Aversa F, Romani L, *et al.* 2013. Human genetic susceptibility to invasive aspergillosis. PLoS Pathog **9**, e1003434.

Dagenais TR, Keller NP. 2009. Pathogenesis of Aspergillus fumigatus in Invasive Aspergillosis. Clin Microbiol Rev **22**, 447-465.

Das Gupta M, Fliesser M, Springer J, *et al.* 2014. Aspergillus fumigatus induces microRNA-132 in human monocytes and dendritic cells. Int J Med Microbiol **304**, 592-596.

De Pauw B, Walsh TJ, Donnelly JP, *et al.* 2008. Revised definitions of invasive fungal disease from the European Organization for Research and Treatment of Cancer/Invasive Fungal Infections Cooperative Group and the National Institute of Allergy and Infectious Diseases Mycoses Study Group (EORTC/MSG) Consensus Group. Clin Infect Dis **46**, 1813-1821.

Di Lulio J, Bartha I, Spreafico R, *et al.* 2021. Transfer transcriptomic signatures for infectious diseases. Proc Natl Acad Sci U S A **118**.

Dix A, Czakai K, Leonhardt I, *et al.* 2017. Specific and Novel microRNAs Are Regulated as Response to Fungal Infection in Human Dendritic Cells. Front Microbiol **8**, 270.

Dix A, Hunniger K, Weber M, *et al.* 2015. Biomarker-based classification of bacterial and fungal whole-blood infections in a genome-wide expression study. Front Microbiol **6**, 171.

Donnelly JP, Chen SC, Kauffman CA, *et al.* 2020. Revision and Update of the Consensus Definitions of Invasive Fungal Disease From the European Organization for Research and Treatment of Cancer and the Mycoses Study Group Education and Research Consortium. Clin Infect Dis **71**, 1367-1376.

Downey C. 2016. Serious infection during etanercept, infliximab and adalimumab therapy for rheumatoid arthritis: A literature review. Int J Rheum Dis **19**, 536-550.

Du B, Luo W, Li R, *et al.* 2013. Lgr4/Gpr48 negatively regulates TLR2/4-associated pattern recognition and innate immunity by targeting CD14 expression. J Biol Chem **288**, 15131-15141.

Dunbar A, Joosse ME, de Boer F, *et al.* 2020. Invasive fungal infections in patients treated with Bruton's tyrosine kinase inhibitors. Neth J Med **78**, 294-296.

Dweep H, Gretz N. 2015. miRWalk2.0: a comprehensive atlas of microRNA-target interactions. Nat Methods **12**, 697.

Elkington PT, O'Kane CM, Friedland JS. 2005. The paradox of matrix metalloproteinases in infectious disease. Clin Exp Immunol **142**, 12-20.

Espinosa V, Jhingran A, Dutta O, *et al.* 2014. Inflammatory monocytes orchestrate innate antifungal immunity in the lung. PLoS Pathog **10**, e1003940.

Fabian MR, Sonenberg N, Filipowicz W. 2010. Regulation of mRNA translation and stability by microRNAs. Annu Rev Biochem **79**, 351-379.

Feinstein MB, Habtes I, Giralt S, *et al.* 2021. Utility of Bronchoscopy with Bronchoalveolar Lavage among Hematologic Transplant Recipients in the Era of Noninvasive Testing. Respiration **100**, 339-346.

Femenia F, Huet D, Lair-Fulleringer S, *et al.* 2009. Effects of conidia of various Aspergillus species on apoptosis of human pneumocytes and bronchial epithelial cells. Mycopathologia **167**, 249-262.

Feys S, Almyroudi MP, Braspenning R, *et al.* 2021. A Visual and Comprehensive Review on COVID-19-Associated Pulmonary Aspergillosis (CAPA). J Fungi (Basel) **7**.

Fisher CE, Hohl TM, Fan W, *et al.* 2017. Validation of single nucleotide polymorphisms in invasive aspergillosis following hematopoietic cell transplantation. Blood **129**, 2693-2701.

Fukuda T, Boeckh M, Carter RA, *et al.* 2003. Risks and outcomes of invasive fungal infections in recipients of allogeneic hematopoietic stem cell transplants after nonmyeloablative conditioning. Blood **102**, 827-833.

Ganapule A, Nemani S, Korula A, *et al.* 2017. Allogeneic Stem Cell Transplant for Acute Myeloid Leukemia: Evolution of an Effective Strategy in India. J Glob Oncol **3**, 773-781.

Garcia-Cadenas I, Rivera I, Martino R, *et al.* 2017. Patterns of infection and infection-related mortality in patients with steroid-refractory acute graft versus host disease. Bone Marrow Transplant **52**, 107-113.

Garcia-Vidal C, Peghin M, Cervera C, *et al.* 2015. Causes of death in a contemporary cohort of patients with invasive aspergillosis. PLoS One **10**, e0120370.

Garcia-Vidal C, Upton A, Kirby KA, *et al.* 2008. Epidemiology of invasive mold infections in allogeneic stem cell transplant recipients: biological risk factors for infection according to time after transplantation. Clin Infect Dis **47**, 1041-1050.

Garlanda C, Hirsch E, Bozza S, *et al.* 2002. Non-redundant role of the long pentraxin PTX3 in anti-fungal innate immune response. Nature **420**, 182-186.

Gayathri L, Akbarsha MA, Ruckmani K. 2020. In vitro study on aspects of molecular mechanisms underlying invasive aspergillosis caused by gliotoxin and fumagillin, alone and in combination. Sci Rep **10**, 14473.

Gebhard C, Regitz-Zagrosek V, Neuhauser HK, *et al.* 2020. Impact of sex and gender on COVID-19 outcomes in Europe. Biol Sex Differ **11**, 29.

Gibson PG, Wark PA, Simpson JL, *et al.* 2003. Induced sputum IL-8 gene expression, neutrophil influx and MMP-9 in allergic bronchopulmonary aspergillosis. Eur Respir J **21**, 582-588.

Girmenia C. 2019. New hematologic populations at risk of invasive aspergillosis: focus on new targeted, biological, and cellular therapies. F1000Res **8**.

Gohir W, Klement W, Singer LG, *et al.* 2019. Host miRNA Profile of Invasive Aspergillosis in Lung Transplant Recipients. The Journal of Heart and Lung Transplantation **38**.

Gomez P, Hackett TL, Moore MM, *et al.* 2010. Functional genomics of human bronchial epithelial cells directly interacting with conidia of Aspergillus fumigatus. BMC Genomics **11**, 358.

Goncalves SM, Lagrou K, Rodrigues CS, *et al.* 2017. Evaluation of Bronchoalveolar Lavage Fluid Cytokines as Biomarkers for Invasive Pulmonary Aspergillosis in At-Risk Patients. Front Microbiol **8**, 2362.

Gordon-Alonso M, Bruger AM, van der Bruggen P. 2018. Extracellular galectins as controllers of cytokines in hematological cancer. Blood **132**, 484-491.

Gottlieb AB. 2007. Tumor necrosis factor blockade: mechanism of action. J Investig Dermatol Symp Proc **12**, 1-4.

Gringhuis SI, den Dunnen J, Litjens M, *et al.* 2009. Dectin-1 directs T helper cell differentiation by controlling noncanonical NF-kappaB activation through Raf-1 and Syk. Nat Immunol **10**, 203-213.

Gross J, Lapiere CM. 1962. Collagenolytic activity in amphibian tissues: a tissue culture assay. Proc Natl Acad Sci U S A **48**, 1014-1022.

Guo J, Wang S, Xia H, *et al.* 2021. Cytokine Signature Associated With Disease Severity in COVID-19. Frontiers in Immunology **12**.

Guo Y, Kasahara S, Jhingran A, *et al.* 2020. During Aspergillus Infection, Monocyte-Derived DCs, Neutrophils, and Plasmacytoid DCs Enhance Innate Immune Defense through CXCR3-Dependent Crosstalk. Cell Host Microbe **28**, 104-116 e104.

Hanash SM. 2011. Why have protein biomarkers not reached the clinic? Genome Med **3**, 66.

Harjunpaa H, Llort Asens M, Guenther C, *et al.* 2019. Cell Adhesion Molecules and Their Roles and Regulation in the Immune and Tumor Microenvironment. Front Immunol **10**, 1078.

Harrington CA, Fei SS, Minnier J, *et al.* 2020. RNA-Seq of human whole blood: Evaluation of globin RNA depletion on Ribo-Zero library method. Sci Rep **10**, 6271.

Hatfield KJ, Reikvam H, Bruserud O. 2010. The crosstalk between the matrix metalloprotease system and the chemokine network in acute myeloid leukemia. Curr Med Chem **17**, 4448-4461.

Hefter M, Lother J, Weiss E, *et al.* 2017. Human primary myeloid dendritic cells interact with the opportunistic fungal pathogen Aspergillus fumigatus via the C-type lectin receptor Dectin-1. Med Mycol **55**, 573-578.

Heinekamp T, Schmidt H, Lapp K, *et al.* 2015. Interference of Aspergillus fumigatus with the immune response. Semin Immunopathol **37**, 141-152.

Heldt S, Prattes J, Eigl S, *et al.* 2018. Diagnosis of invasive aspergillosis in hematological malignancy patients: Performance of cytokines, Asp LFD, and Aspergillus PCR in same day blood and bronchoalveolar lavage samples. J Infect **77**, 235-241.

Herrera I, Cisneros J, Maldonado M, *et al.* 2013. Matrix metalloproteinase (MMP)-1 induces lung alveolar epithelial cell migration and proliferation, protects from apoptosis, and represses mitochondrial oxygen consumption. J Biol Chem **288**, 25964-25975.

Heung LJ. 2020. Monocytes and the Host Response to Fungal Pathogens. Front Cell Infect Microbiol **10**, 34.

Hjortdahl P, Landaas S, Urdal P, *et al.* 1991. C-reactive protein: a new rapid assay for managing infectious disease in primary health care. Scand J Prim Health Care **9**, 3-10.

Hohl TM. 2017. Immune responses to invasive aspergillosis: new understanding and therapeutic opportunities. Curr Opin Infect Dis **30**, 364-371.

Hohl TM, Rivera A, Lipuma L, *et al.* 2009. Inflammatory monocytes facilitate adaptive CD4 T cell responses during respiratory fungal infection. Cell Host Microbe **6**, 470-481.

Hotchkiss RS, Chang KC, Swanson PE, *et al.* 2000. Caspase inhibitors improve survival in sepsis: a critical role of the lymphocyte. Nat Immunol **1**, 496-501.

Huang SF, Huang CC, Chou KT, *et al.* 2021. Chronic Pulmonary Aspergillosis: Disease Severity Using Image Analysis and Correlation with Systemic Proinflammation and Predictors of Clinical Outcome. J Fungi (Basel) **7**.

Hulsen T, de Vlieg J, Alkema W. 2008. BioVenn - a web application for the comparison and visualization of biological lists using area-proportional Venn diagrams. BMC Genomics **9**, 488.

Husni RN, Gordon SM, Longworth DL, *et al.* 1998. Cytomegalovirus infection is a risk factor for invasive aspergillosis in lung transplant recipients. Clin Infect Dis **26**, 753-755.

Iglesias-Osma C, Gonzalez-Villaron L, San Miguel JF, *et al.* 1995. Iron metabolism and fungal infections in patients with haematological malignancies. J Clin Pathol **48**, 223-225.

Illumina Inc. 2017. An Introduction to Next-Generation Sequencing Technology. *Brochure*. I, ed. Available at https://www.illumina.com.

Jacobsen H, Klein SL. 2021. Sex Differences in Immunity to Viral Infections. Front Immunol **12**, 720952.

Jaglowski SM, Devine SM. 2014. Graft-versus-host disease: why have we not made more progress? Curr Opin Hematol **21**, 141-147.

Jantunen E, Ruutu P, Niskanen L, *et al.* 1997. Incidence and risk factors for invasive fungal infections in allogeneic BMT recipients. Bone Marrow Transplant **19**, 801-808.

Jenks JD, Hoenigl M. 2018. Treatment of Aspergillosis. J Fungi (Basel) **4**.

Jensen HL. 1931. The fungus flora of the soil. Soil Science **31**, 123–158.

Jin H, Fan Z, Huang F, *et al.* 2019. Invasive fungal disease is associated with chronic graft-versus-host disease after allogeneic hematopoietic stem cell transplant: a single center, retrospective study. Infection **47**, 275-284.

Jouault T, El Abed-El Behi M, Martinez-Esparza M, *et al.* 2006. Specific recognition of Candida albicans by macrophages requires galectin-3 to discriminate Saccharomyces cerevisiae and needs association with TLR2 for signaling. J Immunol **177**, 4679-4687.

Kabbani D, Bhaskaran A, Singer LG, *et al.* 2017. Pentraxin 3 levels in bronchoalveolar lavage fluid of lung transplant recipients with invasive aspergillosis. J Heart Lung Transplant **36**, 973-979.

Katiyar A, Kaur G, Rani L, *et al.* 2021. Genome-wide identification of potential biomarkers in multiple myeloma using meta-analysis of mRNA and miRNA expression data. Sci Rep **11**, 10957.

Kaya S, Gencalioglu E, Sonmez M, *et al.* 2017. The importance of risk factors for the prediction of patients with invasive pulmonary aspergillosis. Rev Assoc Med Bras (1992) **63**, 764-770.

Keystone EC, Schiff MH, Kremer JM, *et al.* 2004. Once-weekly administration of 50 mg etanercept in patients with active rheumatoid arthritis: results of a multicenter, randomized, double-blind, placebo-controlled trial. Arthritis Rheum **50**, 353-363.

Kirschner MB, van Zandwijk N, Reid G. 2013. Cell-free microRNAs: potential biomarkers in need of standardized reporting. Front Genet **4**, 56.

Koch CM, Chiu SF, Akbarpour M, *et al.* 2018. A Beginner's Guide to Analysis of RNA Sequencing Data. Am J Respir Cell Mol Biol **59**, 145-157.

Koehler P, Bassetti M, Chakrabarti A, *et al.* 2021. Defining and managing COVID-19-associated pulmonary aspergillosis: the 2020 ECMM/ISHAM consensus criteria for research and clinical guidance. Lancet Infect Dis **21**, e149-e162.

Koehler P, Cornely OA, Bottiger BW, *et al.* 2020. COVID-19 associated pulmonary aspergillosis. Mycoses **63**, 528-534.

Koulenti D, Garnacho-Montero J, Blot S. 2014. Approach to invasive pulmonary aspergillosis in critically ill patients. Curr Opin Infect Dis **27**, 174-183.

Krel M, Petraitis V, Petraitiene R, *et al.* 2014. Host biomarkers of invasive pulmonary aspergillosis to monitor therapeutic response. Antimicrob Agents Chemother **58**, 3373-3378.

Krueger KP, Nelson AC. 2009. Economic considerations in the treatment of invasive aspergillosis: a review of voriconazole pharmacoeconomic studies. Clinicoecon Outcomes Res **1**, 35-43.

Kuhn DE, Martin MM, Feldman DS, *et al.* 2008. Experimental validation of miRNA targets. Methods **44**, 47-54.

Kukurba KR, Montgomery SB. 2015. RNA Sequencing and Analysis. Cold Spring Harb Protoc **2015**, 951-969.

Kuo CW, Wang SY, Tsai HP, *et al.* 2021. Invasive pulmonary aspergillosis is associated with cytomegalovirus viremia in critically ill patients - A retrospective cohort study. J Microbiol Immunol Infect.

Kwon-Chung KJ, Sugui JA. 2013. Aspergillus fumigatus--what makes the species a ubiquitous human fungal pathogen? PLoS Pathog **9**, e1003743.

Labbe AC, Su SH, Laverdiere M, *et al.* 2007. High incidence of invasive aspergillosis associated with intestinal graft-versus-host disease following nonmyeloablative transplantation. Biol Blood Marrow Transplant **13**, 1192-1200.

Lamoth F. 2016. Aspergillus fumigatus-Related Species in Clinical Practice. Front Microbiol **7**, 683.

Lass-Florl C. 2011. Triazole antifungal agents in invasive fungal infections: a comparative review. Drugs **71**, 2405-2419.

Lass-Florl C. 2017. Current Challenges in the Diagnosis of Fungal Infections. Methods Mol Biol **1508**, 3-15.

Lass-Florl C. 2019. How to make a fast diagnosis in invasive aspergillosis. Med Mycol **57**, S155-S160.

Latge JP. 1999. Aspergillus fumigatus and aspergillosis. Clin Microbiol Rev **12**, 310-350.

Latge JP, Chamilos G. 2019. Aspergillus fumigatus and Aspergillosis in 2019. Clin Microbiol Rev **33**.

Lee RC, Feinbaum RL, Ambros V. 1993. The C. elegans heterochronic gene lin-4 encodes small RNAs with antisense complementarity to lin-14. Cell **75**, 843-854.

Li H, Liu L, Zhou W, *et al.* 2019. Pentraxin 3 in bronchoalveolar lavage fluid and plasma in non-neutropenic patients with pulmonary aspergillosis. Clin Microbiol Infect **25**, 504-510.

Li H, Zhang J, Fang C, *et al.* 2021a. The prognostic value of IL-8 for the death of severe or critical patients with COVID-19. Medicine (Baltimore) **100**, e23656.

Li J, Xu L, Run ZC, *et al.* 2018. Multiple cytokine profiling in serum for early detection of gastric cancer. World J Gastroenterol **24**, 2269-2278.

Li S, Zhao L, Li X, *et al.* 2021b. Mir-204 Regulates LPS-Induced A549 Cell Damage by Targeting FOXK2. J Healthc Eng **2021**, 7404671.

Li XY, Zhang K, Jiang ZY, *et al.* 2014. MiR-204/miR-211 downregulation contributes to candidemia-induced kidney injuries via derepression of Hmx1 expression. Life Sci **102**, 139-144.

Li Y, Li L. 2020. Bioinformatic screening for candidate biomarkers and their prognostic values in endometrial cancer. BMC Genet **21**, 113.

Lin J, Lin Y, Huang Y, *et al.* 2021. Inhibiting miR-129-5p alleviates inflammation and modulates autophagy by targeting ATG14 in fungal keratitis. Exp Eye Res **211**, 108731.

Lu M, Zhan X. 2018. The crucial role of multiomic approach in cancer research and clinically relevant outcomes. EPMA J **9**, 77-102.

Lupianez CB, Villaescusa MT, Carvalho A, *et al.* 2016. Common Genetic Polymorphisms within NFkappaB-Related Genes and the Risk of Developing Invasive Aspergillosis. Front Microbiol **7**, 1243.

Lydon EC, Henao R, Burke TW, *et al.* 2019. Validation of a host response test to distinguish bacterial and viral respiratory infection. EBioMedicine **48**, 453-461.

Ma A, Zhang L, Ye X, *et al.* 2021. High Levels of Circulating IL-8 and Soluble IL-2R Are Associated With Prolonged Illness in Patients With Severe COVID-19. Front Immunol **12**, 626235.

Machata S, Muller MM, Lehmann R, *et al.* 2020. Proteome analysis of bronchoalveolar lavage fluids reveals host and fungal proteins highly expressed during invasive pulmonary aspergillosis in mice and humans. Virulence **11**, 1337-1351.

Maertens J, Verhaegen J, Lagrou K, *et al.* 2001. Screening for circulating galactomannan as a noninvasive diagnostic tool for invasive aspergillosis in prolonged neutropenic patients and stem cell transplantation recipients: a prospective validation. Blood **97**, 1604-1610.

Marr KA, Carter RA, Boeckh M, *et al.* 2002. Invasive aspergillosis in allogeneic stem cell transplant recipients: changes in epidemiology and risk factors. Blood **100**, 4358-4366.

Matsushima K, Isomoto H, Inoue N, *et al.* 2011. MicroRNA signatures in Helicobacter pylori-infected gastric mucosa. Int J Cancer **128**, 361-370.

Matthaiou EI, Sass G, Stevens DA, *et al.* 2018. Iron: an essential nutrient for Aspergillus fumigatus and a fulcrum for pathogenesis. Curr Opin Infect Dis **31**, 506-511.

Mehrad B, Strieter RM, Standiford TJ. 1999. Role of TNF-alpha in pulmonary host defense in murine invasive aspergillosis. J Immunol **162**, 1633-1640.

Meis JF, Chowdhary A, Rhodes JL, *et al.* 2016. Clinical implications of globally emerging azole resistance in Aspergillus fumigatus. Philos Trans R Soc Lond B Biol Sci **371**.

Meliopoulos VA, Van de Velde LA, Van de Velde NC, *et al.* 2016. An Epithelial Integrin Regulates the Amplitude of Protective Lung Interferon Responses against Multiple Respiratory Pathogens. PLoS Pathog **12**, e1005804.

Mercier T, Dunbar A, de Kort E, *et al.* 2020. Lateral flow assays for diagnosing invasive pulmonary aspergillosis in adult hematology patients: A comparative multicenter study. Med Mycol **58**, 444-452.

Mezger M, Kneitz S, Wozniok I, *et al.* 2008a. Proinflammatory response of immature human dendritic cells is mediated by dectin-1 after exposure to Aspergillus fumigatus germ tubes. J Infect Dis **197**, 924-931.

Mezger M, Steffens M, Beyer M, *et al.* 2008b. Polymorphisms in the chemokine (C-X-C motif) ligand 10 are associated with invasive aspergillosis after allogeneic stem-cell transplantation and influence CXCL10 expression in monocyte-derived dendritic cells. Blood **111**, 534-536.

Miotto E, Saccenti E, Lupini L, *et al.* 2014. Quantification of circulating miRNAs by droplet digital PCR: comparison of EvaGreen- and TaqMan-based chemistries. Cancer Epidemiol Biomarkers Prev **23**, 2638-2642.

Moldovan L, Batte KE, Trgovcich J, *et al.* 2014. Methodological challenges in utilizing miRNAs as circulating biomarkers. J Cell Mol Med **18**, 371-390.

Morrison BE, Park SJ, Mooney JM, *et al.* 2003. Chemokine-mediated recruitment of NK cells is a critical host defense mechanism in invasive aspergillosis. J Clin Invest **112**, 1862-1870.

Nahid MA, Yao B, Dominguez-Gutierrez PR, *et al.* 2013. Regulation of TLR2-mediated tolerance and cross-tolerance through IRAK4 modulation by miR-132 and miR-212. J Immunol **190**, 1250-1263.

Nedel WL, Kontoyiannis DP, Pasqualotto AC. 2009. Aspergillosis in patients treated with monoclonal antibodies. Rev Iberoam Micol **26**, 175-183.

Neofytos D, Horn D, Anaissie E, *et al.* 2009. Epidemiology and outcome of invasive fungal infection in adult hematopoietic stem cell transplant recipients: analysis of Multicenter Prospective Antifungal Therapy (PATH) Alliance registry. Clin Infect Dis **48**, 265-273.

Nucci M, Anaissie E. 2009. Fungal infections in hematopoietic stem cell transplantation and solid-organ transplantation--focus on aspergillosis. Clin Chest Med **30**, 295-306, vii.

O'Connell RM, Taganov KD, Boldin MP, *et al.* 2007. MicroRNA-155 is induced during the macrophage inflammatory response. Proc Natl Acad Sci U S A **104**, 1604-1609.

Obeng JA, Amoruso A, Camaschella GL, *et al.* 2016. Modulation of human monocyte/macrophage activity by tocilizumab, abatacept and etanercept: An in vitro study. Eur J Pharmacol **780**, 33-37.

Odabasi Z, Paetznick VL, Rodriguez JR, *et al.* 2006. Differences in beta-glucan levels in culture supernatants of a variety of fungi. Med Mycol **44**, 267-272.

Oeckinghaus A, Ghosh S. 2009. The NF-kappaB family of transcription factors and its regulation. Cold Spring Harb Perspect Biol **1**, a000034.

Oliveira AC, Bovolenta LA, Nachtigall PG, *et al.* 2017. Combining Results from Distinct MicroRNA Target Prediction Tools Enhances the Performance of Analyses. Front Genet **8**, 59.

Ouyang J, Hu J, Chen JL. 2016. lncRNAs regulate the innate immune response to viral infection. Wiley Interdiscip Rev RNA **7**, 129-143.

Ozaki K, Inoue K, Sato H, *et al.* 2004. Functional variation in LGALS2 confers risk of myocardial infarction and regulates lymphotoxin-alpha secretion in vitro. Nature **429**, 72-75.

Paczesny S, Krijanovski OI, Braun TM, *et al.* 2009. A biomarker panel for acute graft-versus-host disease. Blood **113**, 273-278.

Paijo J, Doring M, Spanier J, *et al.* 2016. cGAS Senses Human Cytomegalovirus and Induces Type I Interferon Responses in Human Monocyte-Derived Cells. PLoS Pathog **12**, e1005546.

Pakshir K, Badali H, Nami S, *et al.* 2020. Interactions between immune response to fungal infection and microRNAs: The pioneer tuners. Mycoses **63**, 4-20.

Palucka K, Banchereau J. 1999. Dendritic cells: a link between innate and adaptive immunity. J Clin Immunol **19**, 12-25.

Park SJ, Hughes MA, Burdick M, *et al.* 2009. Early NK cell-derived IFN-{gamma} is essential to host defense in neutropenic invasive aspergillosis. J Immunol **182**, 4306-4312.

Patterson JE, Peters J, Calhoon JH, *et al.* 2000. Investigation and control of aspergillosis and other filamentous fungal infections in solid organ transplant recipients. Transpl Infect Dis **2**, 22-28.

Patterson TF, Donnelly JP. 2019. New Concepts in Diagnostics for Invasive Mycoses: Non-Culture-Based Methodologies. J Fungi (Basel) **5**.

Patterson TF, Thompson GR, 3rd, Denning DW, *et al.* 2016. Practice Guidelines for the Diagnosis and Management of Aspergillosis: 2016 Update by the Infectious Diseases Society of America. Clin Infect Dis **63**, e1-e60.

Pelzer BW, Seufert R, Koldehoff M, *et al.* 2020. Performance of the AsperGenius(R) PCR assay for detecting azole resistant Aspergillus fumigatus in BAL fluids from allogeneic HSCT recipients: A prospective cohort study from Essen, West Germany. Med Mycol **58**, 268-271.

Pfaffl MW. 2013. Transcriptional biomarkers. Methods **59**, 1-2.

Phadke AP, Mehrad B. 2005. Cytokines in host defense against Aspergillus: recent advances. Med Mycol **43 Suppl 1**, S173-176.

Plassmeyer M, Alpan O, Corley MJ, *et al.* 2021. Caspases and therapeutic potential of caspase inhibitors in moderate-severe SARS CoV2 infection and long COVID. Allergy.

Prashar A, Schnettger L, Bernard EM, *et al.* 2017. Rab GTPases in Immunity and Inflammation. Front Cell Infect Microbiol **7**, 435.

Quezada H, Guzman-Ortiz AL, Diaz-Sanchez H, *et al.* 2017. Omics-based biomarkers: current status and potential use in the clinic. Bol Med Hosp Infant Mex **74**, 219-226.

Rashidi A, Khoruts A, Weisdorf DJ. 2017. Infection Followed by Graft-versus-Host Disease: Pathogenic Role of Antibiotics. Biol Blood Marrow Transplant **23**, 1038-1039.

Rawlings SA, Heldt S, Prattes J, *et al.* 2019. Using Interleukin 6 and 8 in Blood and Bronchoalveolar Lavage Fluid to Predict Survival in Hematological Malignancy Patients With Suspected Pulmonary Mold Infection. Front Immunol **10**, 1798.

Reinwald M, Spiess B, Heinz WJ, *et al.* 2012. Diagnosing pulmonary aspergillosis in patients with hematological malignancies: a multicenter prospective evaluation of an Aspergillus PCR assay and a galactomannan ELISA in bronchoalveolar lavage samples. Eur J Haematol **89**, 120-127.

Rezende CP, Martins Oliveira Brito PK, Pessoni AM, *et al.* 2021. Altered expression of genes related to innate antifungal immunity in the absence of galectin-3. Virulence **12**, 981-988.

Ribaud P. 2006. Challenges of patient recruitment for invasive aspergillosis trials. Med Mycol **44**, S295-S297.

Robin C, Cordonnier C, Sitbon K, *et al.* 2019. Mainly Post-Transplant Factors Are Associated with Invasive Aspergillosis after Allogeneic Stem Cell Transplantation: A Study from the Surveillance des Aspergilloses Invasives en France and Societe Francophone de Greffe de Moelle et de Therapie Cellulaire. Biol Blood Marrow Transplant **25**, 354-361.

Roilides E, Dimitriadou-Georgiadou A, Sein T, *et al.* 1998. Tumor necrosis factor alpha enhances antifungal activities of polymorphonuclear and mononuclear phagocytes against Aspergillus fumigatus. Infect Immun **66**, 5999-6003.

Ross MH, Zick BL, Tsalik EL. 2019. Host-Based Diagnostics for Acute Respiratory Infections. Clin Ther **41**, 1923-1938.

Rossato M, Curtale G, Tamassia N, *et al.* 2012. IL-10-induced microRNA-187 negatively regulates TNF-alpha, IL-6, and IL-12p40 production in TLR4-stimulated monocytes. Proc Natl Acad Sci U S A **109**, E3101-3110.

Ruetten H, Thiemermann C, Perretti M. 1999. Upregulation of ICAM-1 expression on J774.2 macrophages by endotoxin involves activation of NF-kappaB but not protein tyrosine kinase: comparison to induction of iNOS. Mediators Inflamm **8**, 77-84.

Ruhnke M, Behre G, Buchheidt D, *et al.* 2018. Diagnosis of invasive fungal diseases in haematology and oncology: 2018 update of the recommendations of the infectious diseases working party of the German society for hematology and medical oncology (AGIHO). Mycoses **61**, 796-813.

Rutsaert L, Steinfort N, Van Hunsel T, *et al.* 2020. COVID-19-associated invasive pulmonary aspergillosis. Ann Intensive Care **10**, 71.

Saliminejad K, Khorram Khorshid HR, Ghaffari SH. 2019. Why have microRNA biomarkers not been translated from bench to clinic? Future Oncol **15**, 801-803.

Sato M, Sasaki M, Hojo H. 1994. Differential induction of metallothionein synthesis by interleukin-6 and tumor necrosis factor-alpha in rat tissues. Int J Immunopharmacol **16**, 187-195.

Schaffner A, Douglas H, Braude A. 1982. Selective protection against conidia by mononuclear and against mycelia by polymorphonuclear phagocytes in resistance to Aspergillus. Observations on these two lines of defense in vivo and in vitro with human and mouse phagocytes. J Clin Invest **69**, 617-631.

Schauwvlieghe A, Rijnders BJA, Philips N, *et al.* 2018. Invasive aspergillosis in patients admitted to the intensive care unit with severe influenza: a retrospective cohort study. Lancet Respir Med **6**, 782-792.

Schmittgen TD, Livak KJ. 2008. Analyzing real-time PCR data by the comparative C(T) method. Nat Protoc **3**, 1101-1108.

Scott LJ. 2014. Etanercept: a review of its use in autoimmune inflammatory diseases. Drugs **74**, 1379-1410.

Sedger LM, McDermott MF. 2014. TNF and TNF-receptors: From mediators of cell death and inflammation to therapeutic giants - past, present and future. Cytokine Growth Factor Rev **25**, 453-472.
Seelbinder B, Wolf T, Priebe S, *et al.* 2019. GEO2RNAseq: An easy-to-use R pipeline for complete pre-processing of RNA-seq data. bioRxiv, 771063.
Serbina NV, Cherny M, Shi C, *et al.* 2009. Distinct responses of human monocyte subsets to Aspergillus fumigatus conidia. J Immunol **183**, 2678-2687.
Shahzad A, Knapp M, Lang I, *et al.* 2010. Interleukin 8 (IL-8) - a universal biomarker? Int Arch Med **3**, 11.
Shao W, Guo T, Toussaint NC, *et al.* 2019. Comparative analysis of mRNA and protein degradation in prostate tissues indicates high stability of proteins. Nat Commun **10**, 2524.
Simoneau E, Kelly M, Labbe AC, *et al.* 2005. What is the clinical significance of positive blood cultures with Aspergillus sp in hematopoietic stem cell transplant recipients? A 23 year experience. Bone Marrow Transplant **35**, 303-306.
Siopi M, Karakatsanis S, Roumpakis C, *et al.* 2021. A Prospective Multicenter Cohort Surveillance Study of Invasive Aspergillosis in Patients with Hematologic Malignancies in Greece: Impact of the Revised EORTC/MSGERC 2020 Criteria. J Fungi (Basel) **7**.
Snarr BD, St-Pierre G, Ralph B, *et al.* 2020. Galectin-3 enhances neutrophil motility and extravasation into the airways during Aspergillus fumigatus infection. PLoS Pathog **16**, e1008741.
Spreadbury C, Holden D, Aufauvre-Brown A, *et al.* 1993. Detection of Aspergillus fumigatus by polymerase chain reaction. J Clin Microbiol **31**, 615-621.
Stanzani M, Orciuolo E, Lewis R, *et al.* 2005. Aspergillus fumigatus suppresses the human cellular immune response via gliotoxin-mediated apoptosis of monocytes. Blood **105**, 2258-2265.
Steele C, Rapaka RR, Metz A, *et al.* 2005. The beta-glucan receptor dectin-1 recognizes specific morphologies of Aspergillus fumigatus. PLoS Pathog **1**, e42.
Steinbrink JM, Zaas AK, Betancourt M, *et al.* 2020. A transcriptional signature accurately identifies Aspergillus Infection across healthy and immunosuppressed states. Transl Res **219**, 1-12.
Stewart AG, Henden AS. 2021. Infectious complications of CAR T-cell therapy: a clinical update. Ther Adv Infect Dis **8**, 20499361211036773.
Sticht C, De La Torre C, Parveen A, *et al.* 2018. miRWalk: An online resource for prediction of microRNA binding sites. PLoS One **13**, e0206239.
Sturm A, Lensch M, Andre S, *et al.* 2004. Human galectin-2: novel inducer of T cell apoptosis with distinct profile of caspase activation. J Immunol **173**, 3825-3837.
Subramanian Vignesh K, Deepe GS, Jr. 2017. Metallothioneins: Emerging Modulators in Immunity and Infection. Int J Mol Sci **18**.
Sun WK, Lu X, Li X, *et al.* 2012. Dectin-1 is inducible and plays a crucial role in Aspergillus-induced innate immune responses in human bronchial epithelial cells. Eur J Clin Microbiol Infect Dis **31**, 2755-2764.
Sundaram VK, Sampathkumar NK, Massaad C, *et al.* 2019. Optimal use of statistical methods to validate reference gene stability in longitudinal studies. PLoS One **14**, e0219440.
Taganov KD, Boldin MP, Chang KJ, *et al.* 2006. NF-kappaB-dependent induction of microRNA miR-146, an inhibitor targeted to signaling proteins of innate immune responses. Proc Natl Acad Sci U S A **103**, 12481-12486.
Takahashi T, Ellingson MK, Wong P, *et al.* 2020. Sex differences in immune responses that underlie COVID-19 disease outcomes. Nature **588**, 315-320.

Taub DD, Longo DL, Murphy WJ. 1996. Human interferon-inducible protein-10 induces mononuclear cell infiltration in mice and promotes the migration of human T lymphocytes into the peripheral tissues and human peripheral blood lymphocytes-SCID mice. Blood **87**, 1423-1431.

Thammasit P, Sripetchwandee J, Nosanchuk JD, *et al.* 2021. Cytokine and Chemokine Responses in Invasive Aspergillosis Following Hematopoietic Stem Cell Transplantation: Past Evidence for Future Therapy of Aspergillosis. J Fungi (Basel) **7**.

Thompson A, Orr SJ. 2018. Emerging IL-12 family cytokines in the fight against fungal infections. Cytokine **111**, 398-407.

Tisoncik JR, Korth MJ, Simmons CP, *et al.* 2012. Into the eye of the cytokine storm. Microbiol Mol Biol Rev **76**, 16-32.

Tolnai E, Fidler G, Szasz R, *et al.* 2020. Free circulating mircoRNAs support the diagnosis of invasive aspergillosis in patients with hematologic malignancies and neutropenia. Sci Rep **10**, 16532.

Tomalka J, Hise AG. 2015. Inflammasomes in aspergillosis--it takes two to tango. Cell Host Microbe **17**, 290-292.

Tong J, Duan Z, Zeng R, *et al.* 2021. MiR-146a Negatively Regulates Aspergillus fumigatus-Induced TNF-alpha and IL-6 Secretion in THP-1 Macrophages. Mycopathologia **186**, 341-354.

Tsiodras S, Samonis G, Boumpas DT, *et al.* 2008. Fungal infections complicating tumor necrosis factor alpha blockade therapy. Mayo Clin Proc **83**, 181-194.

Tsitsiou E, Lindsay MA. 2009. microRNAs and the immune response. Curr Opin Pharmacol **9**, 514-520.

Ullmann AJ, Aguado JM, Arikan-Akdagli S, *et al.* 2018. Diagnosis and management of Aspergillus diseases: executive summary of the 2017 ESCMID-ECMM-ERS guideline. Clin Microbiol Infect **24 Suppl 1**, e1-e38.

Vasta GR. 2009. Roles of galectins in infection. Nat Rev Microbiol **7**, 424-438.

Veselenak RL, Miller AL, Milligan GN, *et al.* 2015. Development and utilization of a custom PCR array workflow: analysis of gene expression in mycoplasma genitalium and guinea pig (Cavia porcellus). Mol Biotechnol **57**, 172-183.

Vidal-Acuna MR, Ruiz-Perez de Pipaon M, Torres-Sanchez MJ, *et al.* 2018. Identification of clinical isolates of Aspergillus, including cryptic species, by matrix assisted laser desorption ionization time-of-flight mass spectrometry (MALDI-TOF MS). Med Mycol **56**, 838-846.

Vigorito E, Kohlhaas S, Lu D, *et al.* 2013. miR-155: an ancient regulator of the immune system. Immunol Rev **253**, 146-157.

Volling K, Brakhage AA, Saluz HP. 2007. Apoptosis inhibition of alveolar macrophages upon interaction with conidia of Aspergillus fumigatus. FEMS Microbiol Lett **275**, 250-254.

Wang Z, Gerstein M, Snyder M. 2009. RNA-Seq: a revolutionary tool for transcriptomics. Nat Rev Genet **10**, 57-63.

Weinberger M, Elattar I, Marshall D, *et al.* 1992. Patterns of infection in patients with aplastic anemia and the emergence of Aspergillus as a major cause of death. Medicine (Baltimore) **71**, 24-43.

Weiss LA, Lester LA, Gern JE, *et al.* 2005. Variation in ITGB3 is associated with asthma and sensitization to mold allergen in four populations. Am J Respir Crit Care Med **172**, 67-73.

White LP, Price JS. 2021. Recent Advances and Novel Approaches in Laboratory-Based Diagnostic Mycology. J Fungi (Basel) **7**.

White PL, Dhillon R, Cordey A, *et al.* 2020. A national strategy to diagnose COVID-19 associated invasive fungal disease in the ICU. Clin Infect Dis.

White PL, Parr C, Barnes RA. 2018. Predicting Invasive Aspergillosis in Hematology Patients by Combining Clinical and Genetic Risk Factors with Early Diagnostic Biomarkers. J Clin Microbiol **56**.

Wu Y, Xu H, Li Y, *et al.* 2019. miRNA-344b-1-3p modulates the autophagy of NR8383 cells during Aspergillus fumigatus infection via TLR2. Exp Ther Med **18**, 139-146.

Wudhikarn K, Palomba ML, Pennisi M, *et al.* 2020. Infection during the first year in patients treated with CD19 CAR T cells for diffuse large B cell lymphoma. Blood Cancer J **10**, 79.

Xi X, Li T, Huang Y, *et al.* 2017. RNA Biomarkers: Frontier of Precision Medicine for Cancer. Noncoding RNA **3**.

Xu P, Wu Q, Yu J, *et al.* 2020. A Systematic Way to Infer the Regulation Relations of miRNAs on Target Genes and Critical miRNAs in Cancers. Front Genet **11**, 278.

Yoon H, Belmonte KC, Kasten T, *et al.* 2017. Intra- and Inter-individual Variability of microRNA Levels in Human Cerebrospinal Fluid: Critical Implications for Biomarker Discovery. Sci Rep **7**, 12720.

Young RC, Bennett JE, Vogel CL, *et al.* 1970. Aspergillosis. The spectrum of the disease in 98 patients. Medicine (Baltimore) **49**, 147-173.

Zaas AK, Chen M, Varkey J, *et al.* 2009. Gene expression signatures diagnose influenza and other symptomatic respiratory viral infections in humans. Cell Host Microbe **6**, 207-217.

Zhang F, Lin X, Yang X, *et al.* 2019. MicroRNA-132-3p suppresses type I IFN response through targeting IRF1 to facilitate H1N1 influenza A virus infection. Biosci Rep **39**.

Zhang Y, Wang H. 2012. Integrin signalling and function in immune cells. Immunology **135**, 268-275.

Zhao S, Gordon W, Du S, *et al.* 2017. QuickMIRSeq: a pipeline for quick and accurate quantification of both known miRNAs and isomiRs by jointly processing multiple samples from microRNA sequencing. BMC Bioinformatics **18**, 180.

Zhao Y, Nagasaki Y, Paderu P, *et al.* 2019. Applying host disease status biomarkers to therapeutic response monitoring in invasive aspergillosis patients. Med Mycol **57**, 38-44.

Zollner H, Hahn SA, Maghnouj A. 2014. Quantitative RT-PCR specific for precursor and mature miRNAs. Methods Mol Biol **1095**, 121-134.

Zoran T, Seelbinder B, White PL, *et al.* 2022. Molecular Profiling Reveals Characteristic and Decisive Signatures in Patients after Allogeneic Stem Cell Transplantation Suffering from Invasive Pulmonary Aspergillosis. J Fungi (Basel) **8**.

Zoran T, Weber M, Springer J, *et al.* 2019. Treatment with etanercept and low monocyte concentration contribute to the risk of invasive aspergillosis in patients post allogeneic stem cell transplantation. Sci Rep **9**, 17231.

Appendix

Investigation of characteristic molecular signatures indicating IPA in patients post alloSCT

Supplementary Table S1: Clinical characteristics of additional alloSCT patients obtained from the University Hospital of Würzburg (Würzburg, Germany) and Public Health Wales Microbiology Cardiff (Cardiff, United Kingdom, UK). Adapted from Zoran *et al.*, 2022.

Patient ID	Cohort	Sex	Age	Origin	Disease status	Underlying disease
Ca1	Cardiff I	M	56	UK	Probable IPA	AML
Ca2	Cardiff I	M	46	UK	Probable IPA	Myelofibrosis
Ca3	Cardiff I	M	52	UK	Probable IPA	AML
Ca4	Cardiff I	M	67	UK	Probable IPA	AML
Ca5	Cardiff I	F	24	UK	Probable IPA	CIVD
Ca6	Cardiff I	F	65	UK	Probable IPA	AML
Ca7	Cardiff I	M	52	UK	Control	AML/MDS
Ca8	Cardiff I	F	71	UK	Control	AML
Ca9	Cardiff I	M	64	UK	Control	MDS
Ca10	Cardiff I	F	64	UK	Control	MDS
Ca11	Cardiff I	M	18	UK	Control	ALL
Ca12	Cardiff I	M	69	UK	Control	AML
Ca13	Cardiff I	F	24	UK	Possible IPA	CGD
Ca14	Cardiff I	M	55	UK	Possible IPA	AML
Ca15	Cardiff I	F	67	UK	Possible IPA	AML
Ca16	Cardiff I	M	63	UK	Possible IPA	AML
Ca17	Cardiff I	M	48	UK	Possible IPA	AML/MDS
P23	Würzburg	M	52	Germany	Possible IPA	MDS
P33	Würzburg	M	68	Germany	Possible IPA	PCL
P85	Würzburg	M	48	Germany	Possible IPA	AML
P31	Würzburg	M	68	Germany	Control	AML
P44	Würzburg	M	77	Germany	Control	MDS
P53	Würzburg	M	59	Germany	Control	AML
P26	Würzburg	F	44	Germany	GvHD (intestinal, IV)	AML
P67	Würzburg	M	55	Germany	GvHD (skin, III)	AML
P79	Würzburg	M	20	Germany	GvHD (intestinal III, skin II)	ALL

MDS, myelodysplastic syndrome; **CIVD**, Common variable immunodeficiency; **ALL**, Acute Lymphocytic Leukemia; **CGD**, Chronic Granulomatous Disease; **PCL**, Plasma cell leukaemia

Supplementary Table S2: Clinical characteristics of independent COVID-19 cohort obtained from the Public Health Wales Microbiology Cardiff (Cardiff, United Kingdom, UK). The cohort consisted of CAPA cases and COVID-19 controls. Adapted from Zoran *et al*., 2022.

COVID-19 controls			**CAPA cases**		
Patient ID	**Sex**	**Age**	**Patient ID**	**Sex**	**Age**
C6	M	63	C1	M	58
C7	F	59	C2	M	53
C8	M	71	C3	M	83
C9	M	64	C4	F	53
C10	F	45	C5	M	75
C11	M	56	C52	M	58
C12	F	45	C53	M	74
C13	M	63	C54	F	73
C14	F	46	C55	F	53
C15	M	58	C56	M	74
C16	M	53	C57	F	43
C17	F	55	C58	M	60
C18	M	36	C59	F	69
C19	M	59	C60	M	32
C20	M	63	C61	M	85
C21	M	74	C62	F	61
C22	F	62	C63	F	74
C23	F	62	C64	F	55
C24	M	48	C65	M	59
C25	M	58	C66	M	61
C26	M	49			
C27	M	81			
C28	M	38			
C29	F	52			
C30	M	47			
C31	M	70			
C32	M	50			
C33	M	51			
C34	M	57			
C35	M	69			
C36	M	73			
C38	F	58			
C39	M	70			
C40	M	61			
C41	M	54			
C42	M	68			
C43	F	50			
C44	M	57			
C45	M	47			
C46	M	40			
C47	M	45			

C48	M	83
C49	F	71
C50	M	56
C51	M	68

Supplementary Table S3: The list of samples used for the balanced data analysis (first five weeks after IPA onset) based on the established relative time (RelTime). Patients samples were collected at the University Hospital of Würzburg (Würzburg, Germany). Taken from Zoran *et al*., 2022.

Sample	After alloSCT (days)	RelTime (days)
P015-15	82	0
P015-16	92	10
P015-17	106	24
P015-18	113	31
P053-13	82	0
P053-15	91	9
P053-16	100	18
P053-17	113	31
P055-4	12	4
P055-5	15	7
P055-8	28	20
P055-9	41	33
P063-4	12	4
P063-5	15	7
P063-9	28	20
P063-10	40	32
P043-7	46	4
P043-9	53	11
P043-11	60	18
P043-13	67	25
P018-13	46	4
P018-14	56	14
P018-16	67	25
P018-17	70	28

Investigation of human risk factors contributing to the risk of invasive pulmonary aspergillosis in patients post alloSCT

Supplementary Table S4: Collected dynamic and binary clinical variables from investigated alloSCT patients obtained from the University Hospital of Würzburg. Taken from Zorant *et al*., 2019.

Clinical variables		
loperamide	galactomannan	sex
nitroimidazoles	neutropenia >10d	summer
fluorchinolone	Epstein Barr virus	fall
acylaminopenicillines	*Staphylococcus epidermidis*	winter
betalactamase-inhibitors	human herpes virus 6	spring
cephalosporines	cytomegalovirus	T cell immunosuppression in last 90d
carbapenemes	other_pathogens_than_A*spergillus*	sirolimus
amphotericin B	gram-negative rods	mycophenolat mofetil
fluconazole	*Candida albicans*	antithymocyte globulin (Genzyme)
voriconazole	*Escherichia coli*	prednisolone, dexamethasone, hydrocortisone, fludrocortisone
posaconazole	Klebsiella	muromonab
caspofungin	Proteus	etanercept
anidulafungin	viridans streptococci	budesonide
Aspergillus PCR	herpes simplex virus 1	T-cell immunosuppression
dexamethasone	*Clostridium difficile*	nucleoside analogues: valganciclovir, ganciclovir, foscavir, cidofovir, maribravir (anti-cytomegalovirus drugs)
hydrocortisone	Varicella-zoster virus	anti-herpes simplex virus drugs: aciclovir, brivudin, famciclovir, valaciclovir
prednisolone	vancomycin resistent enterococci	degree of GvHD
corticosteroids >21d >0,3mg/kg KG/d	polyomavirus	arterial hypertension
corticosteroids_yes_no	*Candida Krusei*	thromboembolic events: deep vein thrombosis, vena jugularis interna thrombosis, carotid endarterectomy, pulmonary embolism

betamethason_creme	toxoplasmosis	renal diseases: acute renal failure, chronic renal insufficiency, hydronephrosis, nephrolithiasis
dexamethasone	*Candida glabrata*	heart diseases: cardiac arrhythmia, patent foramen ovale, myocardial infarction, left ventricular insufficiency, coronary heart disease
hydrocortisone	gram-positive coccal bacteria	drug incompatibility
prednisolone	coagulase-negative staphylococci	neurological diseases: migraine, depression, gait ataxia, polyneuropathy, cluster headache, multiple sclerosis, hemiplegia, artery cerebri media infarction
budesonide	*Enterococcus faecalis*	orthopaedic diseases: osteoporosis, knee operation, fractures, lumbar spinal stenosis, avascular necrosis of the femoral head
creatinine normal	immunoglobulins	purine analogues: Fludarabine, Mercaptopurine, Nelarabine, Tioguanine, Clofarabine
human albumin	mouth wash	nitrogen mustard analogues: Bendamustine, Cyclophosphamide, Chlorambucil, Ifosfamide, Trofosfamide
etanercept	Alkyl sulfonates: Busulfan, Treosulfan	allogenic, bone marrow transplantation, umbilical cord blood transfusion
matched, unmatched	ATG	chronic lymphocytic leukaemia
acute myeloid leukaemia	thiotepa	multiple myeloma
myelodysplastic syndrome	total body irradiation	plasmacytoma
acute lymphoblastic leukaemia	age	

Supplementary Table S5: Top 40 significantly induced DEGs in MDM infected with *A. fumigatus* compared to unstimulated MDM. MDM generated from three healthy volunteers were infected with live *A. fumigatus* germ tubes (MOI 0.5; 6 hrs) and gene expression was investigated by RNA-seq. DEGs were identified using DESeq by applying adjusted p-value 0.05 and Log2FC 0.5.

Gene	Fold change	P-value (adj.)	Description
XIRP1	203.425	8.200×10^{-9}	xin actin binding repeat containing 1
MIR210HG	183.400	1.021×10^{-59}	MIR210 host gene
AC109326.1	159.762	4.601×10^{-05}	
CXCL2	158.049	7.585×10^{-31}	C-X-C motif chemokine ligand 2
EGR1	152.458	7.825×10^{-13}	early growth response 1
NR4A1	134.476	1.047×10^{-55}	nuclear receptor subfamily 4 group A member 1
ARC	130.124	2.514×10^{-06}	activity regulated cytoskeleton associated protein
EGR4	125.126	3.082×10^{-05}	early growth response 4
GPRC5A	116.284	1.218×10^{-13}	G protein-coupled receptor class C group 5 member A
EDN1	108.972	2.295×10^{-09}	endothelin 1 [Source:HGNC Symbol;Acc:HGNC:3176]
AC083837.1	105.229	6.014×10^{-10}	
AL078604.2	101.334	5.682×10^{-26}	
CXCL3	88.343	1.580×10^{-122}	C-X-C motif chemokine ligand 3
CCL4	83.713	3.079×10^{-36}	C-C motif chemokine ligand 4
AC011511.5	79.313	3.810×10^{-31}	
NR4A2	78.685	8.927×10^{-20}	nuclear receptor subfamily 4 group A member 2
RRAD	78.117	8.092×10^{-16}	Ras related glycolysis inhibitor and calcium channel regulator
TNF	77.820	6.300×10^{-21}	tumor necrosis factor
LINC00243	72.530	9.706×10^{-08}	long intergenic non-protein coding RNA 243
SERPINB2	70.581	3.934×10^{-70}	serpin family B member 2
CXCL8	67.342	2.082×10^{-38}	C-X-C motif chemokine ligand 8
ACOD1	59.879	9.419×10^{-06}	aconitate decarboxylase 1
CCL3L1	59.306	7.883×10^{-29}	C-C motif chemokine ligand 3 like 1
HES1	57.290	1.884×10^{-06}	hes family bHLH transcription factor 1
CXCL1	56.487	1.316×10^{-04}	C-X-C motif chemokine ligand 1
CCL4L2	56.469	1.040×10^{-48}	C-C motif chemokine ligand 4 like 2
NT5E	55.067	2.542×10^{-05}	5'-nucleotidase ecto
EGLN3	52.820	1.650×10^{-37}	egl-9 family hypoxia inducible factor 3
RPL23AP93	50.561	9.102×10^{-07}	ribosomal protein L23a pseudogene 93
IL6	49.863	9.065×10^{-06}	interleukin 6
FOSB	48.443	3.130×10^{-24}	FosB proto-oncogene, AP-1 transcription factor subunit
HCAR2	46.932	1.515×10^{-80}	hydroxycarboxylic acid receptor 2
OSM	45.450	1.103×10^{-53}	oncostatin M
MMP1	43.169	1.641×10^{-04}	matrix metallopeptidase 1
LINC01679	41.333	6.112×10^{-09}	long intergenic non-protein coding RNA 1679
EREG	38.668	2.242×10^{-08}	epiregulin
CSF3	37.305	2.094×10^{-03}	colony stimulating factor 3
TNFSF15	36.378	1.837×10^{-10}	TNF superfamily member 15
AL133163.1	34.099	4.536×10^{-03}	
HEY1	32.307	1.699×10^{-10}	hes related family bHLH transcription factor with YRPW motif 1

Statement of individual author contributions

In vitro* investigation of human transcriptome profiles in response to *Aspergillus fumigatus infection

Zoran T., Seelbinder B., Schäuble, S., Sieber P., Linde J., Loeffler J.

Participated in	**Author Initials,** Responsibility decreasing from left to right				
Study Design Methods Development	TZ	JLo	JLi SS		
Data Collection	TZ				
Data Analysis and Interpretation	TZ	SS, BS	PS	JLo	

Investigation of characteristic molecular signatures indicating IPA in patients post alloSCT

Publication:

Zoran, T.; Seelbinder, B.; White, P.L.; Price, J.S.; Kraus, S.; Kurzai, O.; Linde, J.; Häder, A.; Loeffler, C.; Grigoleit, G.U.; Einsele, H.; Panagiotou, G.; Loeffler*, J.; Schäuble*, S. Molecular Profiling Reveals Characteristic and Decisive Signatures in Patients after Allogeneic Stem Cell Transplantation Suffering from Invasive Pulmonary Aspergillosis. J. Fungi 2022, 8, 171, https://doi.org/10.3390/jof8020171.

*, equal contribution

Participated in	**Author Initials,** Responsibility decreasing from left to right				
Study Design Methods Development	TZ, JLi, JLo	SS, OK			
Data Collection	TZ	AH	JSP		
Data Analysis and Interpretation	TZ	SS, BS	PLW		
Manuscript Writing	TZ	SS, JLo	PLW, OK, SK	AH, BS, JLi	GUG, GP, HE, CL

Investigation of human risk factors contributing to the risk of invasive pulmonary aspergillosis in patients post alloSCT

Publication:

Zoran*, T.; Weber*, M.; Springer, J.; White, P.L.; Bauer, J.; Schober, A.; Loffler, C.; Seelbinder, B.; Hunniger, K.; Kurzai, O.; Scherag A.; Schäuble S.; Morton C. O.; Einsele H.; Linde* J.; Löffler* J. Treatment with etanercept and low monocyte concentration contribute to the risk of invasive aspergillosis in patients post allogeneic stem cell transplantation. Sci. Rep. 2019, 9, 17231, doi:10.1038/s41598-019-53504-8.

*, equal contribution

Participated in	**Author Initials,** Responsibility decreasing from left to right				
Study Design Methods Development	JLo, JLi	MW, TZ	JS		
Data Collection	TZ, MW	JB, JS	AeS		
Data Analysis and Interpretation	TZ, MW	JLo, JLi, JS	KH, BS	AaS, PLW,	OK, AeS, CL
Manuscript Writing	TZ, MW, JLi	JLo, JS	PLW, KH, SS	COM, OK	HE

JLo, Jürgen Loeffler; JLi, Jörg Linde; AeS, André Scherag; AaS, Annika Schober

The doctoral researcher confirms that she has obtained permission from both the publishers and the co-authors for legal second publication.

The doctoral researcher and the primary supervisor confirm the correctness of the above mentioned assessment.

Tamara Zoran	12.4.2022, Würzburg		
Doctoral Researcher's Name	Date	Place	Signature

Prof. Dr. Jürgen Löffler	12.4.2022, Würzburg		
Primary Supervisor's Name	Date	Place	Signature

Acknowledgements

Affidavit

I hereby confirm that my thesis entitled "Multilevel analysis of the human immune response to *Aspergillus fumigatus* infection: Characteristic molecular signatures and individual risk factors" is the result of my own work. I did not receive any help or support from commercial consultants. All sources and / or materials applied are listed and specified in the thesis. Furthermore, I confirm that this thesis has not yet been submitted as part of another examination process neither in identical nor in similar form.

…….....

Place, Date Signature

Eidesstattliche Erklärung

Hiermit erkläre ich an Eides statt, die Dissertation „Analysen der humanen Immunantwort auf eine Infektion mit *Aspergillus fumigatus*: Charakteristische molekulare Signaturen und individuelle Risikofaktoren" eigenständig, d.h. insbesondere selbständig und ohne Hilfe eines kommerziellen Promotionsberaters, angefertigt und keine anderen als die von mir angegebenen Quellen und Hilfsmittel verwendet zu haben. Ich erkläre außerdem, dass die Dissertation weder in gleicher noch in ähnlicher Form bereits in einem anderen Prüfungsverfahren vorgelegen hat.

…….....

Ort, Datum Unterschrift

Publication list

Curriculum vitae